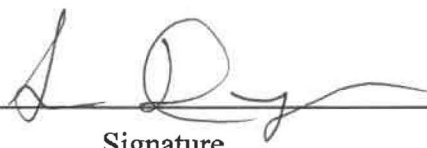


**SANDIA NATIONAL LABORATORIES
WASTE ISOLATION PILOT PLANT**

**ANALYSIS PACKAGE FOR ACTINIDE MOBILIZATION AND
SALADO TRANSPORT IN THE 2019 COMPLIANCE
RECERTIFICATION APPLICATION PERFORMANCE
ASSESSMENT (CRA-2019 PA)**

REVISION 0

Author:	<u>Ramesh Sarathi</u>	<u></u>	<u>7/15/2019</u>
	Print	Signature	Date
Technical Reviewer:	<u>Russell Chris Camphouse</u>	<u></u>	<u>7/15/2019</u>
	Print	Signature	Date
QA Reviewer:	<u>Shelly Nielsen</u>	<u></u>	<u>7-15-19</u>
	Print	Signature	Date
Management Reviewer:	<u>Sean Dunagan</u>	<u></u>	<u>7/15/19</u>
	Print	Signature	Date

ERMS #571371

JULY 11, 2019

WIPP:4.2.1:PA:QA-L:571155

Information Only

1 of 77

This page intentionally left blank.

TABLE OF CONTENTS

EXECUTIVE SUMMARY	VIII
1.0 INTRODUCTION.....	10
1.1 Changes Since the CRA-2014	11
1.1.1 Updates to WIPP Waste Inventory Parameters.....	11
1.1.2 Updates to Radionuclide Solubilities	11
1.1.3 Updates to Colloid Enhancement Parameters	12
1.1.4 Updates to PA Models.....	12
1.1.5 Listing of PA Parameters Related to Radionuclide Solubilities.....	13
1.2 Objectives	18
2.0 CONCEPTUAL APPROACH FOR THE CRA-2019	19
2.1 Actinide Mobilization: PANEL	19
2.2 Salado Transport: NUTS and PANEL	22
3.0 METHODOLOGY	24
4.0 RESULTS	28
4.1 Inventory	29
4.2 Total Mobile Concentration Limits	36
4.3 PANEL Instantaneous Mobile Concentrations	50
4.4 NUTS/PANEL Salado Transport.....	57
5.0 SUMMARY	72
6.0 REFERENCES.....	73

LIST OF TABLES

Table 1 – Solubility and Colloid Parameter Values for the CRA-2014 and CRA-2019 PA Calculations.....	13
Table 2 – Abridged decay chains modeled in PANEL	20
Table 3 – Lumped and Represented Radionuclides.....	21
Table 4 – Decay Chains Modeled in NUTS Code.....	23
Table 5 – Scenario descriptions and borehole intrusion time by simulation	26

LIST OF FIGURES

Figure 1 – Data and computational flow for PANEL calculations	24
Figure 2 – Data and computational flow for NUTS calculations	25
Figure 3– Inventory of Greatest Individual Radionuclides (in Curies)	29
Figure 4– Inventory of Radionuclides (in Curies), Relative.....	29
Figure 5– Isotope:Element Initial Mole Fractions	32
Figure 6– Lumped Radionuclide Solubility Adjustment for Isotope:Element Mole Fraction	33
Figure 7– Inventory of Lumped Radionuclides (in Curies).....	34
Figure 8– Inventory of Lumped Radionuclides (in Curies), Relative	34
Figure 9– Decay of Inventory	35
Figure 10– Baseline Solubilities for Salado Brine.....	36
Figure 11– Baseline Solubilities for Castile Brine	37
Figure 12– Solubility Uncertainty Exponent, SOLMOD3:SOLVAR	38
Figure 13– Solubility Uncertainty Exponent, SOLMOD4:SOLVAR	39
Figure 14– log ₁₀ of Total Mobilization Potential for Base Elements, Castile Brine, All Conditions	40
Figure 15– log ₁₀ of Total Mobilization Potential for Base Elements, Castile Brine, by Brine Redox Condition	40
Figure 16– Absolute Colloidal Contributions to Mobilization Potential: AM	42
Figure 17– Absolute Colloidal Contributions to Mobilization Potential: PU	42
Figure 18– Absolute Colloidal Contributions to Mobilization Potential: TH	43
Figure 19– Absolute Colloidal Contributions to Mobilization Potential: U.....	43
Figure 20– Absolute Colloidal Contributions to Mobilization Potential: NP	44
Figure 21– Fractional Colloidal Contributions to Mobilization Potential: AM	44
Figure 22– Fractional Colloidal Contributions to Mobilization Potential: PU.....	45
Figure 23– Fractional Colloidal Contributions to Mobilization Potential: TH.....	45
Figure 24– Fractional Colloidal Contributions to Mobilization Potential: U	46
Figure 25– Fractional Colloidal Contributions to Mobilization Potential: NP.....	46
Figure 26– log ₁₀ of Total Mobilization Potential, Lumped Radionuclides, Castile Brine, All Conditions	48
Figure 27– log ₁₀ of Total Mobilization Potential, Lumped Radionuclides, Castile Brine, by Brine Redox Condition	48
Figure 28– Means of Concentrations vs Time, Castile Brine, EPA Units.....	50
Figure 29 – Means of Concentrations vs Time, Castile Brine, EPA Units, by Brine Redox Condition.....	50

Figure 30– TOTAL Concentration vs Time, Castile Brine	51
Figure 31– AM241L Concentration vs Time, Castile Brine.....	52
Figure 32– PU239L Concentration vs Time, Castile Brine	52
Figure 33– TOTAL Concentration vs Time, Castile Brine	54
Figure 34– AM241L Concentration vs Time, Castile Brine.....	54
Figure 35– PU239L Concentration vs Time, Castile Brine.....	55
Figure 36– PU238L Concentration vs Time, Castile Brine.....	55
Figure 37– U234L Concentration vs Time, Castile Brine	56
Figure 38– TH230L Concentration vs Time, Castile Brine.....	56
Figure 39– Cumulative Radionuclide Discharge at 10000 Years.....	57
Figure 40– Cumulative Brine Discharge at 10000 Years	57
Figure 41– Cumulative Discharge at 10000 Years, Scenario 2	59
Figure 42– Cumulative Discharge at 10000 Years, Scenario 3	59
Figure 43– Cumulative Discharge at 10000 Years, Scenario 4.....	60
Figure 44– Cumulative Discharge at 10000 Years, Scenario 5	60
Figure 45– Cumulative Discharge at 10000 Years, Scenario 6	61
Figure 46– AM241L Cumulative Discharge vs Time, Scenario 2	62
Figure 47– PU239L Cumulative Discharge vs Time, Scenario 2.....	62
Figure 48– U234L Cumulative Discharge vs Time, Scenario 2.....	63
Figure 49– TH230L Cumulative Discharge vs Time, Scenario 2	63
Figure 50– AM241L Cumulative Discharge vs Time, Scenario 3	64
Figure 51– PU239L Cumulative Discharge vs Time, Scenario 3.....	64
Figure 52– U234L Cumulative Discharge vs Time, Scenario 3	65
Figure 53– TH230L Cumulative Discharge vs Time, Scenario 3	65
Figure 54– AM241L Cumulative Discharge vs Time, Scenario 4	66
Figure 55– PU239L Cumulative Discharge vs Time, Scenario 4.....	66
Figure 56– U234L Cumulative Discharge vs Time, Scenario 4.....	67
Figure 57– TH230L Cumulative Discharge vs Time, Scenario 4	67
Figure 58– AM241L Cumulative Discharge vs Time, Scenario 5	68
Figure 59– PU239L Cumulative Discharge vs Time, Scenario 5.....	68
Figure 60– U234L Cumulative Discharge vs Time, Scenario 5	69
Figure 61– TH230L Cumulative Discharge vs Time, Scenario 5	69
Figure 62– AM241L Cumulative Discharge vs Time, Scenario 6	70

Figure 63– PU239L Cumulative Discharge vs Time, Scenario 6.....70
Figure 64– U234L Cumulative Discharge vs Time, Scenario 671
Figure 65– TH230L Cumulative Discharge vs Time, Scenario 671

This page intentionally left blank.

Executive Summary

The Land Withdrawal Act requires that the U.S. Department of Energy (DOE) apply for recertification of the Waste Isolation Pilot Plant (WIPP) every five years following the initial 1999 waste shipment. The 2019 Compliance Recertification Application (CRA-2019) is the fourth WIPP recertification application submitted for approval by the U.S. Environmental Protection Agency. A performance assessment (PA) has been executed by Sandia National Laboratories in support of the DOE submittal of the CRA-2019. Results found in the CRA-2019 PA are compared to those obtained in the 2014 Compliance Recertification Application (CRA-2014) in order to assess repository performance in terms of the current regulatory baseline. This package documents the actinide mobilization and Salado transport analysis component of the CRA-2019 PA. Changes incorporated into the CRA-2019 PA include repository planned changes, parameter updates, and refinements to PA implementation. Changes included in the CRA-2019 PA that potentially affect the actinide mobilization and Salado transport results as compared to the CRA-2014 are:

- Updates to radionuclide solubilities and their associated uncertainty.
- Refinement to colloid enhancement parameters associated with actinide mobilization.
- Updates to WIPP waste inventory parameters.

Most significantly, the assumed An(III) baseline solubility values decreased substantially, the An(III) solubility uncertainty distribution values increased, and the An(IV) solubility uncertainty distribution values decreased. The result is that Am(III), Pu(III), and especially Pu(IV) median and mean concentrations decreased, and total mobile radioactivity concentrations decreased overall. The reduction in Pu mobile concentrations will reduce late-time releases in particular since little ²⁴¹Am remains in the inventory at late times.

This page intentionally left blank.

1.0 INTRODUCTION

The Waste Isolation Pilot Plant (WIPP), located in southeastern New Mexico, has been developed by the U.S. Department of Energy (DOE) for the geologic (deep underground) disposal of transuranic (TRU) waste. Containment of TRU waste at the WIPP is regulated by the U.S. Environmental Protection Agency (EPA) according to the regulations set forth in Title 40 of the Code of Federal Regulations (CFR), Part 191. The DOE demonstrates compliance with the containment requirements according to the Certification Criteria in Title 40 CFR Part 194 by means of performance assessment (PA) calculations performed by Sandia National Laboratories (SNL). WIPP PA calculations estimate the probability and consequence of potential radionuclide releases from the repository to the accessible environment for a regulatory period of 10,000 years after facility closure. The models used in PA are maintained and updated with new information as part of an ongoing process. Improved information regarding important WIPP features, events, and processes typically results in refinements and modifications to PA models and the parameters used in them. Planned changes to the repository and/or the components therein also result in updates to WIPP PA models. WIPP PA models are used to support the repository recertification process that occurs at five-year intervals following the receipt of the first waste shipment at the site in 1999.

PA calculations were included in the 1996 Compliance Certification Application (CCA) (U.S. DOE 1996), and in a subsequent Performance Assessment Verification Test (PAVT) (MacKinnon and Freeze 1997a, 1997b and 1997c). Based in part on the CCA and PAVT PA calculations, the EPA certified that the WIPP met the regulatory containment criteria. The facility was approved for disposal of transuranic waste in May 1998 (U.S. EPA 1998). PA calculations were an integral part of the 2004 Compliance Recertification Application (CRA-2004) (U.S. DOE 2004). During their review of the CRA-2004, the EPA requested an additional PA calculation, referred to as the CRA-2004 Performance Assessment Baseline Calculation (PABC) (Leigh et al. 2005), be conducted with modified assumptions and parameter values (Cotsworth 2005). Following review of the CRA-2004 and the CRA-2004 PABC, the EPA recertified the WIPP in March 2006 (U.S. EPA 2006).

PA calculations were completed for the second WIPP recertification and documented in the 2009 Compliance Recertification Application (CRA-2009). The CRA-2009 PA resulted from continued review of the CRA-2004 PABC, including a number of technical changes and corrections, as well as updates to parameters and improvements to the PA computer codes (Clayton et al. 2008). To incorporate additional information which was received after the CRA-2009 PA was completed, but before the submittal of the CRA-2009, the EPA requested an additional PA calculation, referred to as the 2009 Compliance Recertification Application Performance Assessment Baseline Calculation (PABC-2009) (Clayton et al. 2010), be undertaken which included updated information (Cotsworth 2009). Following the completion and submission of the PABC-2009, the WIPP was recertified in 2010 (U.S. EPA 2010).

PA calculations were completed for the third WIPP recertification and documented in the 2014 Compliance Recertification Application (CRA-2014). Following the completion and submission of the CRA-2014, the WIPP was recertified in 2017 (U.S. EPA 2017).

The Land Withdrawal Act (U.S. Congress 1992) requires that the DOE apply for WIPP recertification every five years following the initial 1999 waste shipment. The 2019 Compliance Recertification Application (CRA-2019) is the fourth WIPP recertification application submitted

by the DOE for EPA approval. The PA executed by SNL in support of the CRA-2019 is detailed in AP-181 (Zeitler 2019). The CRA-2019 PA includes repository planned changes, parameter updates, and refinements to PA implementation. Results found in the CRA-2019 PA are compared to those obtained in the CRA-2014 in order to assess repository performance in terms of the current regulatory baseline. This analysis package documents the actinide mobilization and Salado transport components of the CRA-2019 PA analysis.

1.1 Changes Since the CRA-2014

Several changes are incorporated in the CRA-2019 PA relative to the CRA-2014 – those changes are outlined in AP-181 (Zeitler 2019). The subset of changes that potentially impact the actinide mobilization and Salado transport results include:

- updates to WIPP waste inventory parameters
- updates to radionuclide solubilities and their associated uncertainty
- updates to colloid enhancement parameters associated with actinide mobilization

1.1.1 Updates to WIPP Waste Inventory Parameters

The CRA-2019 PA is based on the updated radionuclide and waste material inventory reported in the Performance Assessment Inventory Report (PAIR) – 2018 (Van Soest 2018). The radionuclide inventory is screened and PA-specific input parameters are derived in the Radionuclide Inventory Screening Analysis Report for the CRA-2019 (Kicker 2019). Tables D-1 through D-6 of Kicker (2019) summarize the inventory parameter updates.

1.1.2 Updates to Radionuclide Solubilities

The baseline actinide solubilities were recalculated for the CRA-2019 PA by Domski and Sisk-Scott (2019). Tables 6 and 7 of Domski and Sisk-Scott (2019) summarize their determination of baseline solubility values for An(III), An(IV), and An(V) (therein listed as Am(III), Th(IV), and Np(V)) in the Salado (GWB) and Castile (ERDA-6) simulated brine compositions. The “1x minimum” through “5x minimum” columns refer to the dilution factor used to determine the concentrations of organic ligands that were input to their calculations (see Table 3 of the reference, also Sisk-Scott 2019b and Brush and Domski 2013a). The reader is referred to the analysis report by Domski and Sisk-Scott (2019), AP 153 rev. 1 (Brush, Domski, and Xiong 2012), the analysis report by Domski (2019a), AP-183 rev. 1 (Sisk-Scott 2019a), the memo by Domski (2018), AP-182 (Jang 2019), and AP-154 rev. 2 (Xiong 2013) and the references therein for information regarding the changes to the baseline solubility values.

In addition, the actinide solubility uncertainty distributions for An(III) and An(IV) were determined by Domski (2019b) for the CRA-2019 PA. Tables 9 and 6 of Domski (2019b) list the cumulative distributions for the actinide solubility uncertainty exponents (SOLVAR) determined for the CRA-2019. The reader is referred to that reference, along with AP 153 rev. 1 (Brush, Domski, and Xiong 2012), for additional information regarding the causes of the changes.

1.1.3 Updates to Colloid Enhancement Parameters

The parameters related to actinide association with humic, microbial, and intrinsic colloids were updated for the CRA-2019 PA. The mineral colloid parameters and the brine redox state distribution remains the same as was used in the CRA-2014 PA.

The linear proportionality constant for actinide association with humic colloids (PHUMSIM and PHUMCIM (the “S” and “C” signify Salado and Castile brines)) were determined by Mariner (2019) for An(III) and An(IV). Table 1 of Mariner (2019) list the recalculated values. A notable change is that PHUMCIM is now a constant parameter for CRA-2019 (PHUMOX3:PHUMCIM was a sampled parameter in CRA-2014). No changes were made to the linear proportionality constants for An(V) or An(VI), and no changes were made to the association cap CAPHUM.

Both the linear proportionality constant and the association cap parameters (PROPMIC and CAPMIC) for actinide association with microbial colloids were updated as determined by Reed et al. (2019). Table 3-5 and the executive summary of Reed et al. (2019) list the provided values. In addition, the equation used to calculate the concentration limit for actinides associated with mobile microbial colloids was changed (Sarathi 2019a) in the PA code PANEL to be consistent with the revised CAPMIC unit basis. The CAPMIC values provided and used for both CRA-2014 and CRA-2019 were defined as the concentration of actinide associated with mobile microbial colloids (and were derived as a biomass-sorption limit), whereas in prior PA calculations the CAPMIC values represented a total mobile actinide concentration (and were derived as an extrapolated toxicity limit). The change in unit basis without a change in the corresponding equation caused an error in the CRA-2014 microbial colloid enhancement values. See Sarathi (2019a) for further details.

Reed et al. (2019) also provided updated parameter values for the intrinsic colloid concentrations (CONCINT) in Table 3-3 and the executive summary.

1.1.4 Updates to PA Models

The code PANEL was updated from version 4.04 to version 5.00. Pertinent changes include:

- Performing mass balance calculations over a group of “interconnected” waste panels rather than only a single waste panel. The change was motivated by the expected lack of panel closures between waste panels in the southern portion of the repository, which negates the prior assumption that each waste panel is isolated from the others. PANEL now accepts a “number of waste panels” as input. For CRA-2019, this value is set to five to represent all waste panels in the southern portion of the repository. See AP-181 Section 2.1.1 (Zeitler 2019) for additional information.
- Forcing the concentration limit of actinide associated with microbial colloids to plateau at the CAPMIC value (rather than decreasing to zero) if the calculated concentration limit is greater than CAPMIC. This change corrects for the altered unit basis of the parameter CAPMIC.
- Including the isotopes of Cf, Pm, and Pa listed in the inventory in the mobilization calculations.

- Additional details can be found in the updated PANEL Version 5.00 RD/VD/VVP (Sarathi 2019c) and DD/UM (Sarathi 2019b).

The code NUTS was updated from version 2.06 to version 2.07 to correct a minor bug involving selecting material maps when the time-shifting functionality is invoked (i.e. NUTS INTrusion runs). The impact on results was negligible. This is discussed further in Sarathi (2019d).

The NUTS input control files were modified to force NUTS to model precipitation/dissolution sequential to solving the transport/decay equation. This change makes the behavior more consistent with what was described in the CRA-2014 Appendix PA (PA-2014 Section 4.3) and is more robust. The previously-used “implicit” precipitation/dissolution model (NUTS UM, Treadway 1997) combined a penalty method with Picard iteration to attempt control mobile concentrations, but it lacked robust logic to evaluate that the solution had converged to the correct solution. In addition, to improve convergence, the frequency of BRAGFLO binary output times was increased, resulting in smaller NUTS transport time steps (NUTS takes one step for every BRAGLFO binary output time).

Changes to the BRAGFLO code and input control files are discussed in the Salado Flow Analysis Report (Day 2019). BRAGFLO brine flux results are used in the computation of the Salado transport results.

1.1.5 Listing of PA Parameters Related to Radionuclide Solubilities

Table 1 lists the solubility and colloid enhancement parameter values used in the CRA-2014 and CRA-2019 PA calculations, as retrieved from the WIPP PA Parameter Database (PA PDB).

Table 1 – Solubility and Colloid Parameter Values for the CRA-2014 and CRA-2019 PA Calculations

Material	Property	Description	Units	CRA14	CRA19
SOLMOD3	SOLCOH	Solubility in Castile Brine with Organics included Controlled by Mg(OH) ₂ /Hydromagnisite buffer(5424)	mol/L	1.48E-06	1.78E-07
SOLMOD3	SOLCOH2	Solubility in 2 X the minimum volume of Castile Brine with Organics included Controlled by Mg(OH) ₂ /Hydromagnisite buffer(5424)	mol/L	8.59E-07	1.63E-07
SOLMOD3	SOLCOH3	Solubility in 3 X the minimum volume of Castile Brine with Organics included Controlled by Mg(OH) ₂ /Hydromagnisite buffer(5424)	mol/L	5.99E-07	1.58E-07
SOLMOD3	SOLCOH4	Solubility in 4 X the minimum volume of Castile Brine with Organics included Controlled by Mg(OH) ₂ /Hydromagnisite buffer(5424)	mol/L	4.69E-07	1.54E-07

SOLMOD3	SOLCOH5	Solubility in 5 X the minimum volume of Castile Brine with Organics included Controlled by Mg(OH) ₂ /Hydromagnisite buffer(5424)	mol/L	3.92E-07	1.52E-07
SOLMOD3	SOLSOH	Solubiltiy in Salado Brine with Organics included Controlled by Mg(OH) ₂ /Hydromagnisite buffer(5424)	mol/L	2.59E-06	1.63E-07
SOLMOD3	SOLSOH2	Solubility in 2 X the minimum volume of Salado Brine with Organics included Controlled by Mg(OH) ₂ /Hydromagnisite buffer(5424)	mol/L	1.38E-06	1.58E-07
SOLMOD3	SOLSOH3	Solubility in 3 X the minimum volume of Salado Brine with Organics included Controlled by Mg(OH) ₂ /Hydromagnisite buffer(5424)	mol/L	9.74E-07	1.56E-07
SOLMOD3	SOLSOH4	Solubility in 4 X the minimum volume of Salado Brine with Organics included Controlled by Mg(OH) ₂ /Hydromagnisite buffer(5424)	mol/L	7.69E-07	1.55E-07
SOLMOD3	SOLSOH5	Solubility in 5 X the minimum volume of Salado Brine with Organics included Controlled by Mg(OH) ₂ /Hydromagnisite buffer(5424)	mol/L	6.47E-07	1.54E-07
SOLMOD3	SOLVAR	Solubility Multiplier	(-)	Min -3.55E+00 Med -8.74E-01 Max 2.97E+00	Min -1.14E+00 Med 3.45E-01 Max 2.97E+00
SOLMOD4	SOLCOH	Solubility in Castile Brine with Organics included Controlled by Mg(OH) ₂ /Hydromagnisite buffer(5424)	mol/L	7.02E-08	5.44E-08
SOLMOD4	SOLCOH2	Solubility in 2 X the minimum volume of Castile Brine with Organics included Controlled by Mg(OH) ₂ /Hydromagnisite buffer(5424)	mol/L	7.14E-08	5.44E-08
SOLMOD4	SOLCOH3	Solubility in 3 X the minimum volume of Castile Brine with Organics included Controlled by Mg(OH) ₂ /Hydromagnisite buffer(5424)	mol/L	7.17E-08	5.44E-08
SOLMOD4	SOLCOH4	Solubility in 4 X the minimum volume of Castile Brine with Organics included Controlled by Mg(OH) ₂ /Hydromagnisite buffer(5424)	mol/L	7.19E-08	5.44E-08
SOLMOD4	SOLCOH5	Solubility in 5 X the minimum volume of Castile Brine with Organics included Controlled by Mg(OH) ₂ /Hydromagnisite buffer(5424)	mol/L	7.20E-08	5.44E-08

SOLMOD4	SOLSOH	Solubility in Salado Brine with Organics included Controlled by Mg(OH) ₂ /Hydromagnisite buffer(5424)	mol/L	6.05E-08	5.45E-08
SOLMOD4	SOLSOH2	Solubility in 2 X the minimum volume of Salado Brine with Organics included Controlled by Mg(OH) ₂ /Hydromagnisite buffer(5424)	mol/L	6.06E-08	5.45E-08
SOLMOD4	SOLSOH3	Solubility in 3 X the minimum volume of Salado Brine with Organics included Controlled by Mg(OH) ₂ /Hydromagnisite buffer(5424)	mol/L	6.07E-08	5.45E-08
SOLMOD4	SOLSOH4	Solubility in 4 X the minimum volume of Salado Brine with Organics included Controlled by Mg(OH) ₂ /Hydromagnisite buffer(5424)	mol/L	6.07E-08	5.45E-08
SOLMOD4	SOLSOH5	Solubility in 5 X the minimum volume of Salado Brine with Organics included Controlled by Mg(OH) ₂ /Hydromagnisite buffer(5424)	mol/L	6.07E-08	5.45E-08
SOLMOD4	SOLVAR	Solubility Multiplier	(-)	Min -1.52E+00 Med 1.03E+00 Max 3.19E+00	Min -2.01E+00 Med -9.96E-02 Max 1.43E+00
SOLMOD5	SOLCOH	Solubility in Castile Brine with Organics included Controlled by Mg(OH) ₂ /Hydromagnisite buffer(5424)	mol/L	8.76E-07	1.20E-06
SOLMOD5	SOLCOH2	Solubility in 2 X the minimum volume of Castile Brine with Organics included Controlled by Mg(OH) ₂ /Hydromagnisite buffer(5424)	mol/L	7.39E-07	7.27E-07
SOLMOD5	SOLCOH3	Solubility in 3 X the minimum volume of Castile Brine with Organics included Controlled by Mg(OH) ₂ /Hydromagnisite buffer(5424)	mol/L	6.86E-07	5.52E-07
SOLMOD5	SOLCOH4	Solubility in 4 X the minimum volume of Castile Brine with Organics included Controlled by Mg(OH) ₂ /Hydromagnisite buffer(5424)	mol/L	6.60E-07	4.61E-07
SOLMOD5	SOLCOH5	Solubility in 5 X the minimum volume of Castile Brine with Organics included Controlled by Mg(OH) ₂ /Hydromagnisite buffer(5424)	mol/L	6.44E-07	4.05E-07
SOLMOD5	SOLSOH	Solubility in Salado Brine with Organics included Controlled by Mg(OH) ₂ /Hydromagnisite buffer(5424)	mol/L	2.77E-07	4.02E-07

SOLMOD5	SOLSOH2	Solubility in 2 X the minimum volume of Salado Brine with Organics included Controlled by Mg(OH) ₂ /Hydromagnisite buffer(5424)	mol/L	2.18E-07	2.83E-07
SOLMOD5	SOLSOH3	Solubility in 3 X the minimum volume of Salado Brine with Organics included Controlled by Mg(OH) ₂ /Hydromagnisite buffer(5424)	mol/L	1.98E-07	2.42E-07
SOLMOD5	SOLSOH4	Solubility in 4 X the minimum volume of Salado Brine with Organics included Controlled by Mg(OH) ₂ /Hydromagnisite buffer(5424)	mol/L	1.88E-07	2.21E-07
SOLMOD5	SOLSOH5	Solubility in 5 X the minimum volume of Salado Brine with Organics included Controlled by Mg(OH) ₂ /Hydromagnisite buffer(5424)	mol/L	1.82E-07	2.09E-07
SOLMOD6	SOLCOH	Solubility in Castile Brine with Organics included Controlled by Mg(OH) ₂ /Hydromagnisite buffer(5424)	mol/L	1.00E-03	1.00E-03
SOLMOD6	SOLSOH	Solubiltiy in Salado Brine with Organics included Controlled by Mg(OH) ₂ /Hydromagnisite buffer(5424)	mol/L	1.00E-03	1.00E-03
PHUMOX3	PHUMCIM	Proportionality Const.,Humic Colloids, Castile Brine, MgO controls pH	(-)	1.37E+00	2.00E-01
PHUMOX3	PHUMSIM	Proportionality Const. of Actinides in Salado Brine w/Humic Colloids, Inorganic	(-)	1.90E-01	2.00E-01
PHUMOX4	PHUMCIM	Proportionality Const.,Humic Colloids, Castile Brine, MgO controls pH	(-)	6.30E+00	1.00E-02
PHUMOX4	PHUMSIM	Proportionality Const. of Actinides in Salado Brine w/Humic Colloids, Inorganic	(-)	6.30E+00	1.00E-02
PHUMOX5	PHUMCIM	Proportionality Const.,Humic Colloids, Castile Brine, MgO controls pH	(-)	7.40E-03	7.40E-03
PHUMOX5	PHUMSIM	Proportionality Const. of Actinides in Salado Brine w/Humic Colloids, Inorganic	(-)	9.10E-04	9.10E-04
PHUMOX6	PHUMCIM	Proportionality Const.,Humic Colloids, Castile Brine, MgO controls pH	(-)	5.10E-01	5.10E-01
PHUMOX6	PHUMSIM	Proportionality Const. of Actinides in Salado Brine w/Humic Colloids, Inorganic	(-)	1.20E-01	1.20E-01
AM	CAPHUM	Maximum Concentration of Actinide with Mobile Humic Colloids	mol/L	1.10E-05	1.10E-05
AM	CAPMIC	Maximum Concentration of Actinide on Microbe Colloids	mol/L	3.10E-08	2.30E-09
AM	CONCINT	Actinide Concentration with Mobile Actinide Intrinsic Colloids	mol/L	4.00E-09	9.50E-09
AM	CONCMIN	Actinide Concentration with Mobile Mineral Fragment Colloids	mol/L	2.60E-08	2.60E-08

AM	PROPMIC	Moles of Actinide Mobilized on Microbe Colloids per Moles Dissolved	(-)	3.20E-01	3.00E-02
NP	CAPHUM	Maximum Concentration of Actinide with Mobile Humic Colloids	mol/L	1.10E-05	1.10E-05
NP	CAPMIC	Maximum Concentration of Actinide on Microbe Colloids	mol/L	2.30E-06	3.80E-08
NP	CONCINT	Actinide Concentration with Mobile Actinide Intrinsic Colloids	mol/L	2.00E-08	4.30E-08
NP	CONCMIN	Actinide Concentration with Mobile Mineral Fragment Colloids	mol/L	2.60E-08	2.60E-08
NP	PROPMIC	Moles of Actinide Mobilized on Microbe Colloids per Moles Dissolved	(-)	1.76E+00	2.10E-01
TH	CAPHUM	Maximum Concentration of Actinide with Mobile Humic Colloids	mol/L	1.10E-05	1.10E-05
TH	CAPMIC	Maximum Concentration of Actinide on Microbe Colloids	mol/L	2.30E-06	3.80E-08
TH	CONCINT	Actinide Concentration with Mobile Actinide Intrinsic Colloids	mol/L	2.00E-08	4.30E-08
TH	CONCMIN	Actinide Concentration with Mobile Mineral Fragment Colloids	mol/L	2.60E-08	2.60E-08
TH	PROPMIC	Moles of Actinide Mobilized on Microbe Colloids per Moles Dissolved	(-)	1.76E+00	2.10E-01
U	CAPHUM	Maximum Concentration of Actinide with Mobile Humic Colloids	mol/L	1.10E-05	1.10E-05
U	CAPMIC	Maximum Concentration of Actinide on Microbe Colloids	mol/L	2.30E-06	3.80E-08
U	CONCINT	Actinide Concentration with Mobile Actinide Intrinsic Colloids	mol/L	3.00E-08	1.40E-06
U	CONCMIN	Actinide Concentration with Mobile Mineral Fragment Colloids	mol/L	2.60E-08	2.60E-08
U	PROPMIC	Moles of Actinide Mobilized on Microbe Colloids per Moles Dissolved	(-)	1.76E+00	2.10E-01
PU	CONCINT	Actinide Concentration with Mobile Actinide Intrinsic Colloids	mol/L	2.00E-08	4.30E-08
PU	CONCMIN	Actinide Concentration with Mobile Mineral Fragment Colloids	mol/L	2.60E-08	2.60E-08
PU	PROPMIC	Moles of Actinide Mobilized on Microbe Colloids per Moles Dissolved	(-)	1.76E+00	2.10E-01

1.2 Objectives

The purpose of this report is to analyze and discuss results from the actinide mobilization and Salado transport sub-models employed in the CRA-2019 Performance Assessment (PA). The results are compared to those from the CRA-2014 PA (specifically the Rev. 2 results from the Solaris migration integration tests, Kirchner et al. 2014, Kirchner et al. 2015, Zeitler 2019) to illustrate the impacts of the parameter and model changes since the CRA-2014. The objective is to provide insight as to the causes behind the changes in the Complementary Cumulative Distribution Function (CCDF) curves (presented in Brunell 2019) which are used to assess if the long-term performance of WIPP meets the containment requirements set forth in Title 40 CFR Part 191 and Part 194. Because the report is focused on PA changes and results, background discussion is limited and the reader is frequently referred to the proper references for details.

Section 1.1 gives an overview of parameter and model changes since the CRA-2014 that are relevant to the actinide mobilization and Salado transport results. Section 2.0 gives a brief description of the models and their implementation in the WIPP PA. Section 3.0 gives a brief description of the computational workflow. And Section 4.0 illustrates and discusses the key inputs and results.

For reference, the predecessors of this report include Garner (2003), Garner and Leigh (2005), Garner (2010), and Kim (2013a) for the actinide mobilization sub-model, and Lowry (2003), Lowry (2005), Ismail and Garner (2008), and Kim (2013b) for the Salado transport sub-model.

2.0 CONCEPTUAL APPROACH FOR THE CRA-2019

2.1 Actinide Mobilization: PANEL

In WIPP PA calculations, the code PANEL is used to simulate the radionuclide inventory in the repository waste panels over the 10,000-year regulatory period as it decays and as it is mobilized in brine. Specifically it performs three predominant functions:

1. PANEL computes the total mobile concentration limit (a.k.a. total mobilization potential, source term) for each radionuclide of interest. The total mobile concentration limit is a constant, effective aqueous solubility limit that encompasses the dissolved (speciated and complexed with organic ligands) plus dispersed (i.e. associated with dispersed colloids) concentration limits. The total mobile concentration limits are constant throughout the course of a simulation for a given model realization (MASS-2014 Pg. 18, *Chemical conditions in the repository will be constant. Chemical equilibrium is assumed...*), but vary between model realizations due to the solubility uncertainty factor, brine redox condition, and brine source. These total mobile concentration limit values are used by both PANEL and NUTS (the Salado transport code) to calculate instantaneous aqueous radionuclide concentrations as a function of time (and, for NUTS, space).
2. PANEL calculates the instantaneous aqueous radionuclide concentrations as a function of time in the waste panels. This involves performing a mass balance of the inventory in the waste panels, calculating the amount of radioactive decay and ingrowth, and performing a simple saturation-type calculation that sets the mobile concentration to the lesser value of the total mobile concentration limit and the available inventory (at the specific time) divided by the volume of brine in the waste panels (MASS-2014 Pg. 19: *Radionuclide dissolution to solubility limits is instantaneous*; Pg. 20: *An concentration in the repository will be inventory limited when the mass of an An becomes depleted such that the predicted concentrations cannot be achieved*). For the concentration calculations intended for DBR releases, PANEL assumes that the brine volume in the waste panels is constant over time (and that the panel behaves as a closed system – no mass leaves). PA consequently runs PANEL multiplicatively with a set of brine volumes. These brine volumes, which are defined as multiples of the minimum volume of brine required for a DBR to occur (Clayton 2008), also correspond to the organic ligand concentration dilution factors (PA-2014 Section 1.1.9 and 6.7.3; also Brush and Domski 2013a, Sisk-Scott 2019b) that were used in the calculation of the baseline solubility parameters (the baseline solubility parameters are named according to the brine dilution factor). The reasoning behind the multiple brine volumes is to better correlate panel brine volume with radionuclide concentrations (in particular because organic ligands can substantially enhance actinide solubility, but PA assumes fixed organic ligand concentrations rather than computing them dynamically via mass balance; this can inflate the actinide solubilities when panel brine volumes are large) (PA-2014 Section 1.1.9). The code CCDFGF linearly interpolates between the different PANEL brine volume runs to estimate the appropriate radionuclide concentration (at a given time, for a given BRAGFLO-DBR panel volume) when computing DBR releases (PA-2014 Section 6.8.2.3, CCDFGF UM Section 5.4).

- PANEL calculates the long-term discharge of contaminated brine from the repository through the borehole and shaft to the Culebra in the E2E1 scenario (scenario 6). The calculations are similar as previously described, but instead the panel brine volume varies with time as and the radionuclide inventory decreases with time due to (nonzero) discharge of contaminated brine.

PANEL models the decay and ingrowth of 30 radionuclides

^{241}Am	^{237}Np	^{244}Pu	^{234}U
^{243}Am	^{231}Pa	^{226}Ra	^{235}U
^{252}Cf	^{210}Pb	^{228}Ra	^{236}U
^{243}Cm	^{147}Pm	^{147}Sm	^{238}U
^{244}Cm	^{238}Pu	^{90}Sr	
^{245}Cm	^{239}Pu	^{229}Th	
^{248}Cm	^{240}Pu	^{230}Th	
^{137}Cs	^{241}Pu	^{232}Th	
	^{242}Pu	^{233}U	

subject to the abridged decay chains:

Table 2 – Abridged decay chains modeled in PANEL

		^{238}Pu											
		↓											
^{242}Pu	→	^{238}U	→	^{234}U	→	^{230}Th	→	^{226}Ra	→	^{210}Pb	→		
		^{243}Cm											
		↓											
^{243}Am	→	^{239}Pu	→	^{235}U	→	^{231}Pa	→						
				^{244}Cm									
				↓									
^{252}Cf	→	^{248}Cm	→	^{244}Pu	→	^{240}Pu	→	^{236}U	→	^{232}Th	→	^{228}Ra	→
^{245}Cm	→	^{241}Pu	→	^{241}Am	→	^{237}Np	→	^{233}U	→	^{229}Th	→		
^{147}Pm	→	^{147}Sm	→										
^{137}Cs	→												
^{90}Sr	→												

*The last radioisotope in a chain decays to a stable isotope that is not tracked in PANEL.

The first four chains in Table 2 follow (or are collinear to) the Uranium Series, the Actinium Series, the Thorium Series, and the Neptunium Series (KAPL 2002, Sarathi 2019b Appendix-A).

The abridged chains were originally formulated to include radionuclides called out in 40 CFR §191 Appendix A (i.e. radionuclides with half-lives longer than 20 years) and deemed potentially significant to releases based on criteria set forth in the CCA Appendix-WCA (especially Pg. 23). Certain radionuclides with half-lives longer than 20 years were historically screened out based on small initial inventory and small potential for ingrowth during the 10,000 year regulatory period (CCA Appendix WCA, Kicker and Zeitler 2013, Kicker 2019). Certain radionuclides with half-lives shorter than 20 years, but with significant inventories and which decay to radionuclides with half-lives longer than 20 years are included (e.g. ²⁴¹Pu).

In the abridged chains, intermediate radionuclides with short half-lives (i.e. less than 2 years) are excluded (PANEL assumes the parent decays directly to the next long-lived radionuclide), and stable isotopes are not tracked. Furthermore the Uranium Series chain omits ²⁵⁰Cf, ²⁴⁶Cm, and ²⁵⁰Cm; the Actinium Series chain omits ²⁵¹Cf, ²⁴⁷Cm, ²⁴⁷Bk, and ²²⁷Ac; the Thorium Series chain omits ²³⁶Pu and ²³²U (²³⁶Np is not listed in the inventory); and the Neptunium Series chain omits ²⁴⁹Cf, radionuclides with half-lives greater than 20 years (Sarathi 2019b Appendix-A).

While PANEL performs the decay and mass balance calculations on the full set of 30 individual radionuclides, it reports concentrations/discharges in terms of 5 “lumped” radionuclides that represent 10 of the 30 (Table 3). A more detailed discussion of the selection and lumping methodology is given in Garner and Leigh (2005) and has been unchanged since (Kicker and Zeitler 2013, Kicker 2019). PANEL performs this lumping procedure internally and at each time step.

Table 3 – Lumped and Represented Radionuclides

Surrogate, “Lumped” Radionuclide	Constituent Radionuclides
AM241L	²⁴¹ Am + ²⁴¹ Pu
PU239L	²³⁹ Pu + ²⁴⁰ Pu + ²⁴² Pu
PU238L	²³⁸ Pu
U234L	²³⁴ U + ²³³ U
TH230L	²³⁰ Th + ²²⁹ Th

PANEL calculates the total mobile concentration limits as the sum of the “dissolved” solubility limit and the concentration limits for association with four types of colloids – mineral-fragment, intrinsic, humic, and microbial (SOTERM-2014, MASS-2014). These terms are calculated from the database parameters (indicated as MATERIAL:PROPERTY) as follows

$$S_{baseline} = SOLMOD\{valency\}:SOL\{S|C\}OH\{dilution\ factor\}$$

$$S_{dissolved} = S_{baseline} \cdot 10^{SOLMOD\{valency\}:SOLVAR}$$

$$S_{mineral} = \{actinide\}:CONCMIN$$

$$S_{intrinsic} = \{actinide\}:CONCINT$$

$$S_{humic} = \min(S_{dissolved} \cdot PHUMOX\{valency\}:PHUM\{S|C\}IM, \quad \{actinide\}:CAPHUM)$$

$$S_{microbial} = \min(S_{dissolved} \cdot \{actinide\}:PROPMIC, \quad \{actinide\}:CAPMIC)$$

$$S_{total} = S_{dissolved} + S_{mineral} + S_{intrinsic} + S_{humic} + S_{microbial}$$

The terms inside the braces are substituted with the actinide, valence state, or brine type of interest. The mineral-fragment and intrinsic colloid-associated concentration limits are constant while the humic and microbial colloid-associated concentration limits are linearly proportional to the dissolved concentration limit (but subject to a cap).

Additional assumptions related to the actinide mobilization sub-model/PANEL are enumerated in MASS-2014, Pg. 18-21, and additional background about the actinide mobilization assumptions can be found in SOTERM-2014. Practical discussion of PANEL's functionality, input parameters, and calculation methods for concentration limit, decay, and mass balance is given in the PANEL DD/UM (Sarathi 2019b).

2.2 Salado Transport: NUTS and PANEL

In WIPP PA calculations, the code NUTS is used to simulate radionuclide transport due to advection in the aqueous phase in the Salado formation. It is used to track radionuclides exiting the repository, specifically through the anhydrite marker beds, shafts, and a future intrusion borehole, as a function of time over the 10,000 year regulatory period. The cumulative radionuclide discharges through the (conceptually-combined) shaft and borehole are assumed to flow into the overlying Culebra member of the Rustler formation. These cumulative radionuclide discharge versus time results are used by CCDFGF (but with the mineral-, intrinsic-, and microbial-colloid-bound actinides removed, MASS-2014 Pg 25-26) to calculate reported *from the Culebra* releases to the land withdrawal boundary (LWB).

NUTS (used for scenarios 1-5, the undisturbed, E1 intrusion, and E2 intrusion scenarios) uses the same two-dimensional grid as BRAGFLO, and relies on BRAGFLO (PA-2014 Sections 4.2, 6.7.1) results for the brine flux (i.e. volumetric flow rate) fields and other fluid and rock properties. It models only contaminant advection in the aqueous phase, dissolution/precipitation (controlled by the total mobile concentration limit values), and radioactive decay. Cumulative discharges are tabulated at the intersection of the borehole and the bottom of the Culebra formation. PANEL (used for scenario 6, the E2E1 intrusion scenario) simply performs a mass balance calculation over a fixed number of waste panels (one for CRA-2014, five for CRA-2019), and similarly relies on BRAGFLO results for brine volume and brine discharge inputs. The reader is referred to the NUTS User's Manual (Shinta 1997), the PANEL DD/UM (Sarathi 2019b), and PA-2014 Sections 4.3, 4.4, 6.7.2, and 6.7.3 for additional background. PA-2014 Sections 4.8, 4.9, 6.7.7, and 6.7.8 and Kuhlman (2010) discuss the related Culebra transport sub-model.

NUTS, as a simplification and for computational economy, performs decay and mass balance calculations using only the five lumped radionuclides (the inventory lumping used as input to NUTS is discussed in Garner and Leigh (2005), Kicker and Zeitler (2013), and Kicker (2019)). This is in contrast to PANEL, which performs the decay and mass balance calculations on the full set of 30 individual radionuclides and lumps and reports the lumped values at each timestep. NUTS models three reduced decay chains (Table 4) assuming that the lumped isotopes assume the atomic properties of the named isotope.

Table 4 – Decay Chains Modeled in NUTS Code

AM241L	→
--------	---

PU238L	→	U234L	→	TH230L	→
--------	---	-------	---	--------	---

PU239L	→
--------	---

*The last radioisotope in a chain decays to a stable isotope that is not tracked in NUTS.

3.0 METHODOLOGY

The overall methodology for the PA calculations remains consistent with the methodology used in the CRA-2014. Additional background is given in PA-2014 Section 6, especially 6.7. Code executable versions, execution sequences and loops, and file names and locations for the CRA-2019 PA are given in Long (2019).

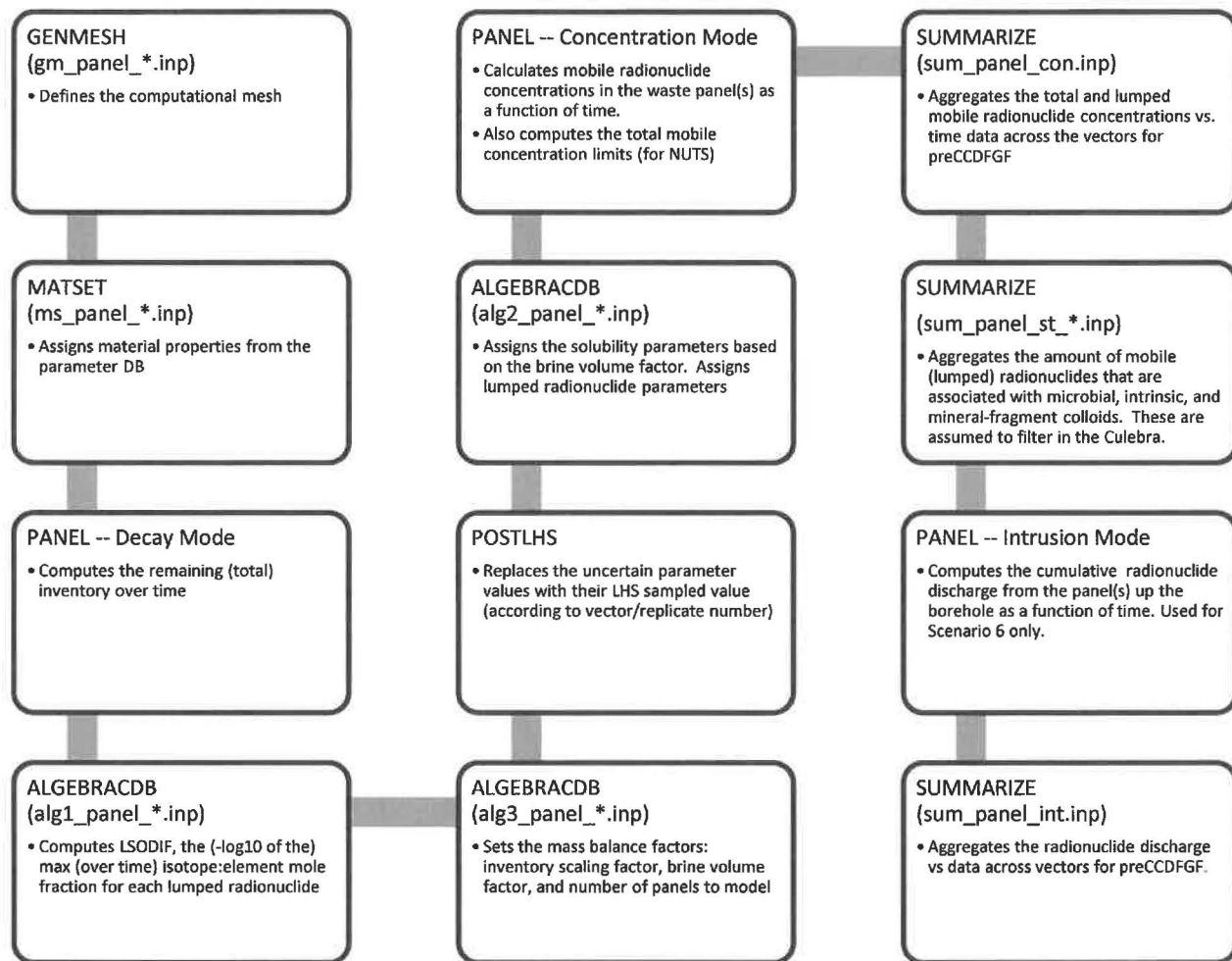


Figure 1 – Data and computational flow for PANEL calculations

Figure 1 gives an overview of the code execution process for the PANEL computations and illustrates (logically) the sequence used to assign fixed and sampled parameters (via the codes MATSET and POSTLHS), perform intermediate pre- and post- processing of PANEL input/output data, and ultimately generate tabular output data (across the different vectors, via the code SUMMARIZE) that is passed to (pre-)CCFGF for the construction of the futures. PANEL is run in three different roles. The first role, Decay Mode, is solely to fulfill the need to estimate the maximum (over time) isotope-to-element mole fraction value for each radionuclide.

These maximum isotope-to-element mole fraction values are used to compute a fixed isotope-to-element mole fraction for the lumped radionuclides (LSOLDIF is the $-\log_{10}$ of these values). This factor is used to scale the elemental mobile concentration limit values to apply to the isotopes that represent the lumped isotope species (see the PANEL DD/UM, Sarathi 2019b, for additional information). The second role, Concentration Mode, is to calculate the total mobile concentration limits and the instantaneous mobile concentrations of the radionuclides as a function of time. The total mobile concentration limits are used by the code NUTS (and by PANEL internally), and the (SUMMARIZED) instantaneous mobile concentrations are used by CCDFGF to compute DBR releases. The third role, Intrusion Mode, is to calculate the long-term radionuclide discharge from the waste panels in the E2E1 scenario (scenario 6; NUTS performs these computations for scenarios 1-5). These (SUMMARIZED) *to the Culebra* discharges are used by CCDFGF to compute *from Culebra* releases.

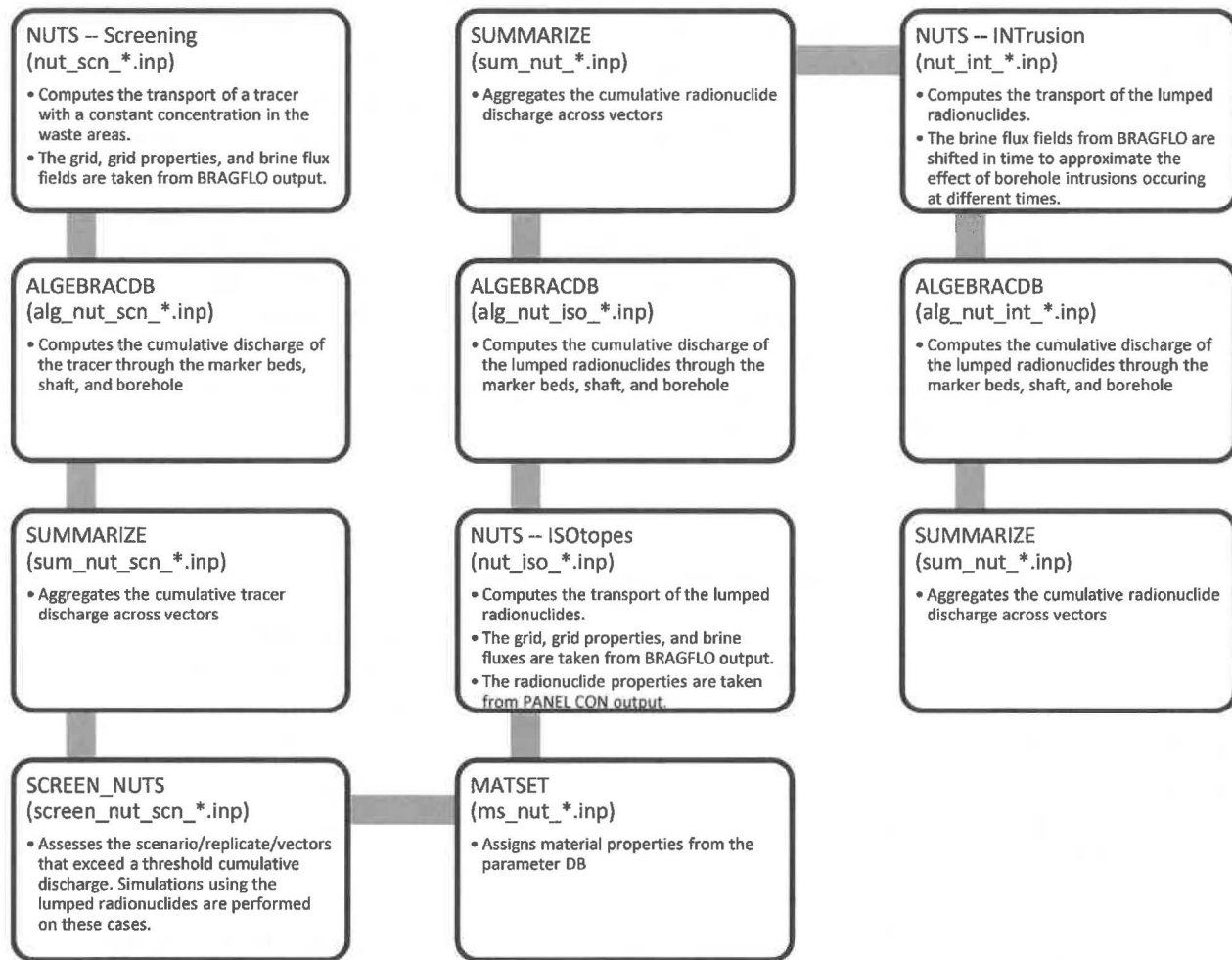


Figure 2 – Data and computational flow for NUTS calculations

Figure 2 gives a similar overview of the code execution process for NUTS computations. NUTS relies on BRAGFLO simulation output for the grid, grid-based (static and dynamic) material

properties, and the time-varying brine flux field data. It relies on PANEL simulation output for the radionuclide solubility properties. This is why it lacks initial GENMESH and POSTLHS executions (the intermediate MATSET step only sets reference constants, atomic properties, and the inventory Waste Unit Factor). PA performs three types of NUTS simulations. The purpose of the first type, the screening simulations, is to assess which vectors have the potential for radionuclides to enter the Culebra via the borehole and shaft or cross the LWB through the anhydrite marker beds. The waste areas are modeled as maintaining a constant nonreactive tracer concentration of 1 kg/m³ (i.e. those grid cells are assigned Dirichlet concentration boundary conditions), and those vectors where the cumulative tracer discharge through any of the borehole, shaft, or anhydrite marker beds exceeds a cutoff of 1.0e-7 kg are screened in (Lowery 2003). The screening is performed per-scenario, but any vector that is screened in for scenarios 2-5 is also screened in for scenario 1. The purpose of the second type, the ISOtope simulations, is to model transport of the lumped radionuclides for scenarios 1-5, for those vectors that have been previously screened-in. The purpose of the third type, the INTrusion simulations, is also to model transport of the lumped radionuclides, but to simulate borehole intrusions occurring at times other than those simulated by BRAGFLO (Table 5, adapted from PA-2014 Sections 6.7.1-6.7.3). This is done for the benefit of CCDFGF, which constructs futures with drilling intrusions occurring at random times between year 100 and 10,000, to better capture the effects of the inventory changing with time due to decay/ingrowth (i.e. later intrusions will release a different composition than earlier intrusions). NUTS and PANEL approximate the effect of different intrusion times by shifting the supplied BRAGFLO simulation results (for the corresponding intrusion) forward or backward in time relative to the approximated intrusion time. The time shifting functionality is described further in the NUTS User’s Manual (Shinta 1997) and the PANEL DD/UM (Sarathi 2019), and the motivation is discussed further in Lowry (2003) and Garner (2003). Ultimately, the (SUMMARIZED) NUTS ISO and NUTS INT (and PANEL INT) simulation results for long term radionuclide discharge *to the* Culebra are used by CCDFGF to compute *from Culebra* releases.

Table 5 – Scenario descriptions and borehole intrusion time by simulation

Scenario	BRAGFLO Intrusion Time (years post-closure)	NUTS/PANEL Intrusion Time (years post-closure)
S1-BF (undisturbed scenario)	N/A	N/A
S2-BF (single E1 intrusion that penetrates the Castile brine reservoir)	350	NUTS ISO: 350 NUTS INT: 100
S3-BF (single E1 intrusion that penetrates the Castile brine reservoir)	1000	NUTS ISO: 1000 NUTS INT: 3000, 5000, 7000, 9000
S4-BF (single E2 intrusion that penetrates no deeper than the repository)	350	NUTS ISO: 350 NUTS INT: 100

<p>S5-BF (single E2 intrusion that penetrates no deeper than the repository)</p>	<p>1000</p>	<p>NUTS ISO: 1000 NUTS INT: 3000, 5000, 7000, 9000</p>
<p>S6-BF (two intrusions separated in time – first an E2, later an E1)</p>	<p>E2 at year-1000, then E1 at year-2000</p>	<p>PANEL INT : Second (E1) intrusion at 100, 350, 1000, 2000, 4000, 6000, 9000</p>

4.0 RESULTS

The discussion of the results is broken into sections, and each section builds on the inputs to and results from the previous section. First, the radionuclide inventory (Kicker 2019, van Soest 2018) used in the CRA-2019 is briefly reviewed to provide context for the radionuclide concentrations and release results. Second, the key inputs to and results from the total mobile concentration limit (total mobilization potential) calculations are presented. Third, the instantaneous radionuclide concentrations simulation results are presented. And finally, the transport results are presented. A limited discussion of the related sub-models is also included. This report and the included results focus on the epistemic uncertainty (as addressed by sampling parameters with LHS and running multiple simulations), though results are typically presented for multiple scenarios (which form the inputs for the aleatory uncertainty simulations constructed by the code CCDFGF). The CCDF results, which couple the aleatory and epistemic uncertainties, are not discussed – the reader is referred to Brunell (2019) for the final CCDF curves.

The following sections contain numerous box plots to facilitate visualizing and comparing distributions of results. The convention used in this report is that the “box” bottom and top edges indicate the 25th and 75th percentiles, the box interior line indicates the 50th percentile (median), and the green triangle marker indicates the mean. The “whiskers” (the extended vertical lines with horizontal bars) indicate the 2nd and 98th percentiles, and the diamond markers exterior to the bars are discrete outliers (i.e. less than the 2nd percentile or greater than the 98th percentile). Upon occasion, a particular dependent variable is constant (its independent parameters may not be sampled), and the box is collapsed to a single horizontal bar. At the other extreme, some dependent variables may have distributions where the mean is dominated by a few outliers. In those plots, only the top whisker and the outliers are visible – the box would be located below the range of the figure.

4.1 Inventory

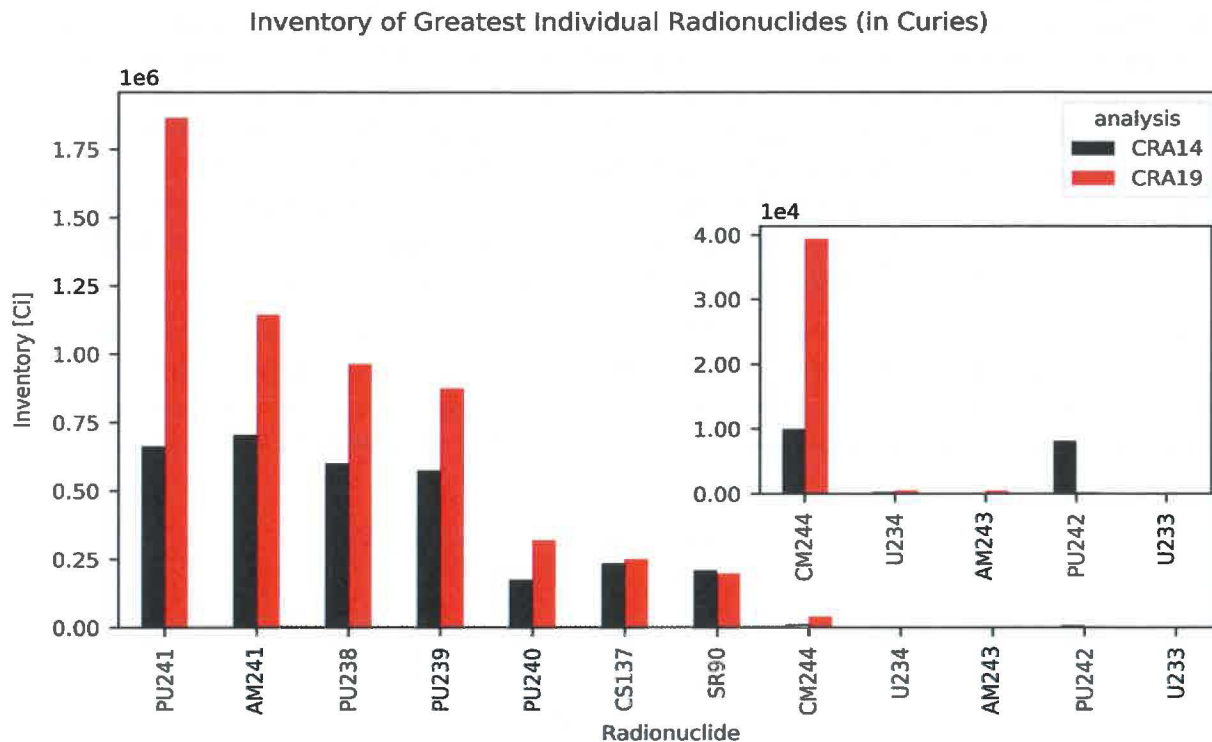


Figure 3– Inventory of Greatest Individual Radionuclides (in Curies)

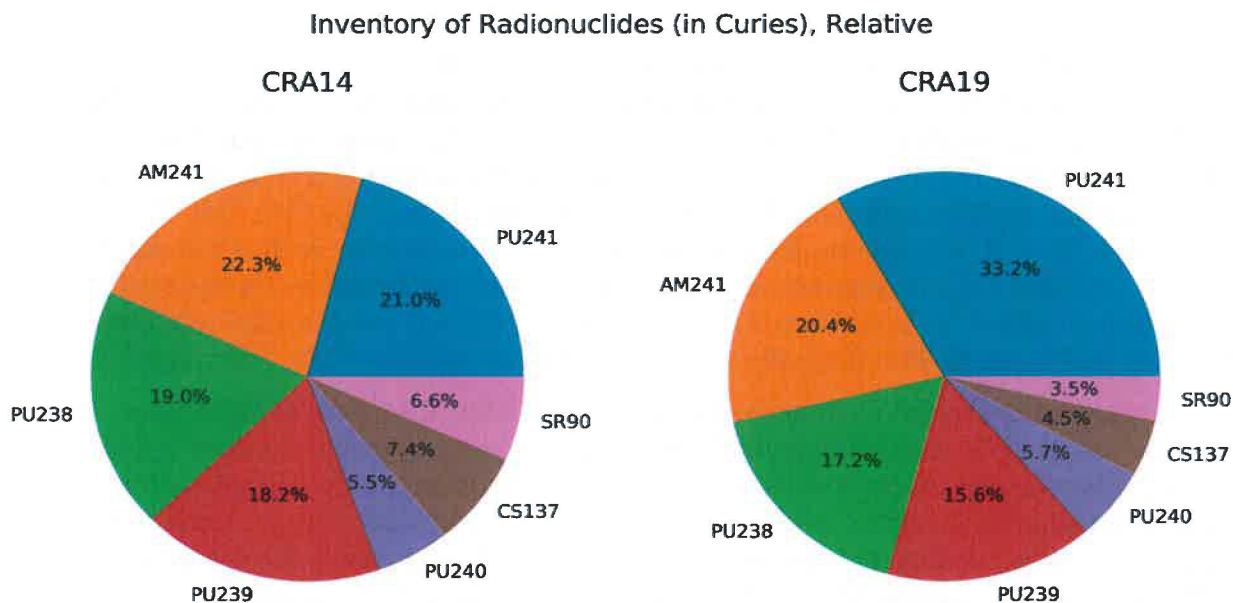


Figure 4– Inventory of Radionuclides (in Curies), Relative

Figure 3 and Figure 4 illustrate the largest contributors (on a Curie basis) to the initial radionuclide inventory (see Kicker 2019, WIPP PA PDB for the input values). ^{241}Pu , which has a half-life of 14.3 years (which is less than the 20-year threshold for it to be assigned an EPA release limit) and decays to ^{241}Am , has increased substantially for CRA-2019. This effectively increases the amount of available ^{241}Am , which is significant because ^{241}Am has a low release limit (100 Ci/WUF; 40 CFR §191 Appendix C Table 1, WIPP PA PDB (parameter EPAREL)), but ^{241}Pu has none and thus does not increase the Waste Unit Factor (parameter BOREHOLE:WUF). ^{238}Pu inventory has also increased and will act as an increased source for ^{234}U . ^{241}Am , ^{239}Pu , and ^{240}Pu have also increased – these contribute to an increase in the WUF from 2.06 for CRA-2014 to 3.30 for CRA-2019 (calculated in Kicker 2019).

The WUF (the Unit of Waste in 40 CFR §191 Appendix C, Note 1, Item e), defined as “an amount of transuranic (TRU) wastes containing one million curies of alpha-emitting transuranic radionuclides with half-lives greater than 20 years” acts as an (initial-inventory-dependent) normalization factor when scaling Curies to “EPA units.” For reference, the WUF is calculated as

$$WUF = \frac{\sum_{iso \in \{TRU \cap \alpha\text{-emitter} \cap t_{1/2} > 20yr\}} A_{iso}}{10^6 Ci}$$

where A is the inventory in Ci. The unit conversion factor from Ci to EPA release units then is:

$$\frac{EPA \text{ unit}}{Ci} = \frac{1}{EPAREL \cdot WUF}$$

note that this unit conversion factor is isotope-specific because the EPAREL value is isotope-specific.

The larger WUF in CRA-2019 indicates that a larger number of Curies are embodied by an EPA unit.

The PANEL and NUTS inventory screening analyses for the CRA-2019 PA and CRA-2014 PA (Kicker 2019, Kicker and Zeitler 2014, predated by CCA Appendix-WCA, Fox 2003, Leigh and Fox 2005, Fox et al. 2009) exclude a number of radionuclides that comprise a small percentage of the total inventory (<1-2% combined) but exceed the initial screening criteria of 0.001 EPA units set forth in the CCA Appendix-WCA (Pg. 23), notably ^{246}Cm , ^{232}U , ^{63}Ni , ^{59}Ni , ^{249}Cf , ^{227}Ac , ^{242m}Am , and ^{99}Tc (^{14}C was historically screened out due to reasons given in the CCA Appendix-WCA Pg. 26: “Any C-14 transported out of the repository will be diluted by the large excess of nonradioactive carbon.”). In addition, PANEL (Garner 1998), sets the elemental solubility limits for Ra, Pb, and Sm to 1e-99 (effectively zero), which further excludes ^{226}Ra , ^{228}Ra , and ^{210}Pb .

While screening based on an absolute minimum cutoff of 0.001 EPA units allows unaccounted release potentials to be bounded (provided that the number of unaccounted isotopes is limited), screening based on percentage of overall inventory (in EPA units) is only appropriate for bounding potential unaccounted solids releases. This is because solids releases are assumed to, in aggregate (across random release events), have a composition similar to the overall inventory in EPA units, thus accounting for >99.9% of the inventory translates to accounting for >99.9% of potential solids releases. However, this is not true for brine releases (DBRs and long-term transport). Radionuclides are assumed to dissolve according to mole-unit-based solubility limits and mole-based isotope-to-element mole fractions. Furthermore, different isotopes have vastly different molar radioactivities (i.e. Ci/mol or EPA-units/mol). Taken together, this means that the EPA-unit composition of contaminated brine will be very different from that of the overall total

inventory, and that radionuclides that comprise a small portion of the total inventory may comprise a large portion of the radioactivity in contaminated brine. This does not appear to be explicitly addressed in the references prior to 2019; radionuclides were historically screened based on absolute or relative amount in/of the total inventory in EPA-units (and parent/daughter relationships). The CCA Appendix-WCA obliquely mentions this phenomena, but in the context of including additional isotopes of the same element in order to adequately represent the isotope-to-element mole fractions (CCA Appendix-WCA Pg. 22).

For DBR releases, a simple calculation can be made to bound the unaccounted for potential releases. At year 100 the unaccounted for (CRA-2019) inventory is ~2.8 EPA units. Assuming this dissolves in 1x the minimum volume of brine necessary for a DBR to occur (parameter GLOBAL:DBRMINBV, Clayton 2008), 17400 m³, and the maximum DBR volume is 200 m³ (from 40 CFR §191 Appendix C, *Frequency and Severity of Inadvertent Human Intrusion into Geologic Repositories*; the maximums simulated are ~100 m³), the unaccounted for potential DBR release is ~0.03 EPA units (per DBR occurrence). This is below the lower release limit of < 0.1 probability of 1 EPA unit, thus it is unlikely that the unaccounted for DBR releases alone will lead to a failure to demonstrate compliance with the containment requirements.

Unfortunately, such a bounding calculation is not so straightforward or conclusive for transport releases. One could presume that for substantial long-term brine discharge to the Culebra to occur, the repository will be flooded, and (using the same consolidated room volumes as in Clayton 2008) assume that the radionuclides are dissolved in 63,000 m³ of brine. Neglecting dilution by continual mixing with source brine and inventory segmentation by panel closures (in addition to decay and transport through the Culebra, which will act differently on different radionuclides), one could compare the cumulative brine discharges (calculated by BRAGFLO) to this volume. The 90th percentile of cumulative brine discharges from scenario 6 is ~23,000 m³ (~20,000 m³ for scenario 2) (Section 4.4). Thus, with these assumptions, less than 37% of the unaccounted for inventory would enter the Culebra. Additional analysis is required to adequately bound the results or better represent the unaccounted for inventory in PA calculations. This is to be discussed further in a forthcoming memo.

Isotope:Element Initial Mole Fractions

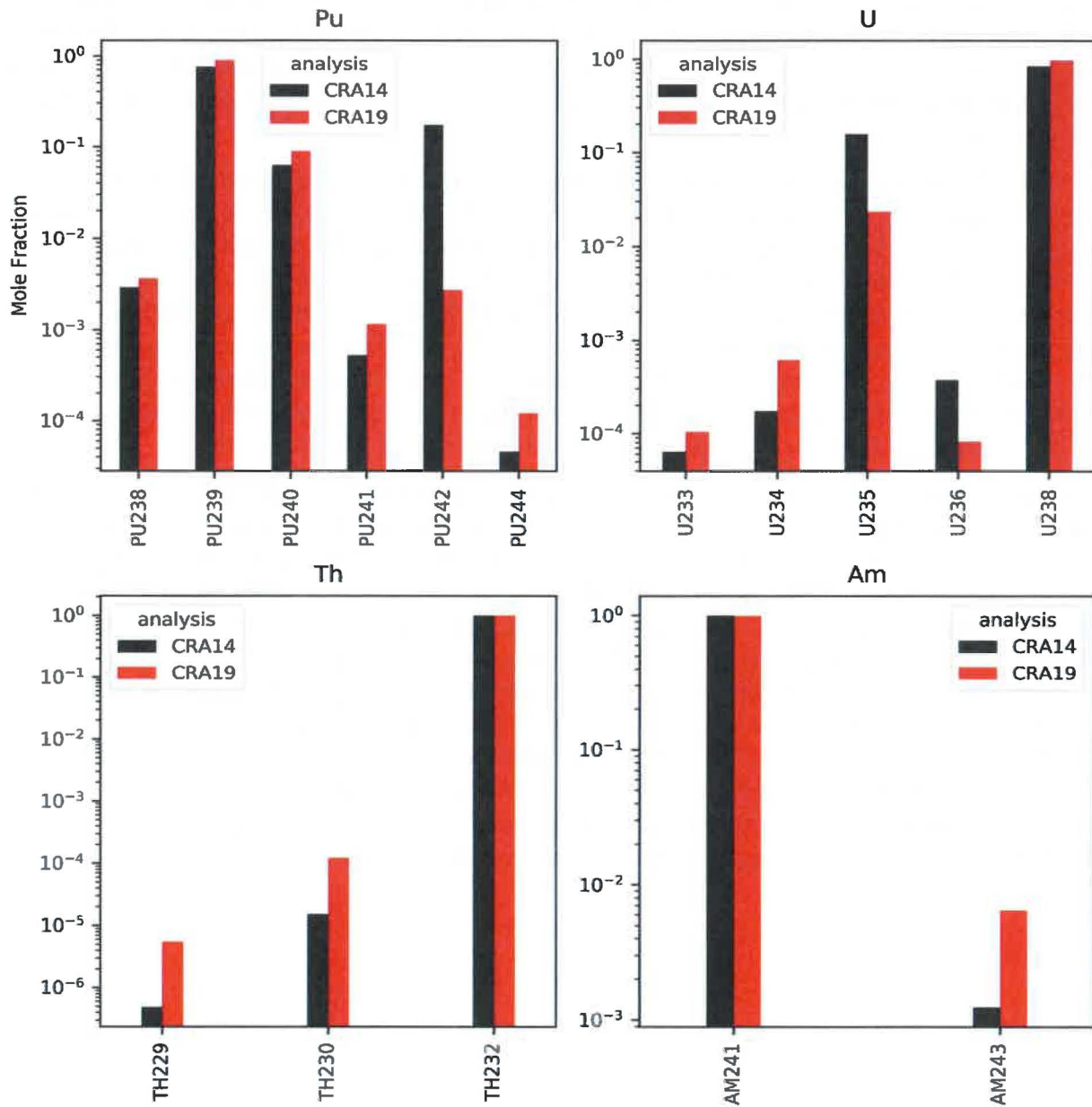


Figure 5– Isotope:Element Initial Mole Fractions

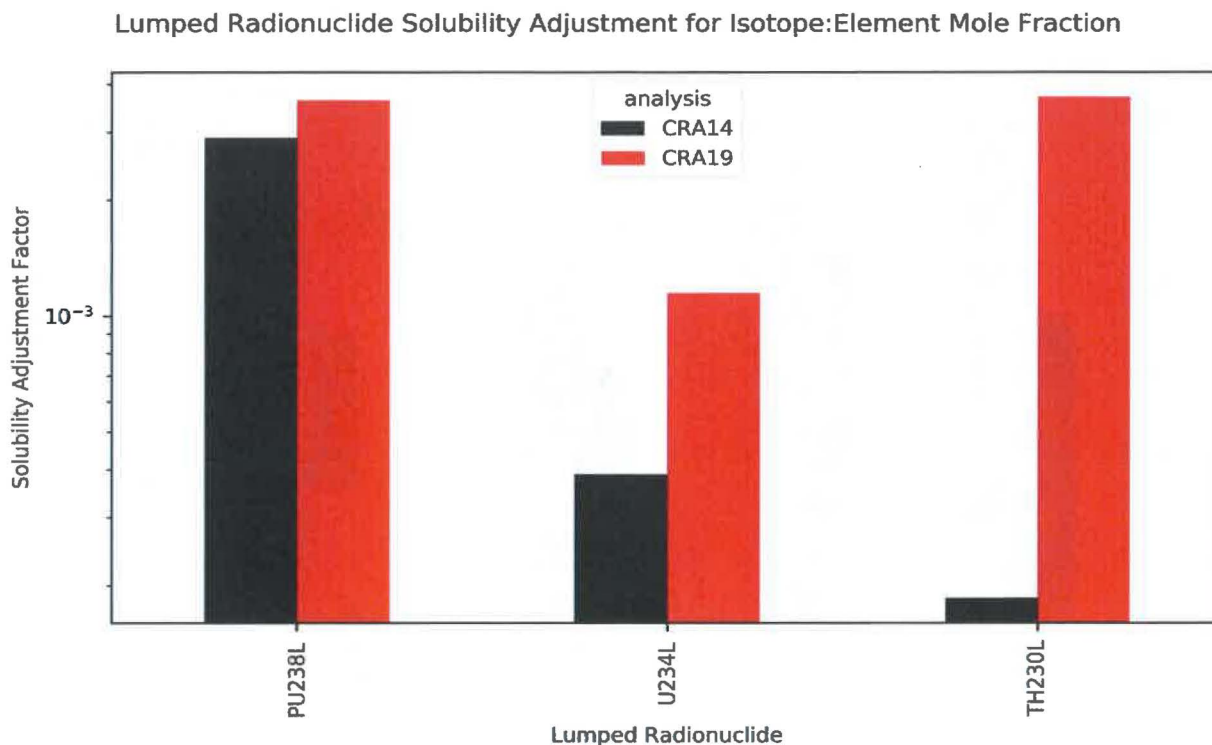


Figure 6-- Lumped Radionuclide Solubility Adjustment for Isotope:Element Mole Fraction

Because isotopes are assumed to dissolve in proportion to their isotope-to-element mole fraction, these mole fractions can have a significant impact on the concentrations of the radionuclides of interest. The initial isotope-to-element mole fraction ratios are shown in Figure 5. ²³³U and ²³⁴U, which have shorter half-lives (and thus greater molar radioactivities) than ²³⁵U, ²³⁶U, and ²³⁸U, has increased. The same is true for ²²⁹Th and ²³⁰Th, as compared to ²³²Th. The maximum (over the 10,000-year regulatory period) isotope-to-element mole fraction ratios are used when computing the mobile concentration limits of the lumped radionuclides used in the transport calculations (see discussion of LSOLDIF in Sarathi 2019, Leigh and Garner 2005). These are shown in Figure 6 (AM241L and PU239L have assumed mole fractions of one). Analogous to the initial individual isotope-to-element mole fractions, the maximum lumped isotope-to-element mole fractions for U234L (²³³U + ²³⁴U,) and TH230L (²²⁹Th + ²³⁰Th) have increased. This will act to increase the mobile concentration limits of those lumped radionuclides (Section 4.2).

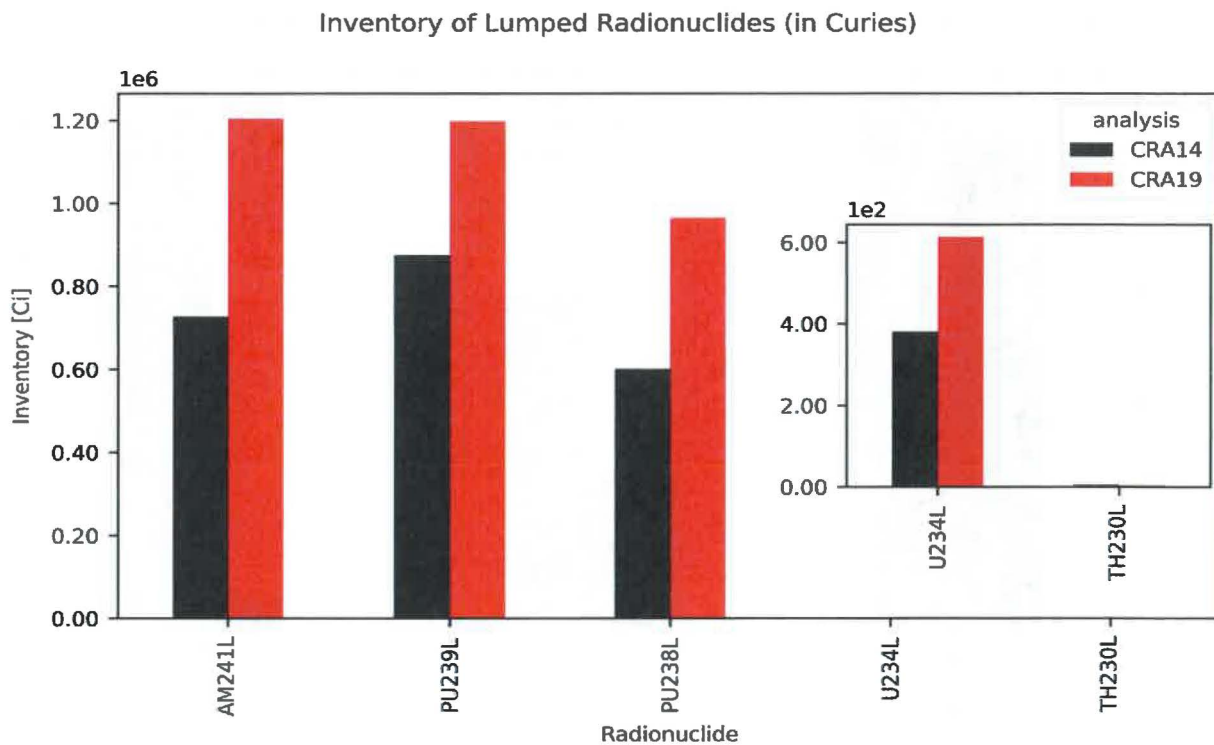


Figure 7– Inventory of Lumped Radionuclides (in Curies)

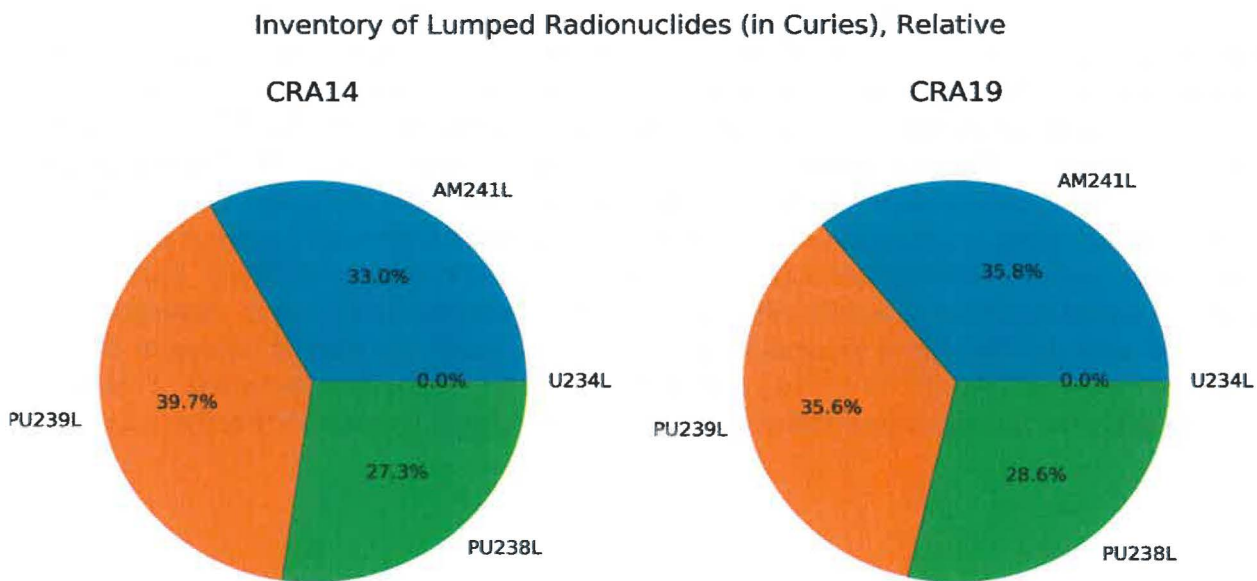


Figure 8– Inventory of Lumped Radionuclides (in Curies), Relative

For computation of the transport releases, and to ease presentation of radionuclide-specific concentrations and releases, the inventory is lumped and reduced to five surrogate radionuclides

(Kicker 2019, Garner and Leigh 2005, also, Section 2.2). The lumped inventory is compared in Figure 7 and Figure 8. Similar to the individual inventory, AM241L ($^{241}\text{Am} + ^{241}\text{Pu}$) has increased, as has PU239L ($^{239}\text{Pu} + ^{240}\text{Pu} + ^{242}\text{Pu}$), and PU238L (^{238}Pu only).

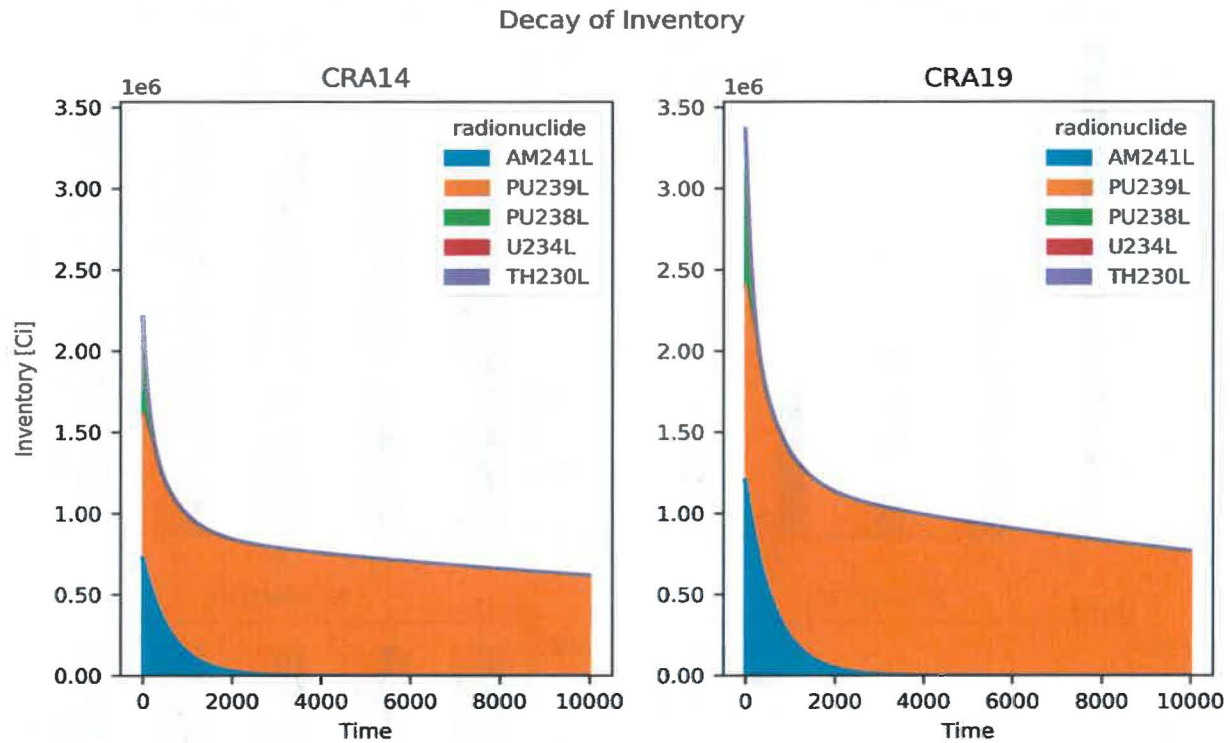


Figure 9– Decay of Inventory

For general reference, Figure 9 illustrates the decay of the lumped inventory over the 10,000-year regulatory period. AM241L, with a half-life of 432 years, decays to ~4% of its initial inventory after 2000 years, leaving PU239L, with a half-life of 24,110 years, as the predominant inventory component.

4.2 Total Mobile Concentration Limits

Baseline Solubilities for Salado Brine

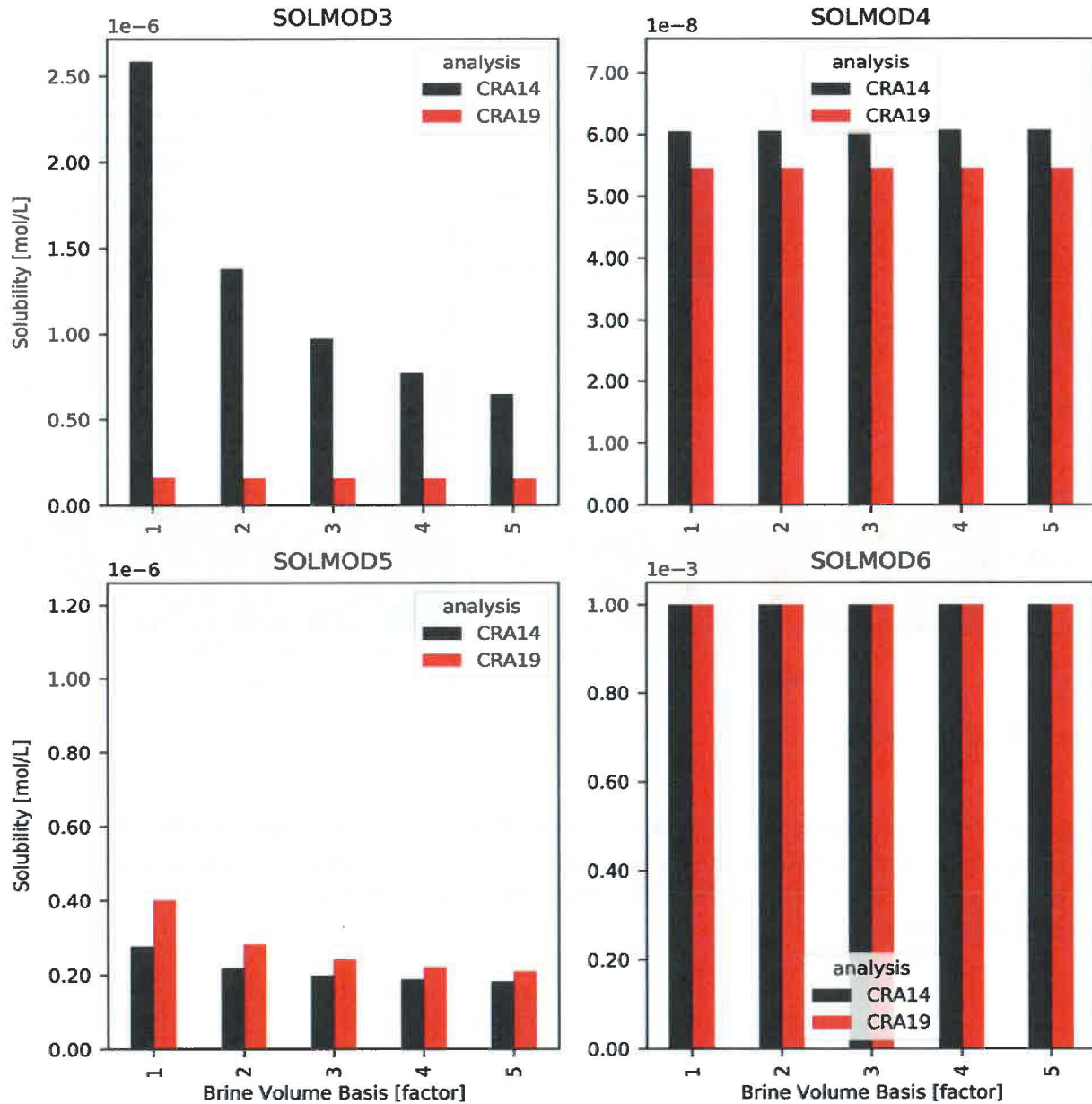


Figure 10– Baseline Solubilities for Salado Brine

Baseline Solubilities for Castile Brine

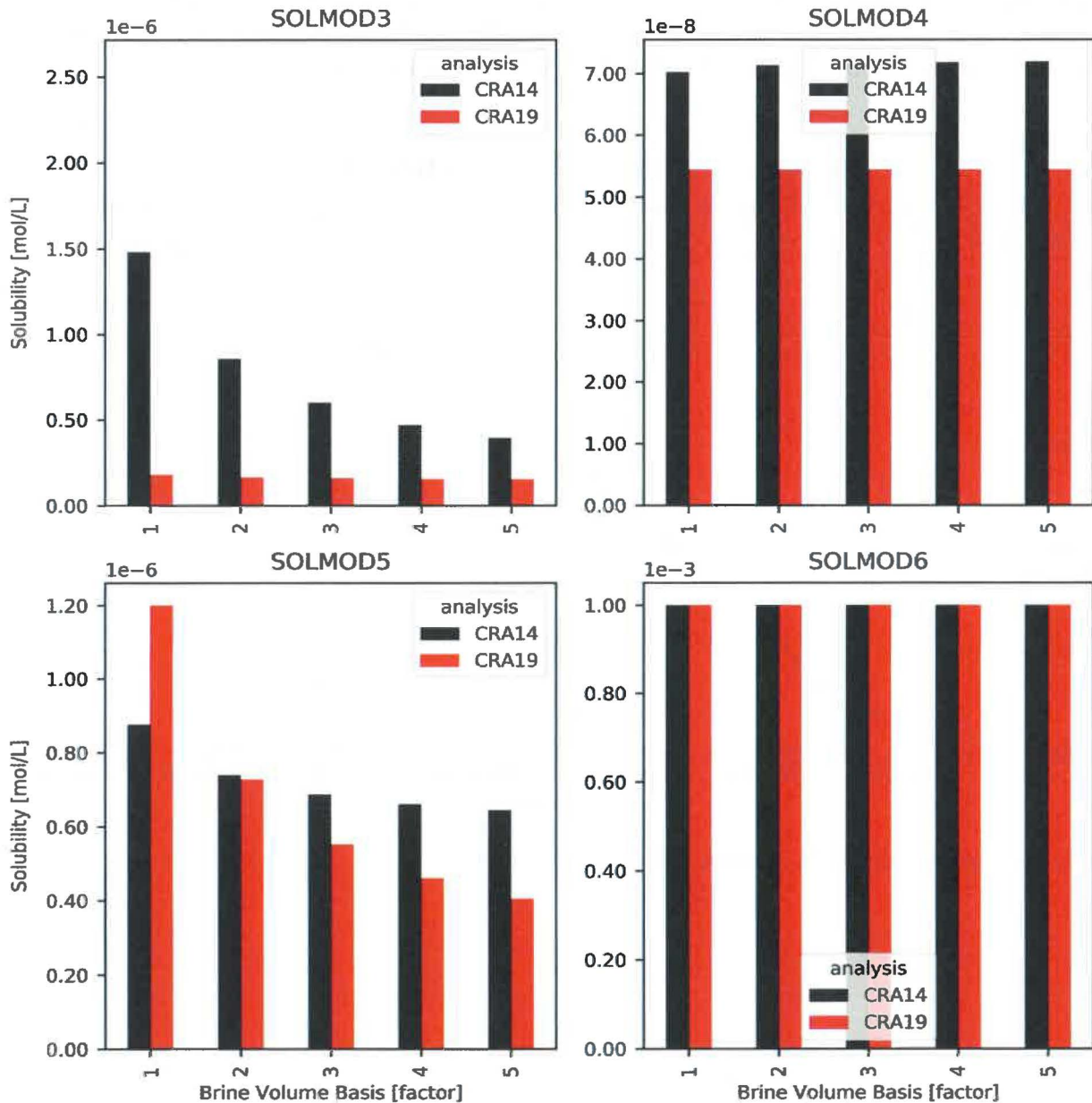


Figure 11– Baseline Solubilities for Castile Brine

Figure 10 and Figure 11 illustrate the baseline solubility values, as determined by Domski and Sisk-Scott (2019), for the +III, +IV, +V, and +VI actinide valence states, for the Salado (GWB) (used for scenarios 1,4, and 5) and Castile (ERDA-6) (used for scenarios 2, 3, and 6) source brines, respectively. The +III (SOLMOD3) baseline solubilities have decreased markedly for CRA-2019 – the reader is referred to Domski and Sisk-Scott (2019) and Domski (2019b) for justification (see Section 1.1.2). The +IV and +V values are similar between CRA-2014 and CRA-2019. The +VI values are fixed as per EPA request (SOTERM-2014) and remain unchanged. From the behavior with respect to the organic ligand dilution factor (brine volume

basis factor), it appears that An(III) interacts dramatically more weakly with EDTA or other organic ligands in the CRA-2019 model, whereas An(V) interacts more strongly. Overall, the Salado and Castile values are similar for the CRA-2019. The remaining illustrations in Section 4.2 and Section 4.3 will focus on the Castile brine (as the Castile brine pocket intrusion scenarios generate more impactful DBR volumes) and the 1x brine volume basis.

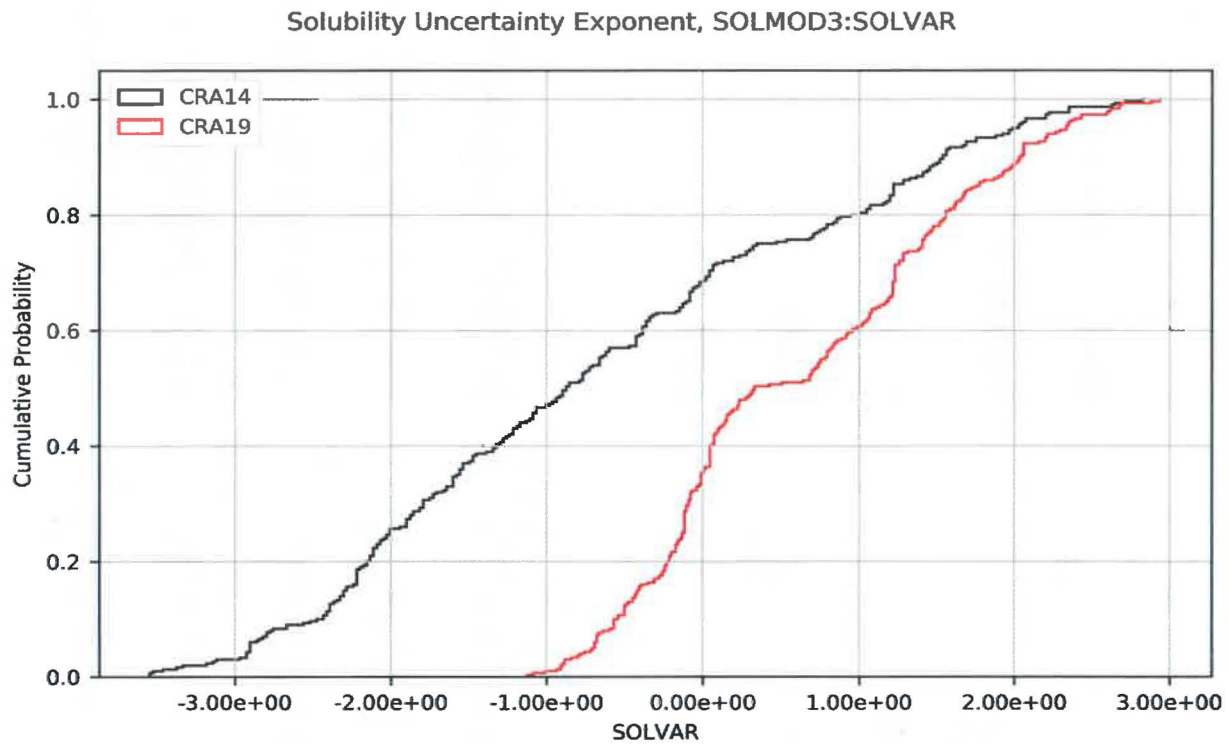


Figure 12– Solubility Uncertainty Exponent, SOLMOD3:SOLVAR

Solubility Uncertainty Exponent, SOLMOD4:SOLVAR

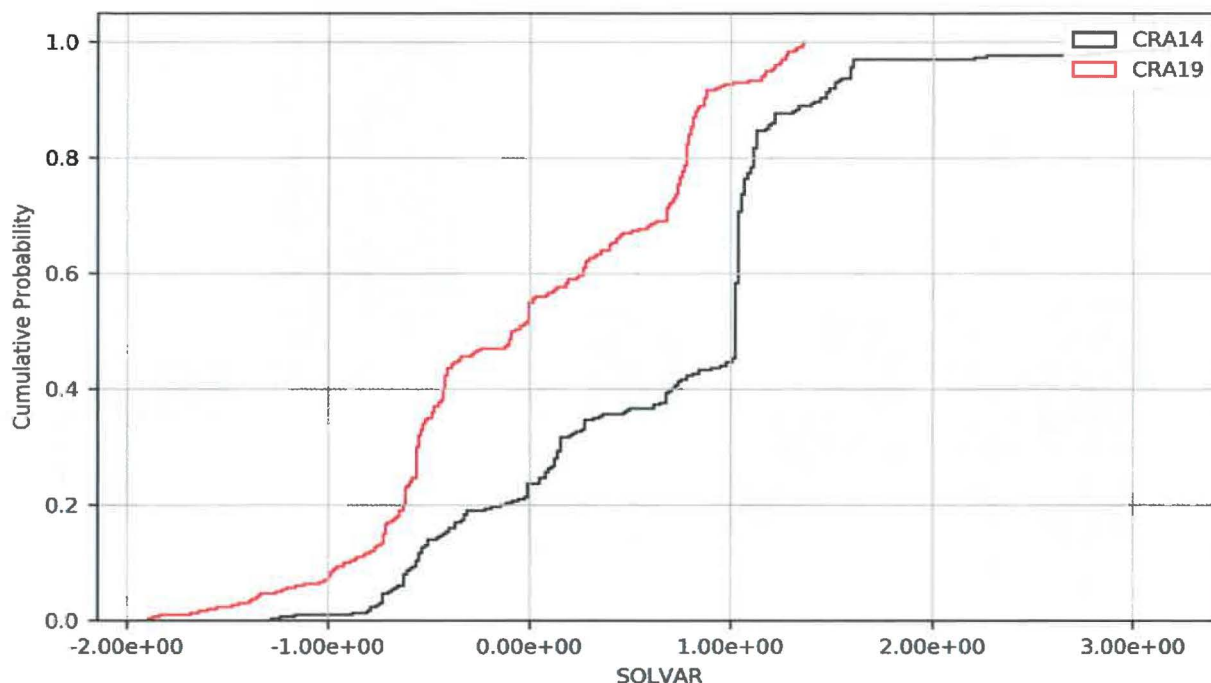


Figure 13– Solubility Uncertainty Exponent, SOLMOD4:SOLVAR

Figure 12 and Figure 13 illustrate the solubility uncertainty exponent (SOLVAR) sampled values for actinides in the +III and +IV valence states (the input distributions were determined by Domski (2019a), see figures 4 and 2 therein). The baseline solubilities are multiplied by ten raised to the power of SOLVAR to calculate the realized (dissolved) solubility limit. For the actinides in the +III state, the minimum and median of the cumulative distribution has dramatically increased and the variance as decreased for the CRA-2019. This will act to increase +III solubilities (and counteract the decrease in the baseline solubilities). For actinides in the +IV state, the minimum, median, and maximum of the cumulative distribution has decreased, as has the variance, for the CRA-2019. This will act to decrease +IV solubilities.

LOG10 of Total Mobilization Potential, Castile Brine, All Conditions

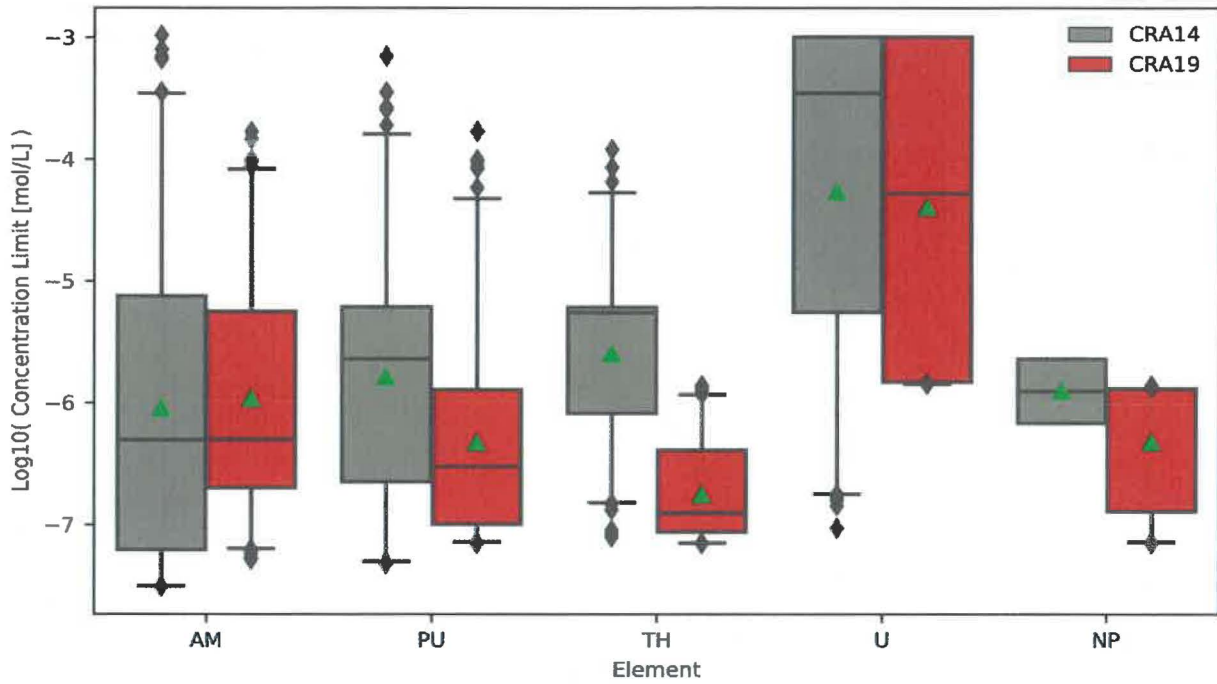


Figure 14– log10 of Total Mobilization Potential for Base Elements, Castile Brine, All Conditions

LOG10 of Total Mobilization Potential, Castile Brine

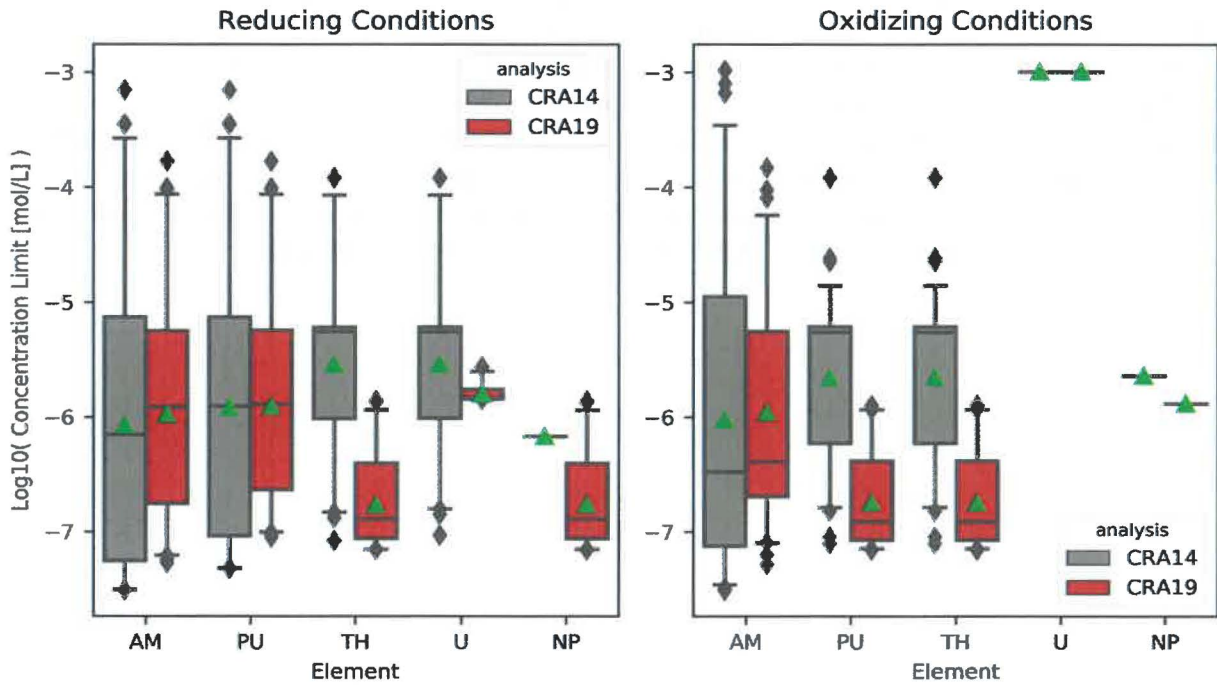


Figure 15– log10 of Total Mobilization Potential for Base Elements, Castile Brine, by Brine Redox Condition

Figure 14 illustrates the log₁₀ of the total mobilization potential (i.e. the total mobile concentration limit) for each of the five primary actinides (the base 10 logarithm (log₁₀) values are plotted because SOLMOD3:SOLVAR and SOLMOD4:SOLVAR uncertainty distributions are defined as the log₁₀ of the solubility uncertainty multiplier, thus it is more appropriate to display the mean/medians of the log₁₀ values rather than the log₁₀ of the mean/median mobilization potentials). Figure 15 illustrates the same, but with the distribution of results split according to the redox condition of the brine (sampled parameter OXSTAT). If the brine exhibits reducing conditions, the Pu(III), U(IV), and Np(IV) are assumed to exist. If the brine exhibits oxidizing conditions, Pu(IV), U(VI), and Np(V) are assumed to exist. Am(III) and Th(IV) are assumed to exist under both brine redox conditions.

For Am(III) and Pu(III), the larger percentile concentration limit values have decreased (evidenced by the decrease in the box-top, whiskers, and outliers), but the median values remain similar. The increase in the median of the input solubility uncertainty distribution (SOLMOD3:SOLVAR) largely offsets the decrease in the baseline solubility. For Pu(IV) and Th(IV), the decrease in the entire solubility uncertainty distribution (SOLMOD4:SOLVAR) causes the concentration limits to decrease markedly, and the median and top percentiles decrease by almost two log units (the floor is set by the mineral and intrinsic colloid concentration limits). For U(IV), the mobile concentration limit is dominated by the (fixed) intrinsic colloid concentration limit (U:CONCINT), which has increased to 1.4e-6 mol/L for CRA-2019 (Reed et al 2019), a value much larger than the baseline solubility (SOLMOD4:SOLSOH) of ~5.4e-8 mol/L. Its distribution has shrunk because most of the dissolved concentration limit values are smaller than the intrinsic colloid concentration limit (see Figure 19 and Figure 24). The Np(IV) values are now sampled for CRA-2019 (the Np(V) values remain fixed) as is consistent with other SOLMOD analogues (SOTERM-2014, Sarathi 2019e). Np(V) values are similar, but slightly decreased due to the decrease in the CAPMIC parameter. Finally, U(VI) remains similar for CRA-2019, as all of the colloid terms remain small compared to its baseline solubility value.

Absolute Colloidal Contributions to Mobilization Potential: AM

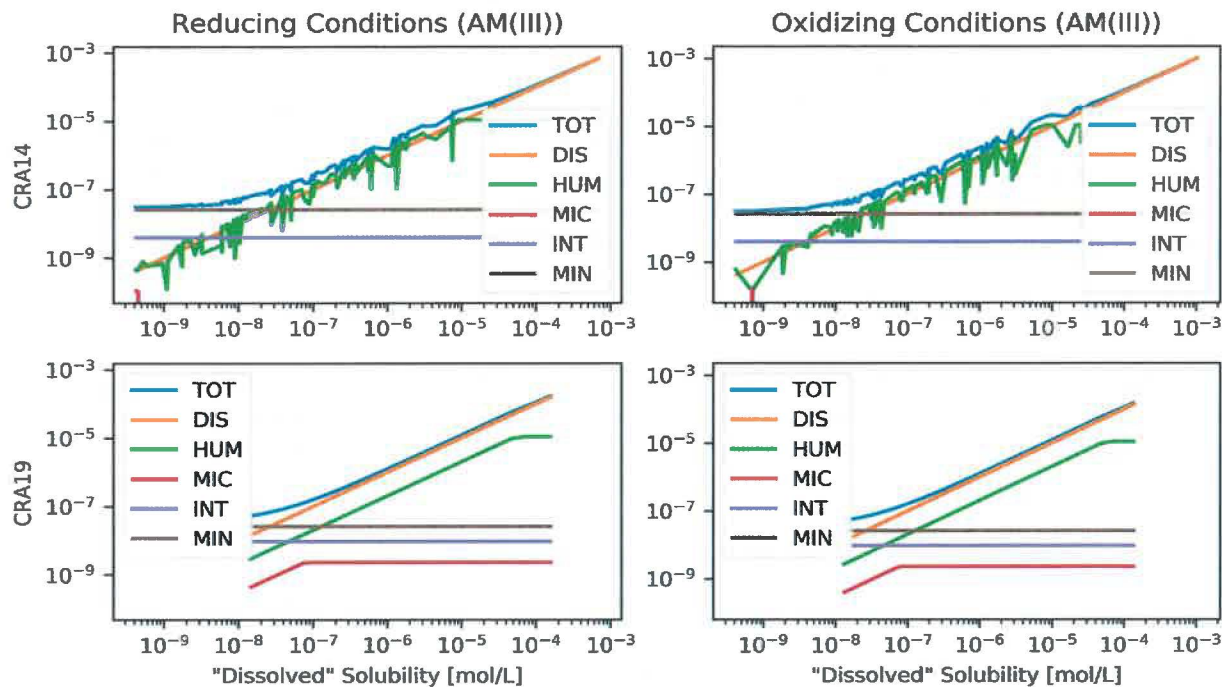


Figure 16– Absolute Colloidal Contributions to Mobilization Potential: AM

Absolute Colloidal Contributions to Mobilization Potential: PU

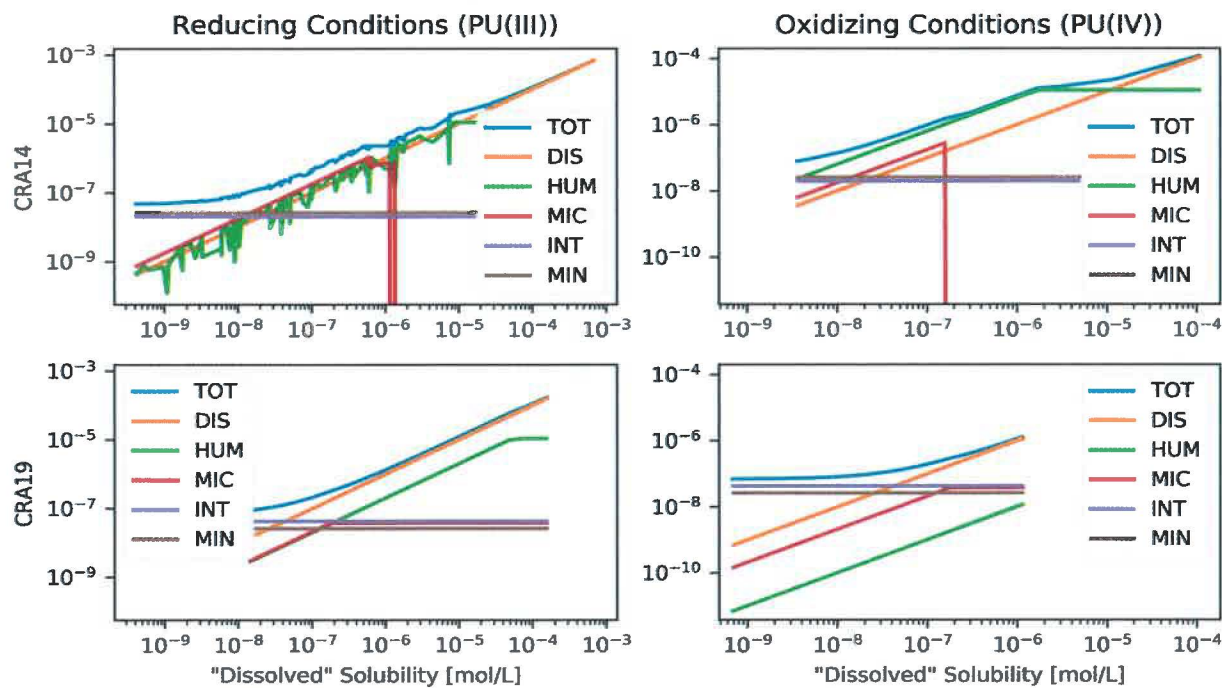


Figure 17– Absolute Colloidal Contributions to Mobilization Potential: PU

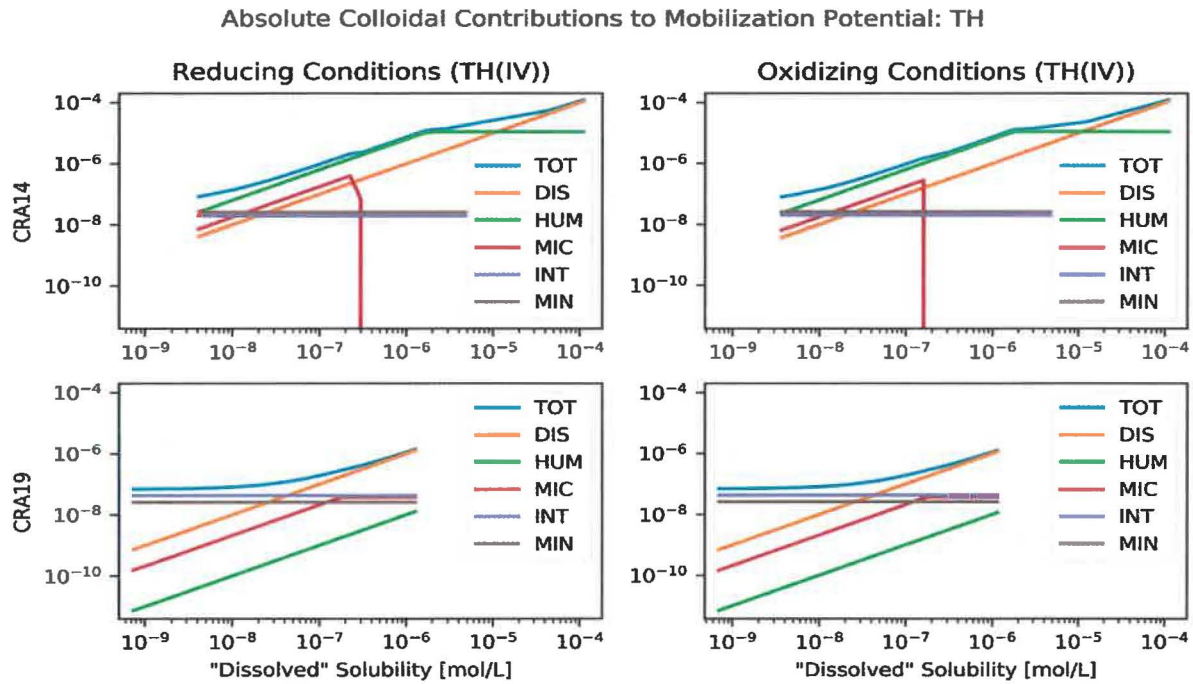


Figure 18– Absolute Colloidal Contributions to Mobilization Potential: TH

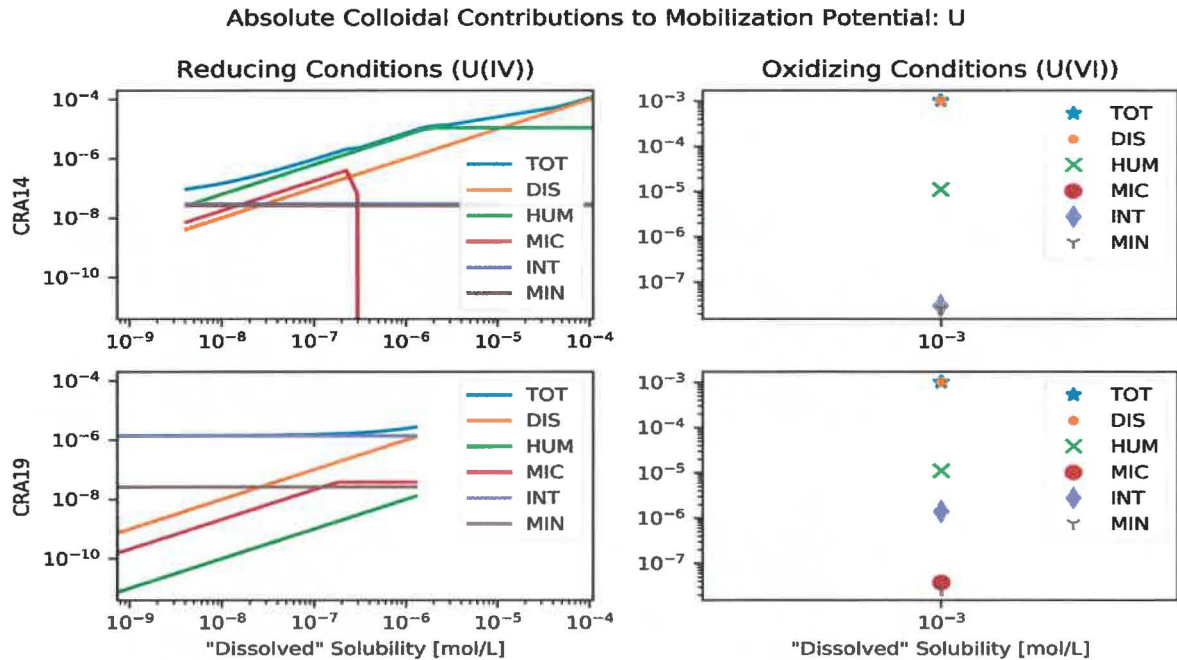


Figure 19– Absolute Colloidal Contributions to Mobilization Potential: U¹

¹ Note that the value of MIC in U(VI) for CRA14 is zero and does not appear on this log scale plot. The value of MIC being zero follows from the sum of the other solubilities (1.011e-03) being greater than CAPMIC (2.3e-06). See Sarathi (2019a) for a more complete discussion of how CAPMIC has been implemented.

Absolute Colloidal Contributions to Mobilization Potential: NP

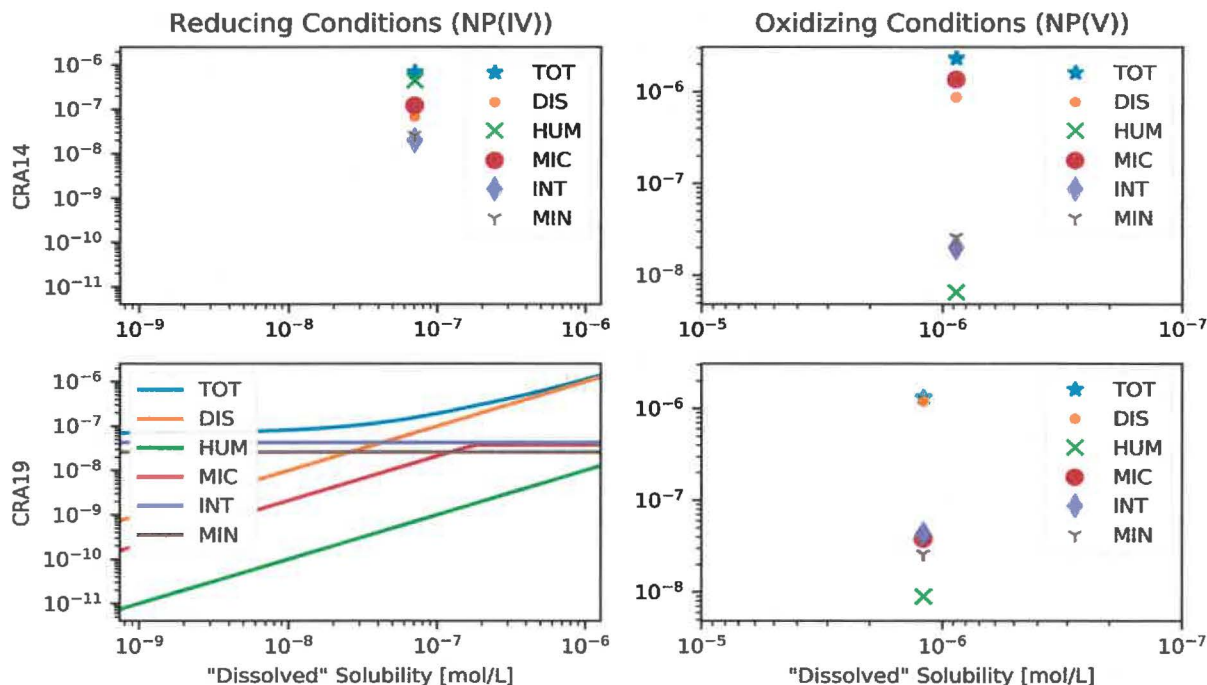


Figure 20– Absolute Colloidal Contributions to Mobilization Potential: NP

Fractional Colloidal Contributions to Mobilization Potential: AM

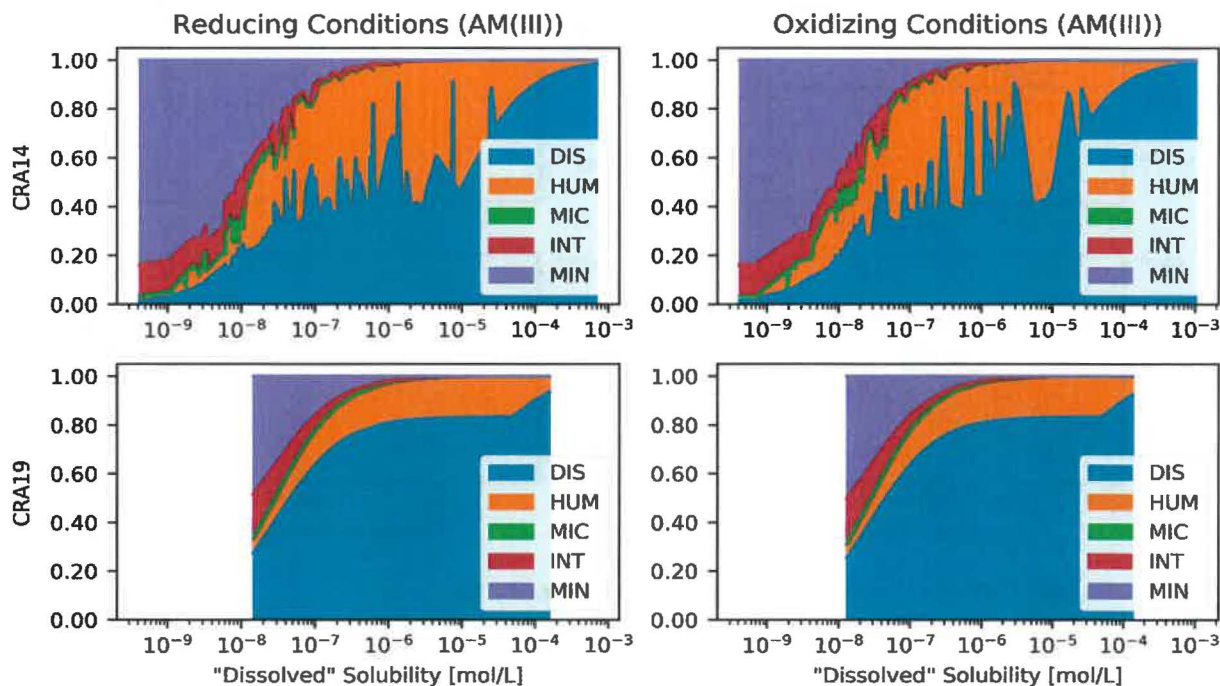


Figure 21– Fractional Colloidal Contributions to Mobilization Potential: AM

Fractional Colloidal Contributions to Mobilization Potential: PU

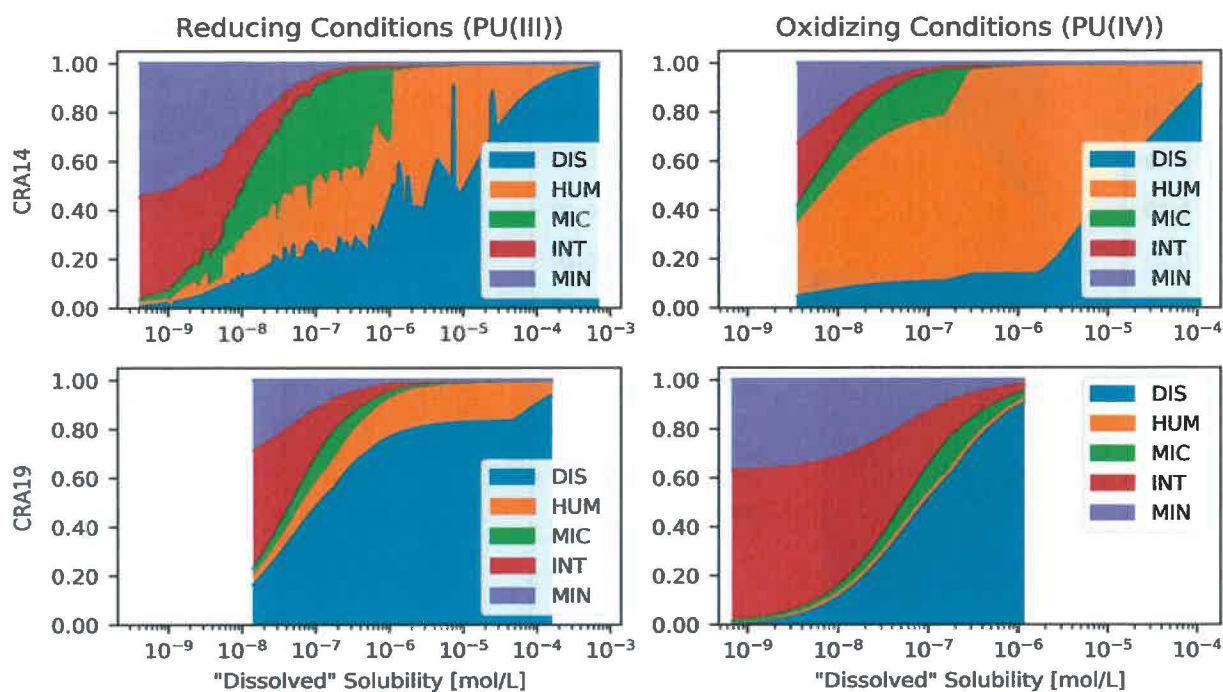


Figure 22– Fractional Colloidal Contributions to Mobilization Potential: PU

Fractional Colloidal Contributions to Mobilization Potential: TH

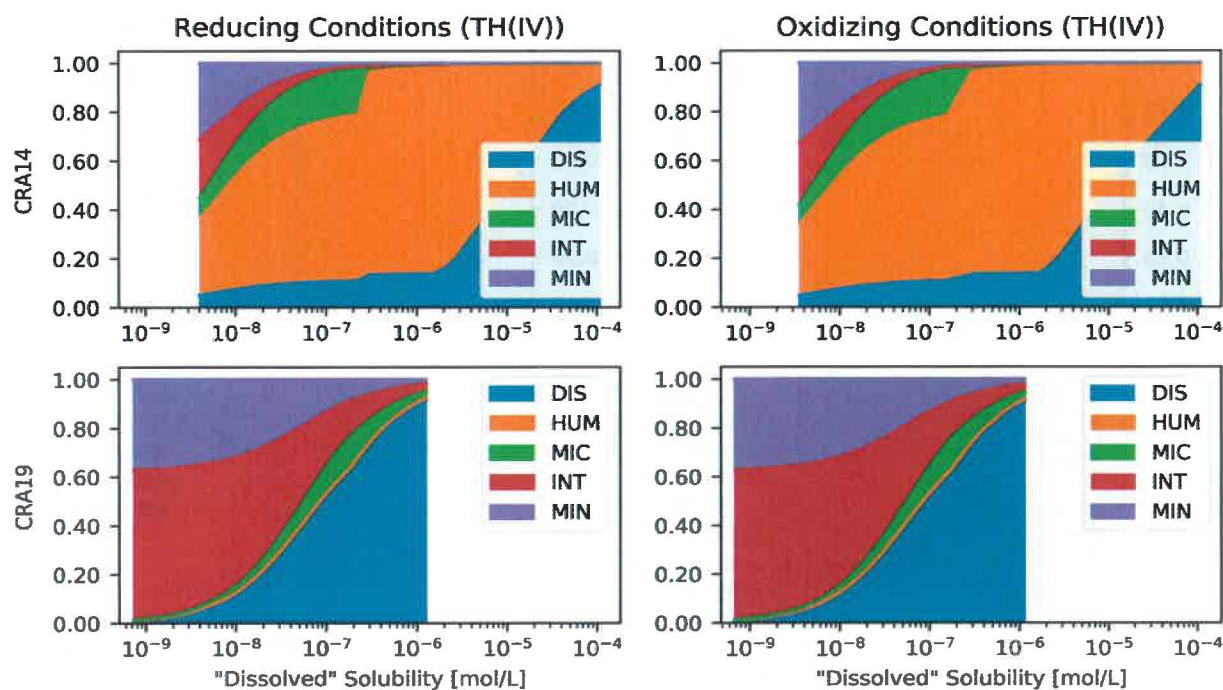


Figure 23– Fractional Colloidal Contributions to Mobilization Potential: TH

Fractional Colloidal Contributions to Mobilization Potential: U

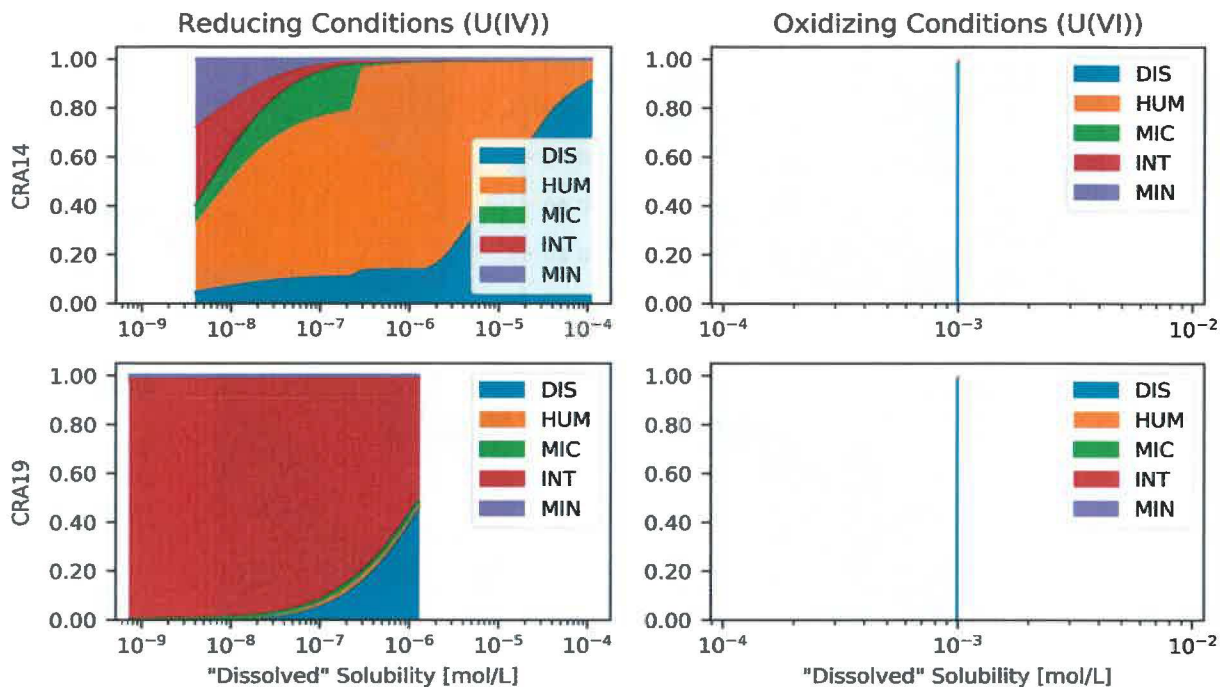


Figure 24– Fractional Colloidal Contributions to Mobilization Potential: U

Fractional Colloidal Contributions to Mobilization Potential: NP

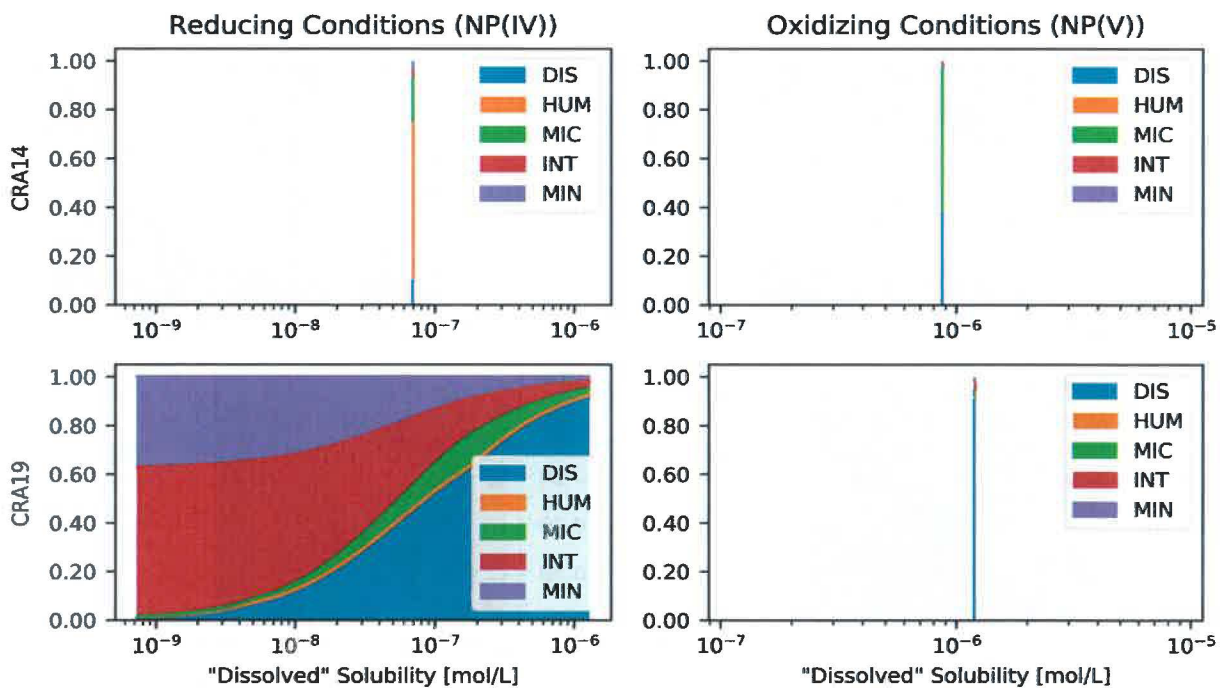


Figure 25– Fractional Colloidal Contributions to Mobilization Potential: NP

Figure 16 through Figure 20 illustrate the dissolved and various colloid (humic, microbial, intrinsic, and mineral) contributions to the total concentration limit as a function of the stochastic dissolved concentration limit (the humic and microbial colloid contributions are proportional to the dissolved concentration limit). Figure 21 through Figure 25 illustrate the fractional contributions of each to the total concentration limit. The results are split according to brine redox condition. In all of the absolute figures, the change in the microbial colloid implementation (Sarathi 2019a) is apparent – the microbial contribution now increases linearly to the parameter CAPMIC and plateaus (previously it ramped to a value derived from CAPMIC and then decreased to zero). For all elements, the microbial colloid term contributes little to the total concentration limit for CRA-2019. For Am(III), the dissolved concentration limit comprises the majority of the total concentration limit except at low sampled solubility uncertainty values. The same is true for Pu(III). For Pu(IV) and Th(IV), the intrinsic and mineral colloid terms contribute a large portion over the range (and especially at the lower dissolved concentration limits). The humic colloid term contributes little due to the decrease in the linear proportionality constant (PHUMOX4:PHUMSIM) for CRA-2019 (from 6.3 to 0.01, see Mariner 2019) (also, for CRA-2019, the humic proportionality constant for An(III) for the Castile brine (PHUMOX3:PHUMCIM) was changed to a constant value; for CRA-2014 it was sampled, and this is why the humic curves are jagged for Am(III) and Pu(III)). For U(IV), the intrinsic colloid term comprises most of the total concentration limit across the entire dissolved concentration limit range because of its increase from $3.0e-8$ to $1.4e-6$ mol/L, and because the An(IV) uncertainty distribution has decreased. U(VI) and Np(V) (and Np(IV) for CRA-2014) solubilities are not sampled, which is why the respective subplots appear to contain a single point or a single line. For U(VI) and Np(V), the colloid terms contribute little to the total concentration limit. For CRA-2019, Np(IV) behaves similarly to Th(IV).

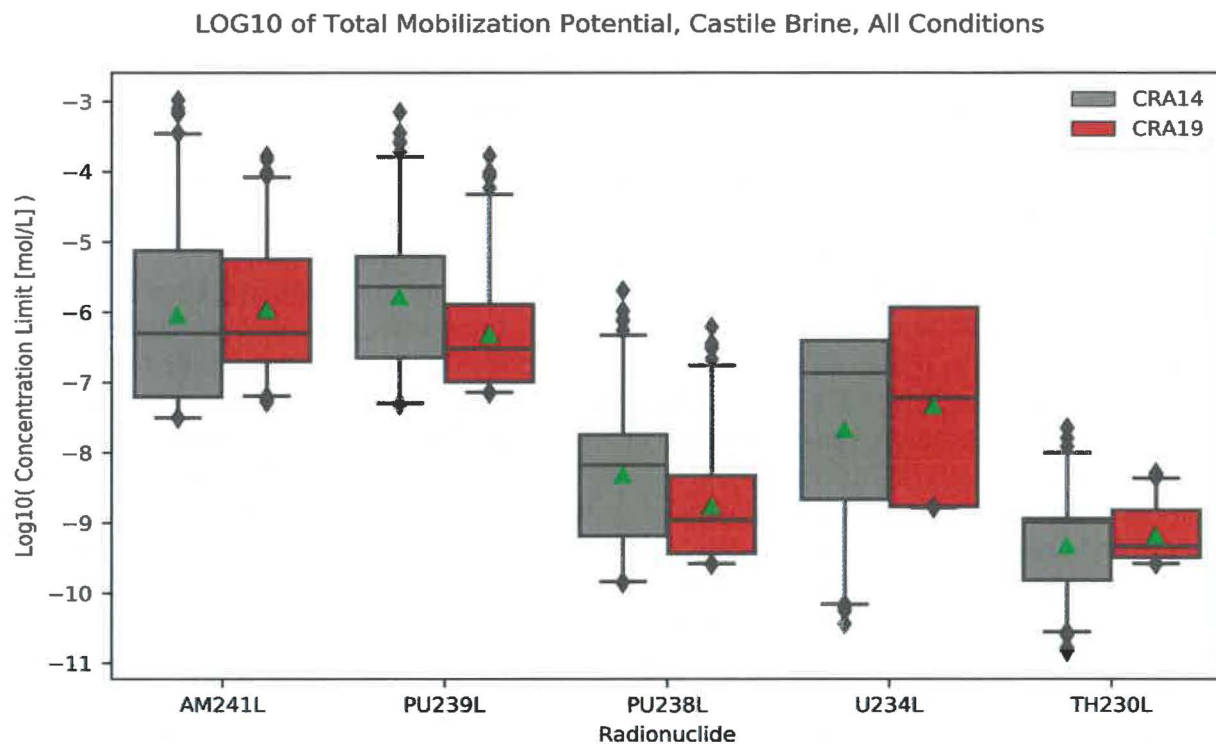


Figure 26– log10 of Total Mobilization Potential, Lumped Radionuclides, Castile Brine, All Conditions

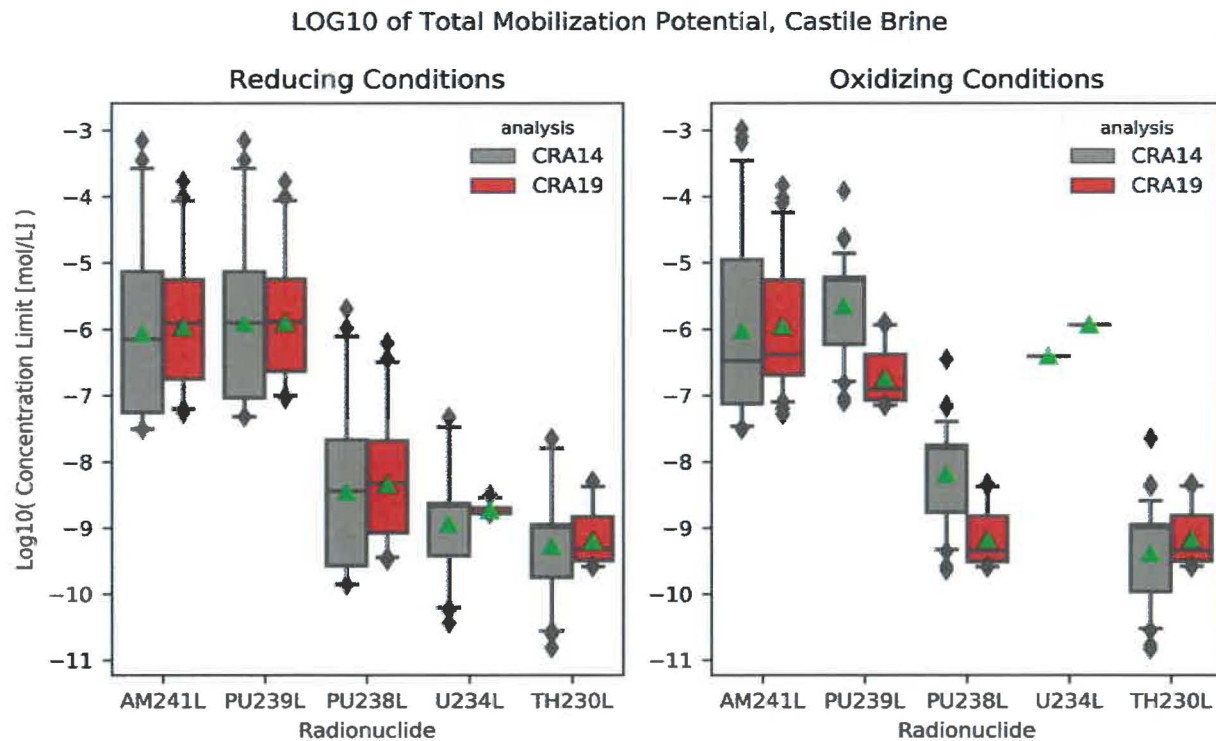


Figure 27– log10 of Total Mobilization Potential, Lumped Radionuclides, Castile Brine, by Brine Redox Condition

The total mobile concentration limits of the lumped radionuclides are illustrated in Figure 26 and Figure 27. These are analogous to the elemental results shown in Figure 14 and Figure 15, but with the fixed lumped isotope-to-element mole fractions (LSOLDIF) of Figure 6 applied (while indicative of the overall behavior, these values are used as input to the NUTS transport simulations; PANEL determines the isotope-to-element mole fractions at each timestep for its calculations). AM241L and PU239L are the same as the elemental values because no adjustment is applied. U234L and TH230L values are smaller than the elemental values (because other, nonlumped isotopes comprise the bulk of the dissolved U and Th, Figure 5). However, the U(VI) value increases because of the increased portions of ^{233}U and ^{234}U , and this increases the maximum of the overall U234L results distribution.

4.3 PANEL Instantaneous Mobile Concentrations

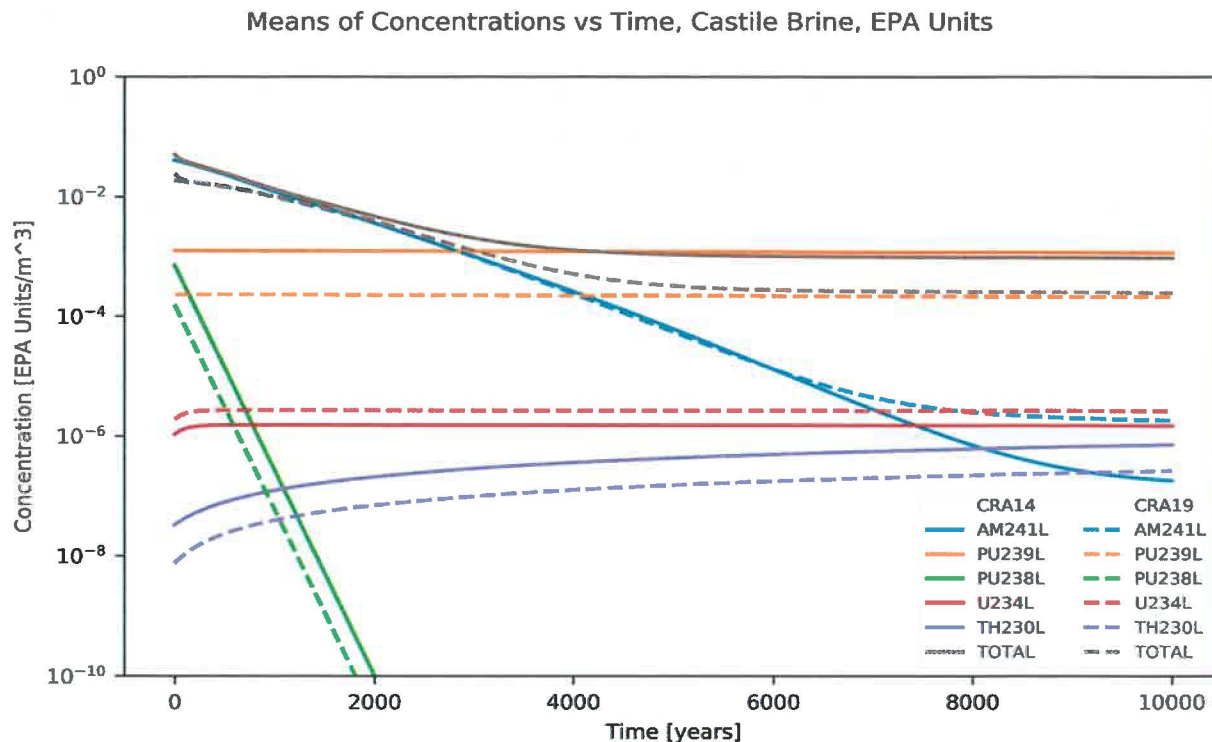


Figure 28– Means of Concentrations vs Time, Castile Brine, EPA Units

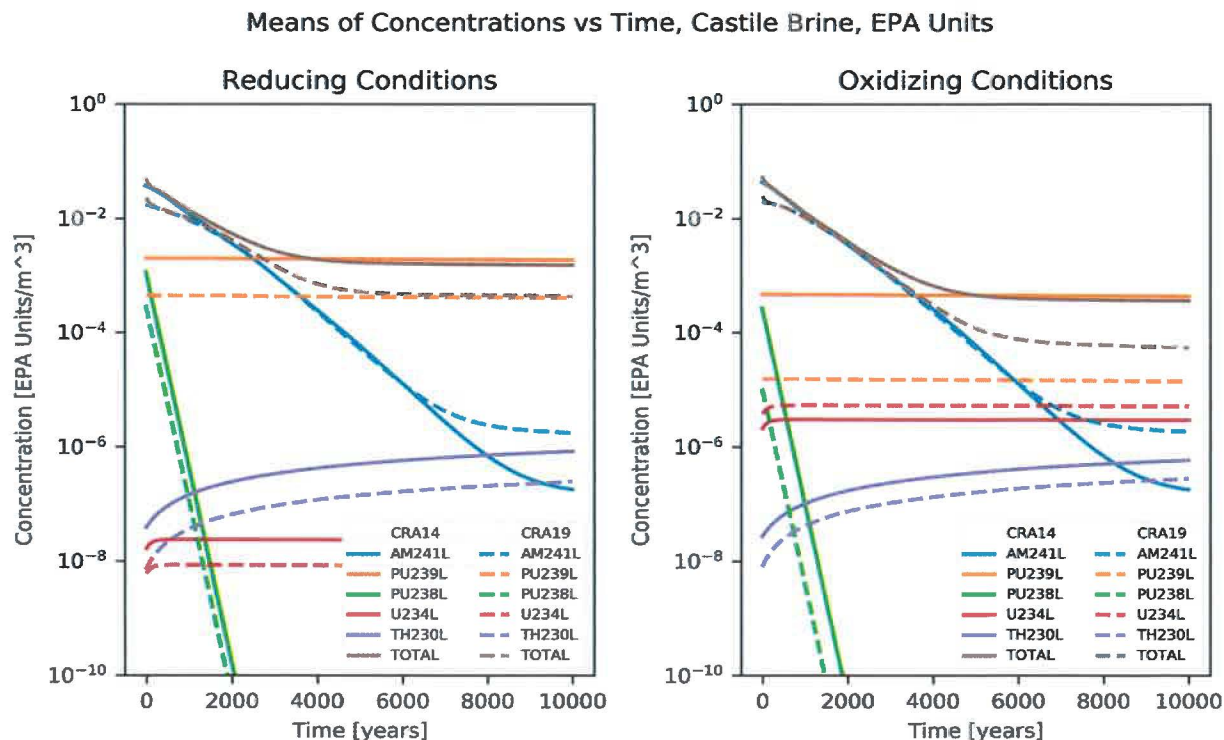


Figure 29 – Means of Concentrations vs Time, Castile Brine, EPA Units, by Brine Redox Condition

The total mobile concentration limits presented in Section 4.2 are used to calculate instantaneous radionuclide concentrations in the waste panels as a function of time. These calculations, performed by the code PANEL, consider the effects of decay/ingrowth and mass balance. The mean (across all vectors and replicates) mobile concentrations for the lumped radionuclides in 1x the minimum DBR volume is shown in Figure 28 with units EPA units/m³. The mean total radioactivity concentration at early times is dominated by AM241L and at later times by PU239L. The mean total radioactivity concentration has decreased for CRA-2019, following the trends for the overall reduction in the An(III) and An(IV) concentration limits discussed in Section 4.2. The increase in the late-time plateau for AM241L is due to an increase in the initial inventory of ²⁴⁵Cm (from 1.225 to 24.47 Ci in CRA-2019), which decays with a half-life of 8,500 years to ²⁴¹Pu and then to ²⁴¹Am, and thus acts as a slow source for ²⁴¹Am.

Figure 29 illustrates the mean (across vectors) mobile concentrations (in EPA units/m³) versus time, similar to Figure 28, but separated according to the sampled brine redox condition. At early times, the mean radioactivity concentrations are similar because the radioactivity concentration is dominated by redox-insensitive elements, but at late times they differ due to the oxidation state of Pu.

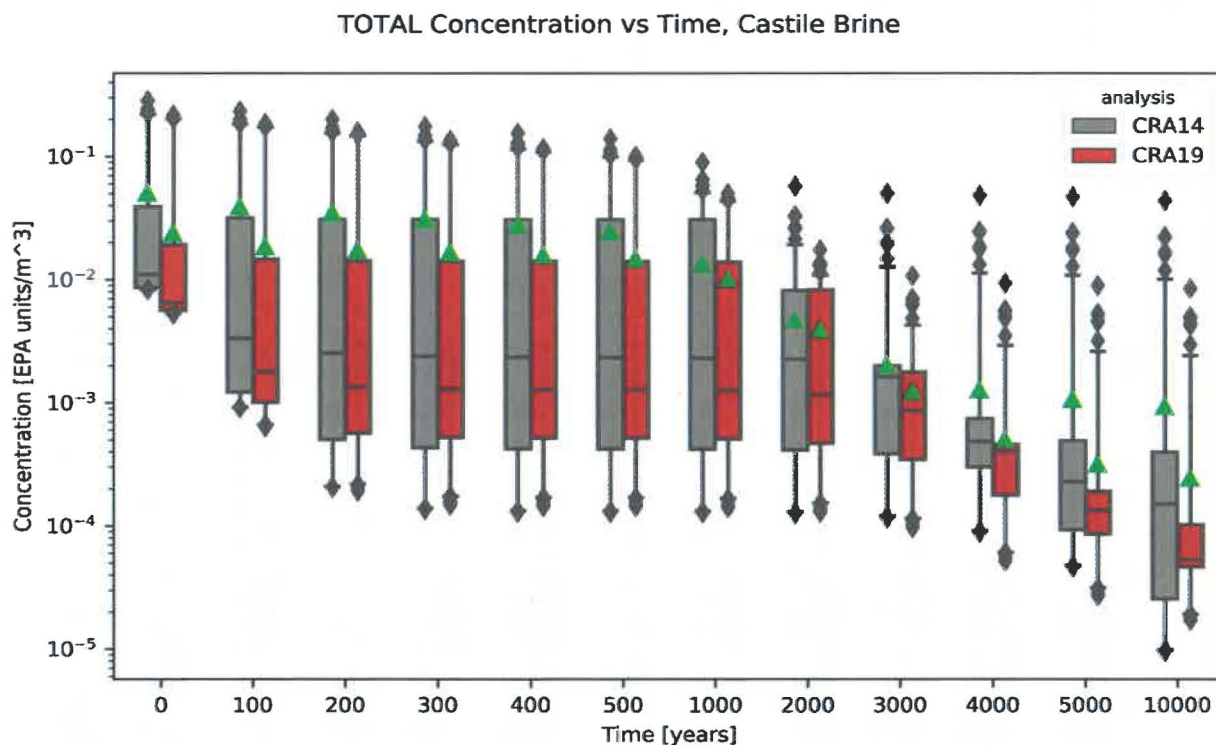


Figure 30– TOTAL Concentration vs Time, Castile Brine

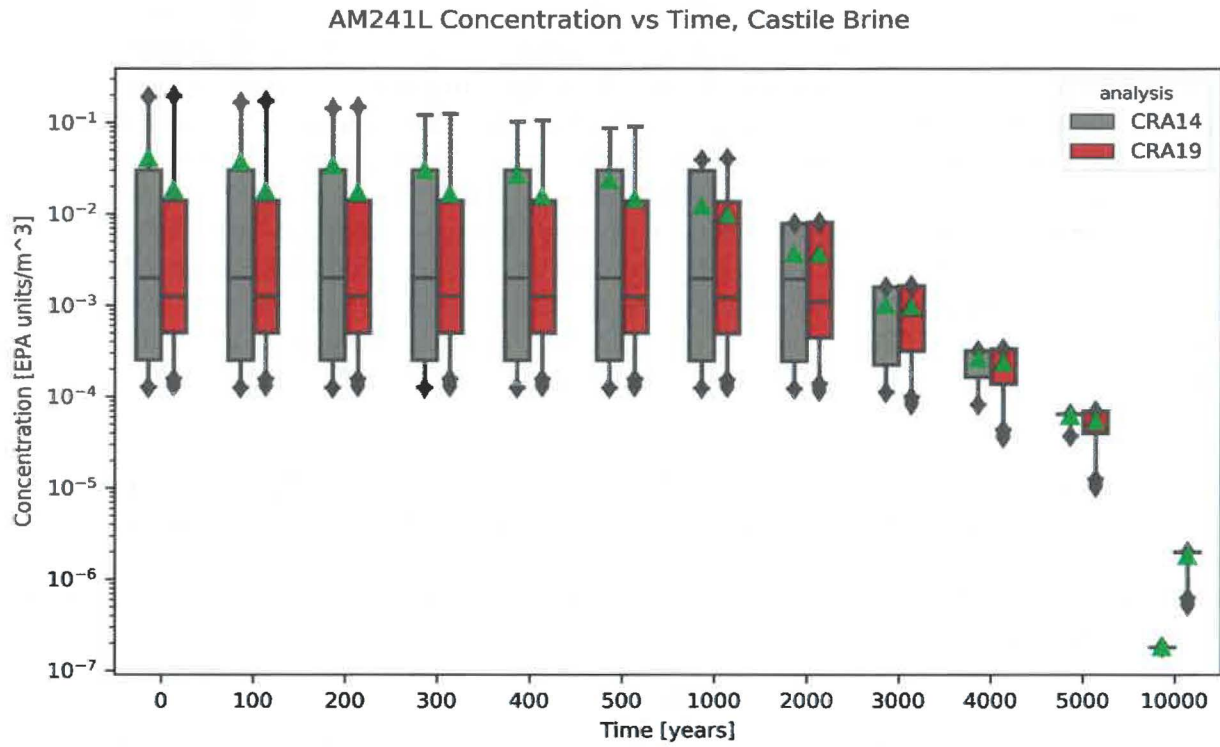


Figure 31– AM241L Concentration vs Time, Castile Brine

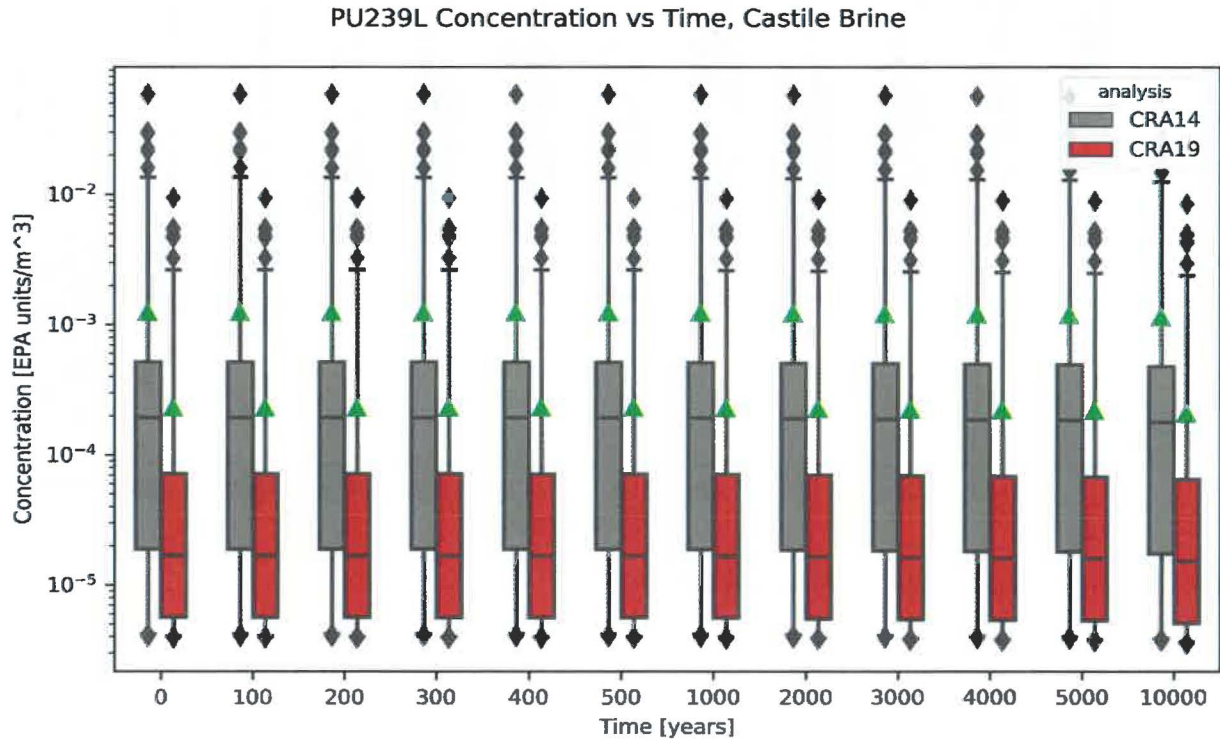


Figure 32– PU239L Concentration vs Time, Castile Brine

Figure 30 illustrates the distribution of the total radioactivity concentration (in EPA units/m³) at discrete points in time (note, the displayed times are not regularly spaced), and Figure 31 and Figure 32 illustrate the same for AM241L and PU239L. The statistics illustrated in these boxplots are calculated over the concentration values and are plotted on a log scale (the statistics for the concentration limits illustrated in Figure 14 were calculated over the logarithm of the concentration limits to be consistent with the nature of the input uncertainty distribution, while the statistics for the instantaneous concentrations are calculated over the untransformed values to be consistent with the usage of the output uncertainty). Because of this, the output distribution appears highly skewed and the means are in many instances larger than the 75th percentile. The overall reduction and the reduction in variance in the total radioactivity concentration at late times is due to the decay of AM241L; the total radioactivity concentration distribution approaches that of PU239L at late times.

For reference, the horsetail plots of mobile concentration vs. time are shown in Figure 33 through Figure 38 (the red line indicates the mean across vectors vs time). The envelope line to which the various simulation results converge in the AM241L and PU238L plots shows the behavior when the mobile concentrations are inventory limited (rather than solubility limited), and the decrease in this line over time illustrates decay. For U234L, the horsetails cluster onto the upper (non-sampled) U(VI) concentration line and the much lower (sampled) U(IV) concentration lines.

TOTAL Concentration vs Time, Castile Brine

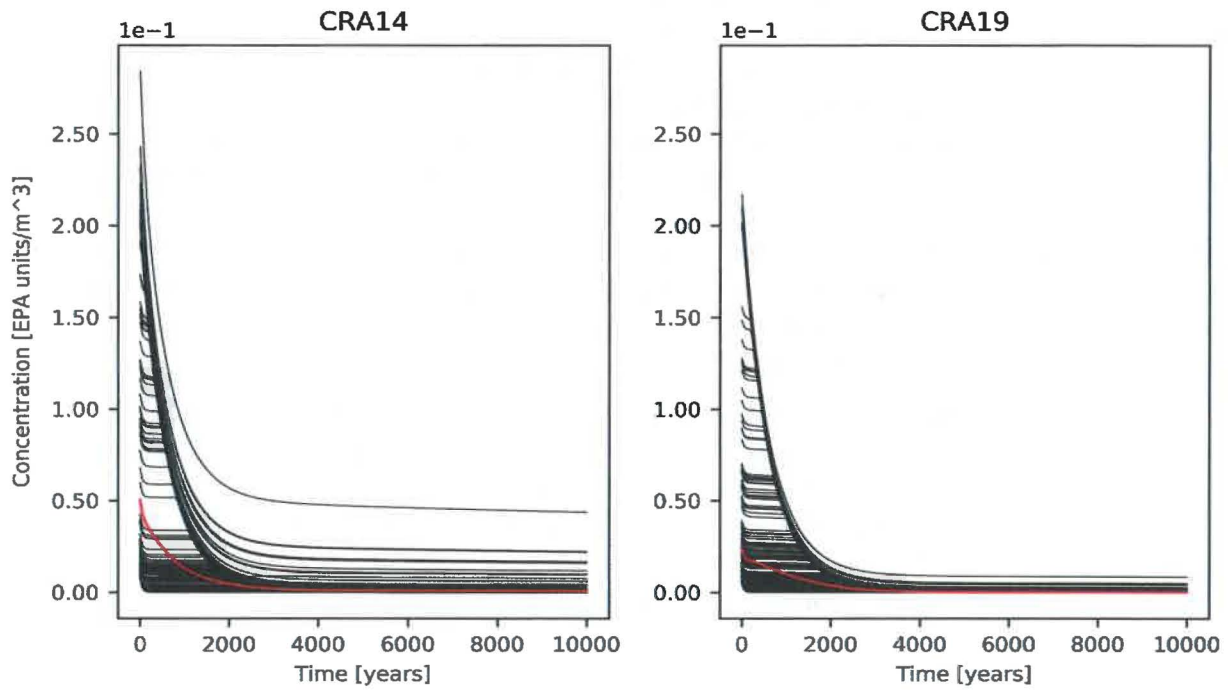


Figure 33– TOTAL Concentration vs Time, Castile Brine

AM241L Concentration vs Time, Castile Brine

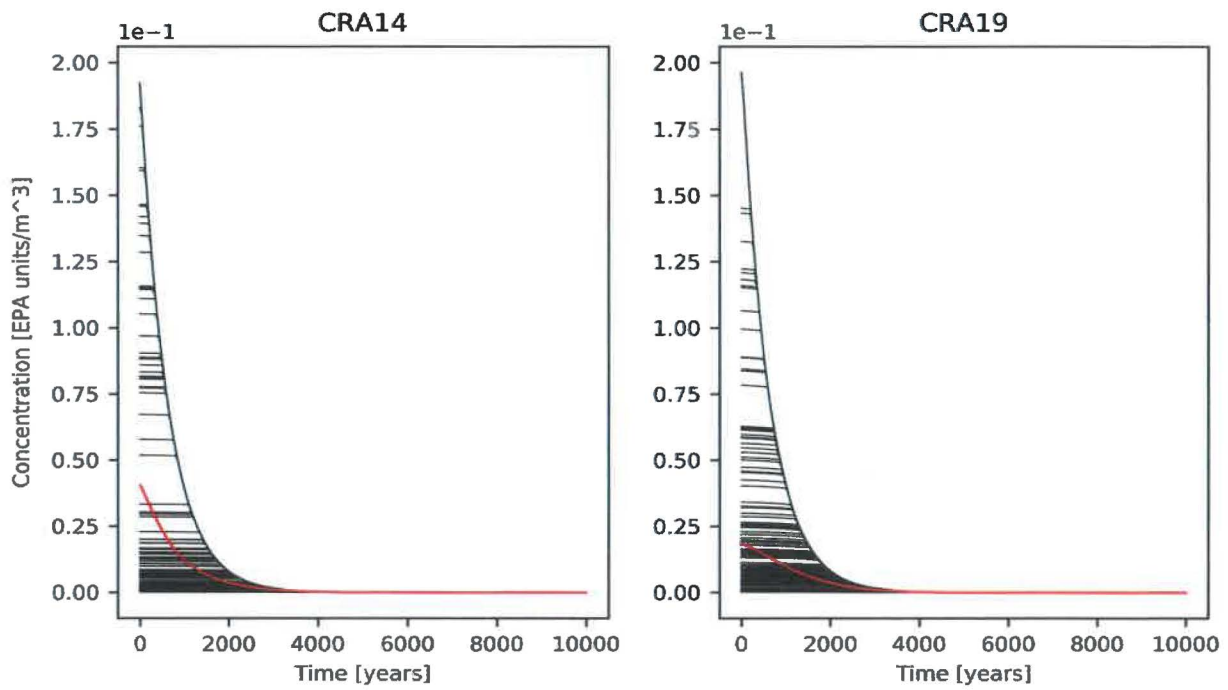


Figure 34– AM241L Concentration vs Time, Castile Brine

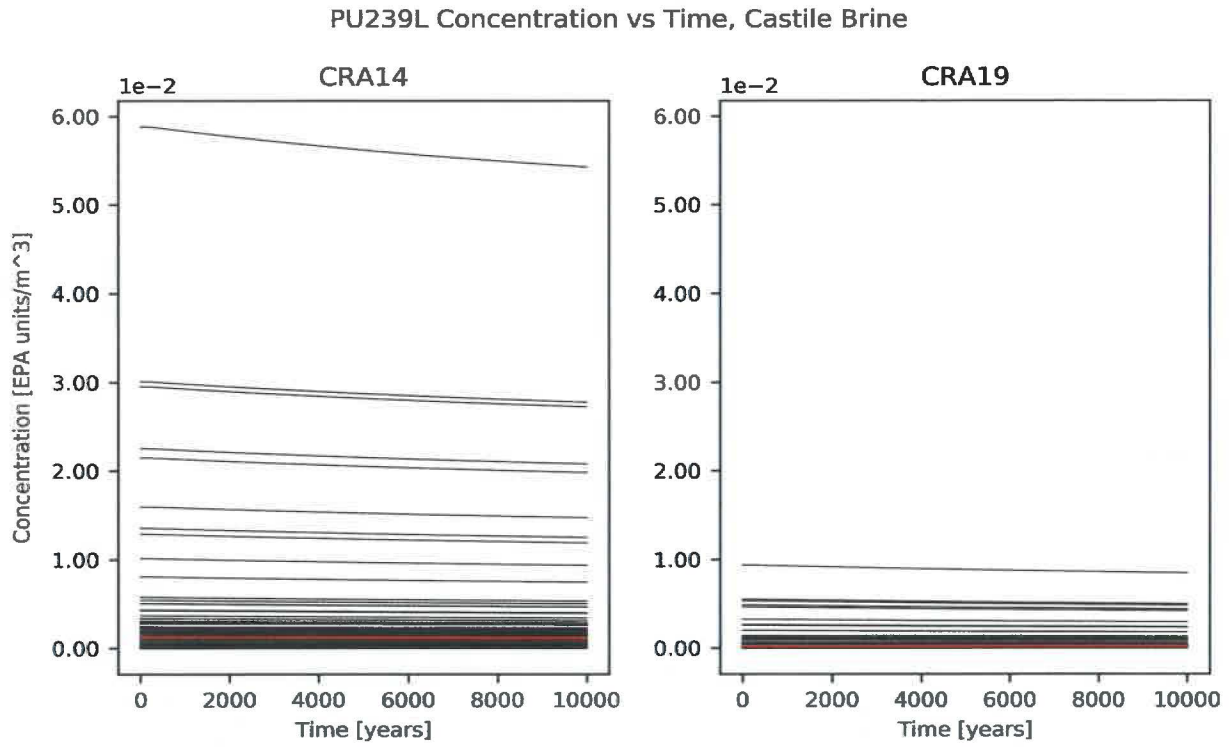


Figure 35-- PU239L Concentration vs Time, Castile Brine

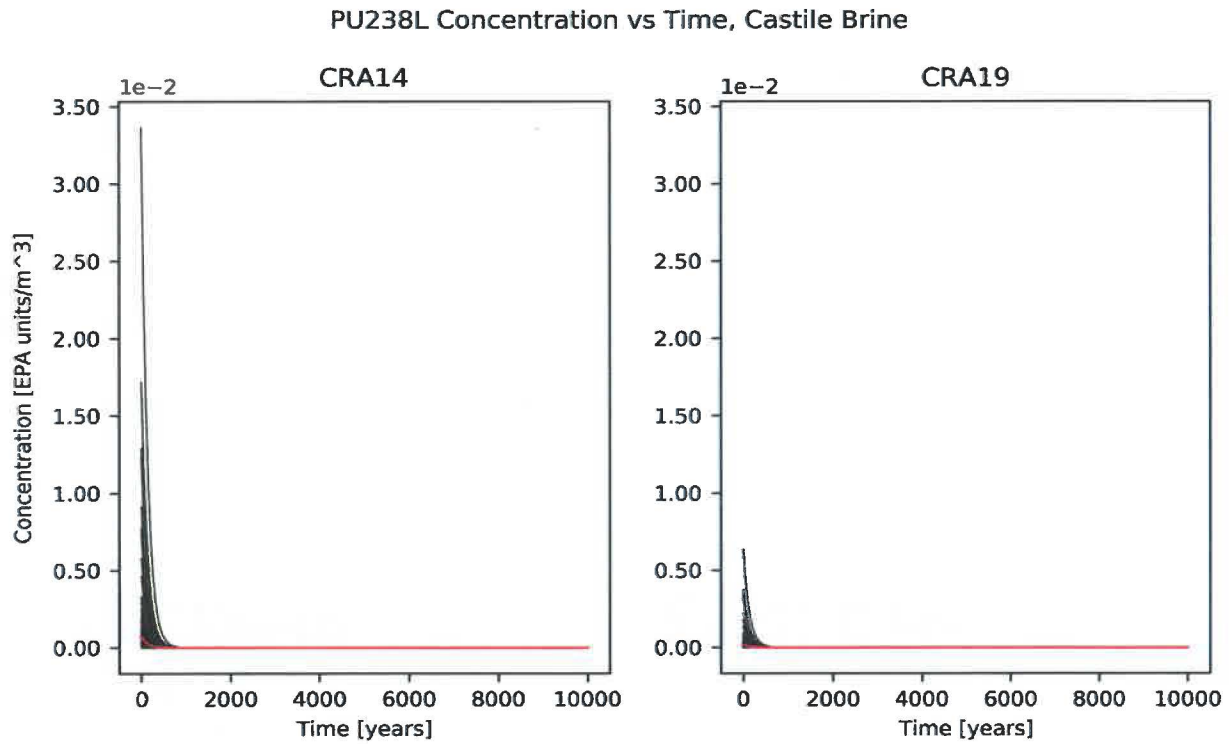


Figure 36-- PU238L Concentration vs Time, Castile Brine

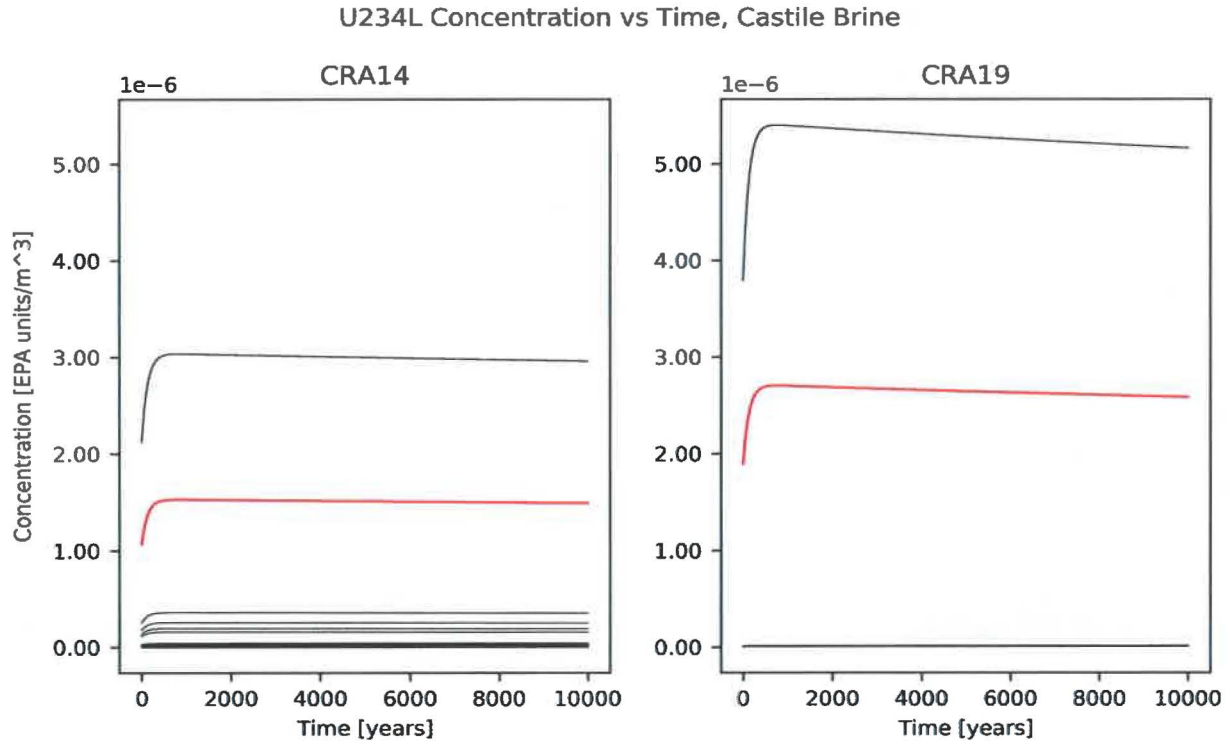


Figure 37– U234L Concentration vs Time, Castile Brine

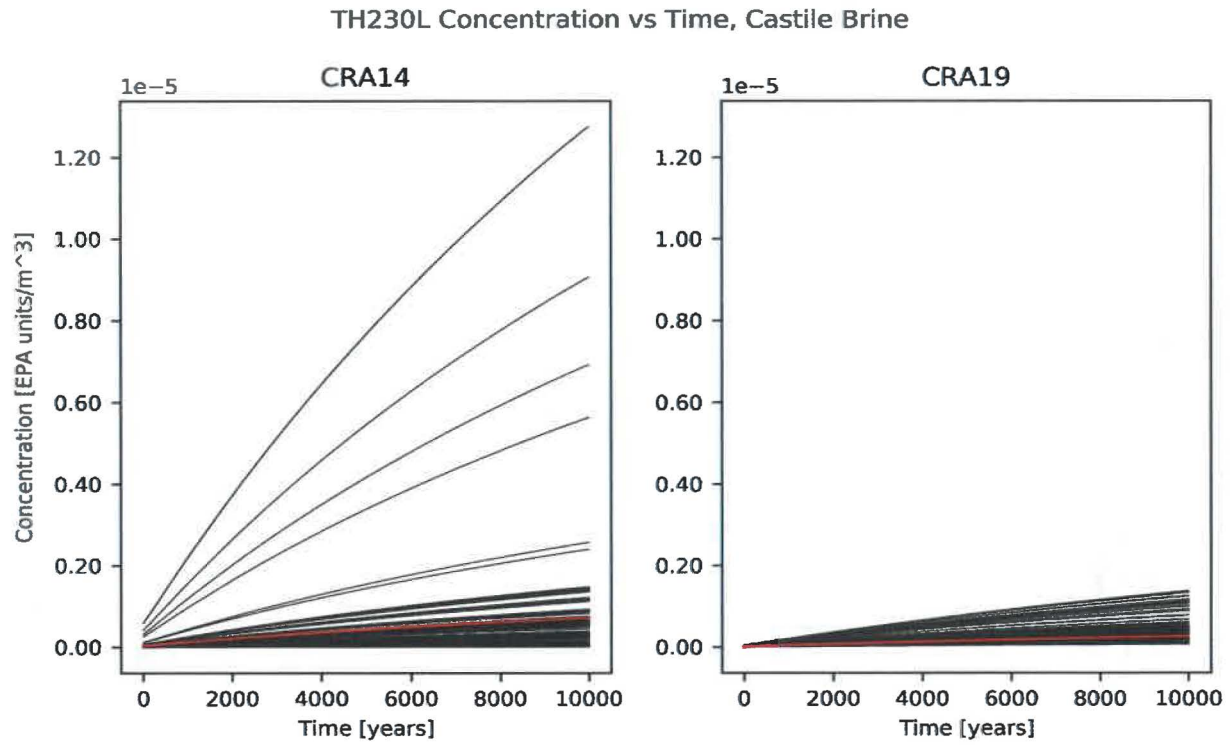


Figure 38– TH230L Concentration vs Time, Castile Brine

4.4 NUTS/PANEL Salado Transport

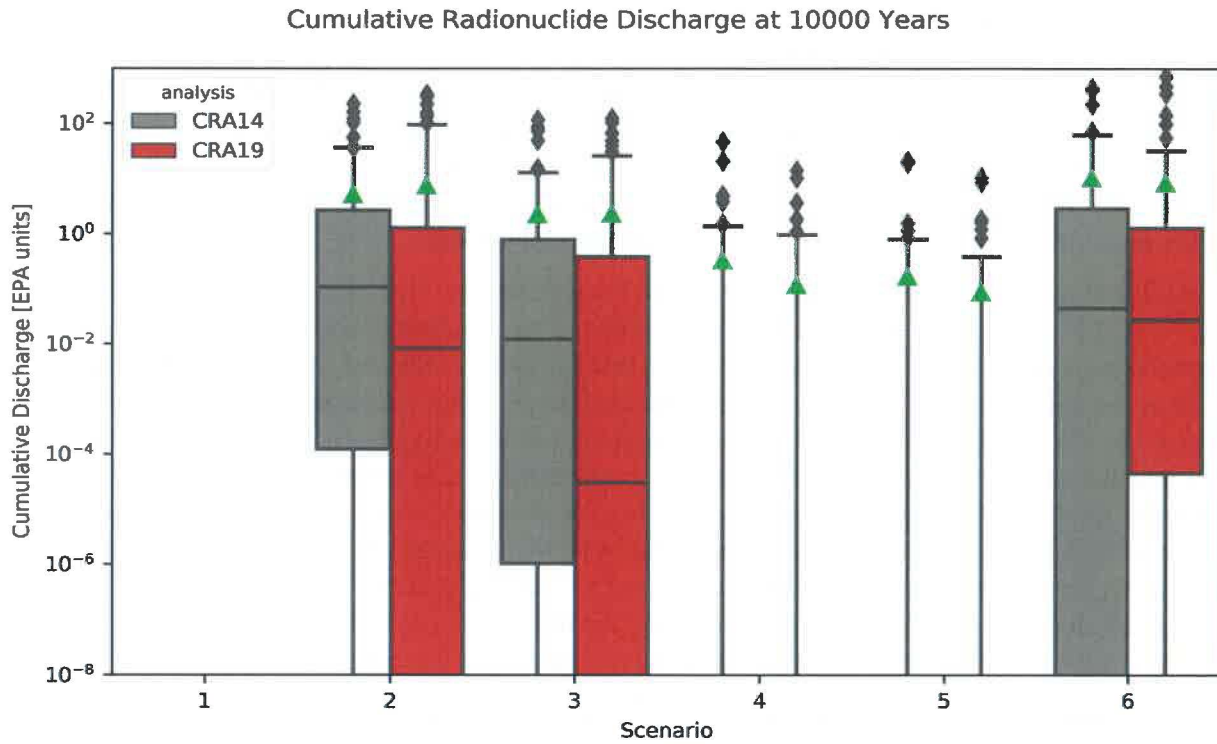


Figure 39– Cumulative Radionuclide Discharge at 10000 Years

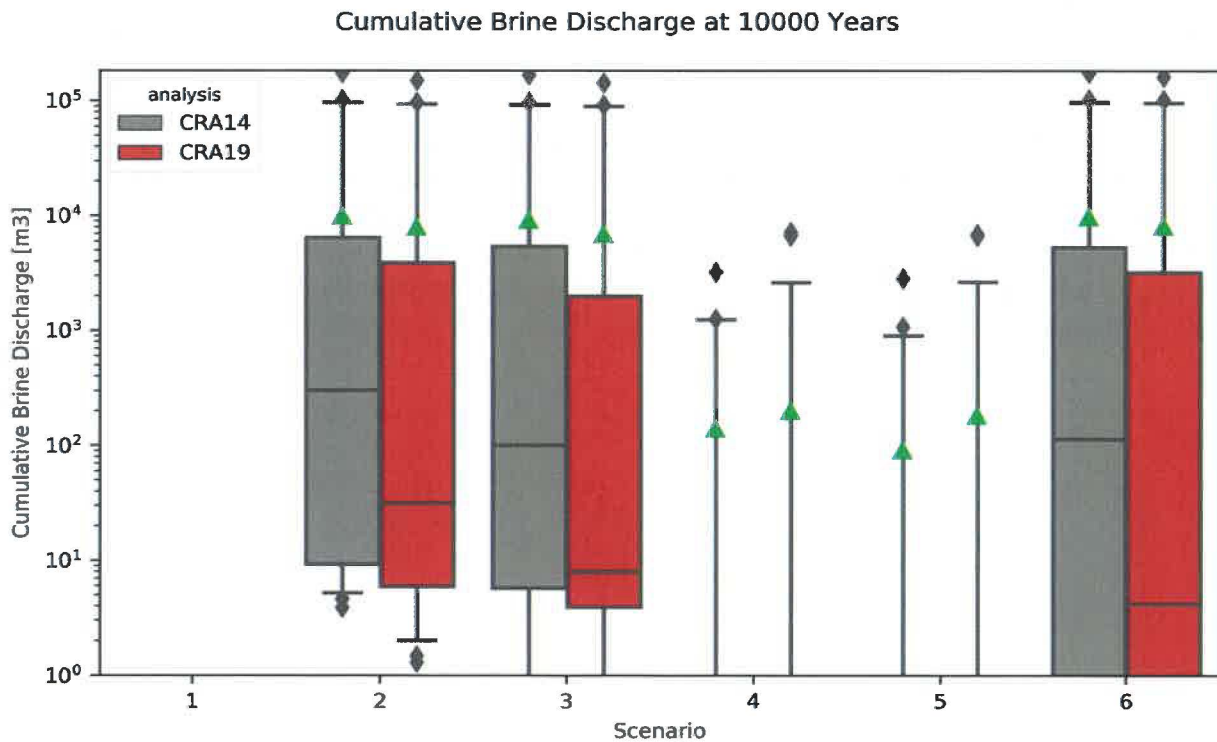


Figure 40– Cumulative Brine Discharge at 10000 Years

The total mobile concentration limits presented in Section 4.2 are also used in the radionuclide transport simulations. The code NUTS is used to model radionuclide transport in the Salado for scenarios 1-5 (the discrete BRAGFLO scenarios with zero or one borehole intrusions), and the code PANEL is used for scenario 6 (the discrete scenario with a sequence of two borehole intrusions). Both codes rely on BRAGFLO simulation results for brine flux and brine volume data. The cumulative discharges up the borehole are tabulated and comprise the *to Culebra* discharges. These are the source for the *from Culebra* releases. For scenarios 1-5, the radionuclide discharge through the shaft and the radionuclide discharge through the anhydrite marker beds (all three combined) to the LWB are also tabulated.

For the Undisturbed Scenario (scenario 1), one vector produced a nonzero discharge through the shaft of $1e-133$ EPA units, which is within the noise of the numerical methods. The maximum (across vectors) discharge through all anhydrite marker beds combined was $3e-10$ EPA units, which is insignificant compared to other release pathways. Thus calculated long term releases through the shaft and anhydrite marker beds continue to be negligible for the CRA-2019. For the disturbed scenarios 2-5, the results are similar. Radionuclide discharges through the shaft were within the noise of the numerical methods (the largest computed value was $\sim 1e-39$ EPA units, but most results were identically zero), and radionuclide discharges through the anhydrite marker beds across the LWB were insignificant compared to other release pathways (the largest computed value was $\sim 2e-7$ EPA units, and again the most of the results were zero). The remainder of the discussion focuses on cumulative discharges through the borehole.

Figure 39 illustrates the cumulative (over 10,000 years) total radionuclide discharge through the borehole for each scenario, and Figure 40 illustrates the cumulative brine discharge through the borehole (computed by BRAGFLO, see Day 2019; for consistency, the brine discharges tabulated just below MB138 are compared as per Garner 2003) for each scenario. Because high consequence radionuclide solubilities are not correlated with high consequence brine discharges, the results are mixed. Overall, the mean radionuclide discharges are similar for the Castile brine pocket intrusion scenarios (scenarios 2, 3, and 6), but the median has decreased while the high-consequence outliers have increased. A somewhat similar trend is apparent in the brine discharges (though the outliers have slightly decreased). The means and outlier radionuclide discharges for scenarios 4 and 5 have slightly decreased, which is contrary to that observed for the brine discharges. However, because there are few simulations in scenarios 4 and 5 with meaningful brine discharges, the change in radionuclide discharges is likely influenced by this small population size more than other phenomena. There is no borehole intrusion for scenario 1.

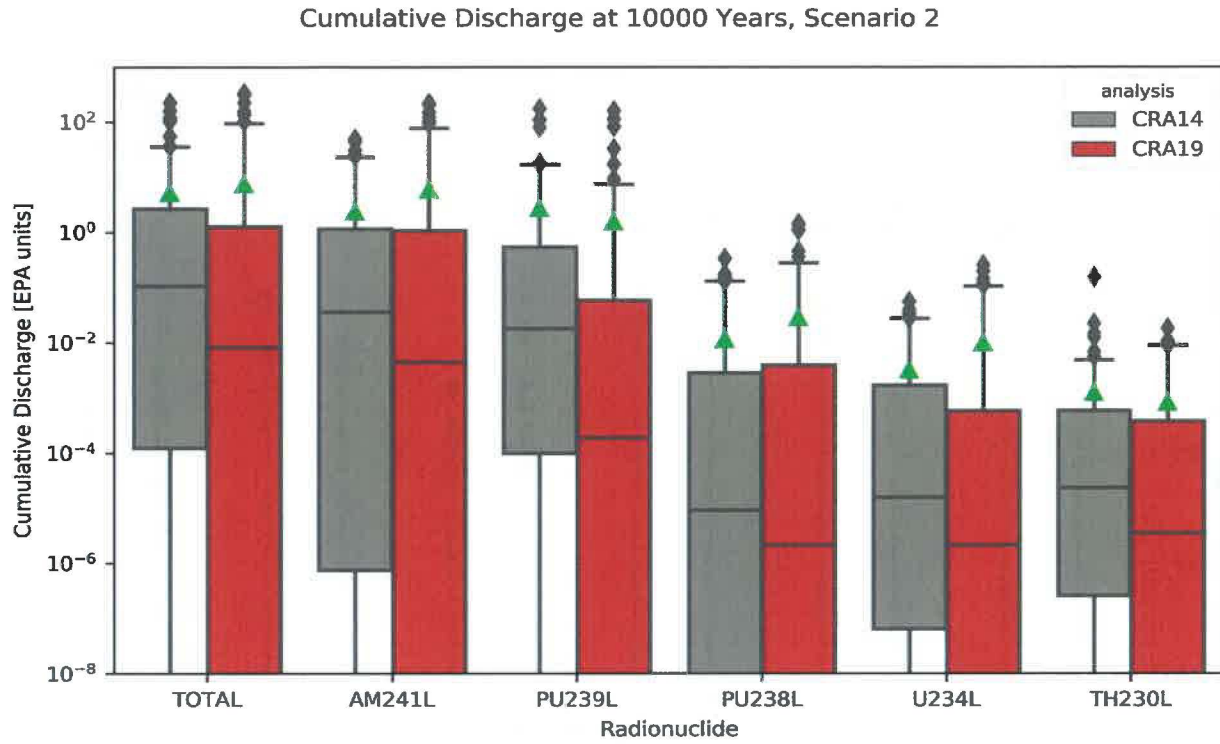


Figure 41– Cumulative Discharge at 10000 Years, Scenario 2

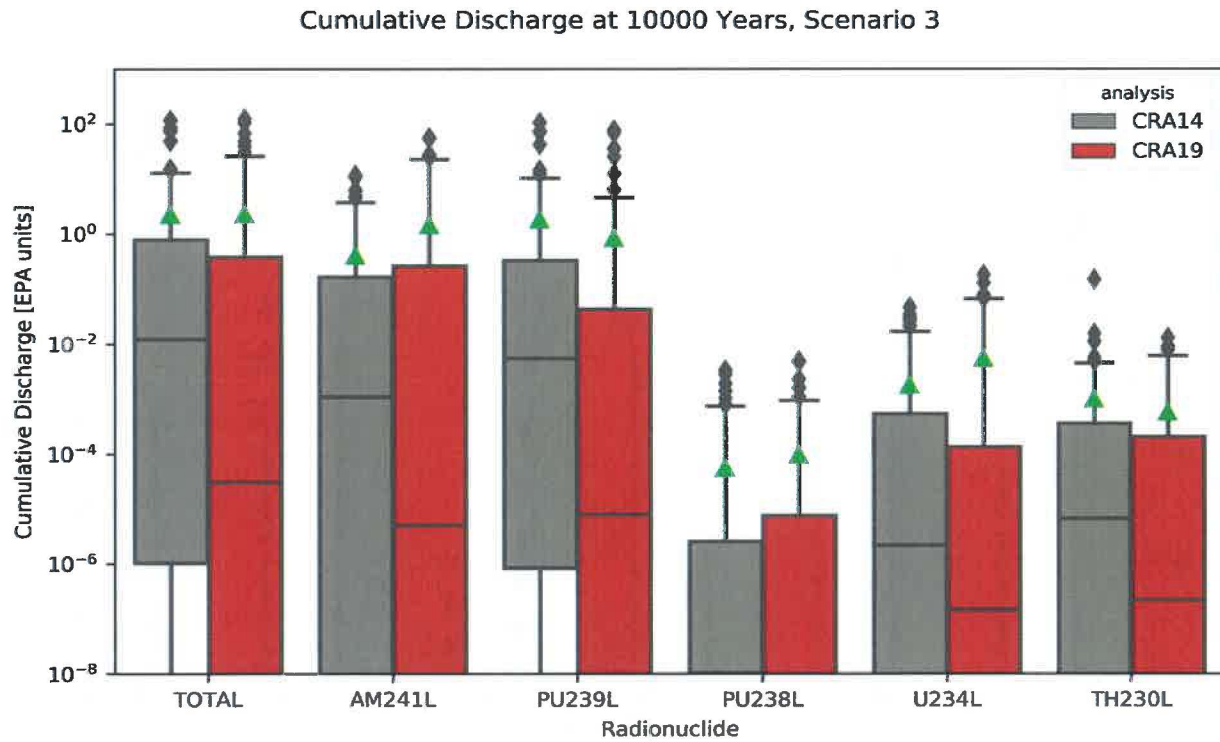


Figure 42– Cumulative Discharge at 10000 Years, Scenario 3

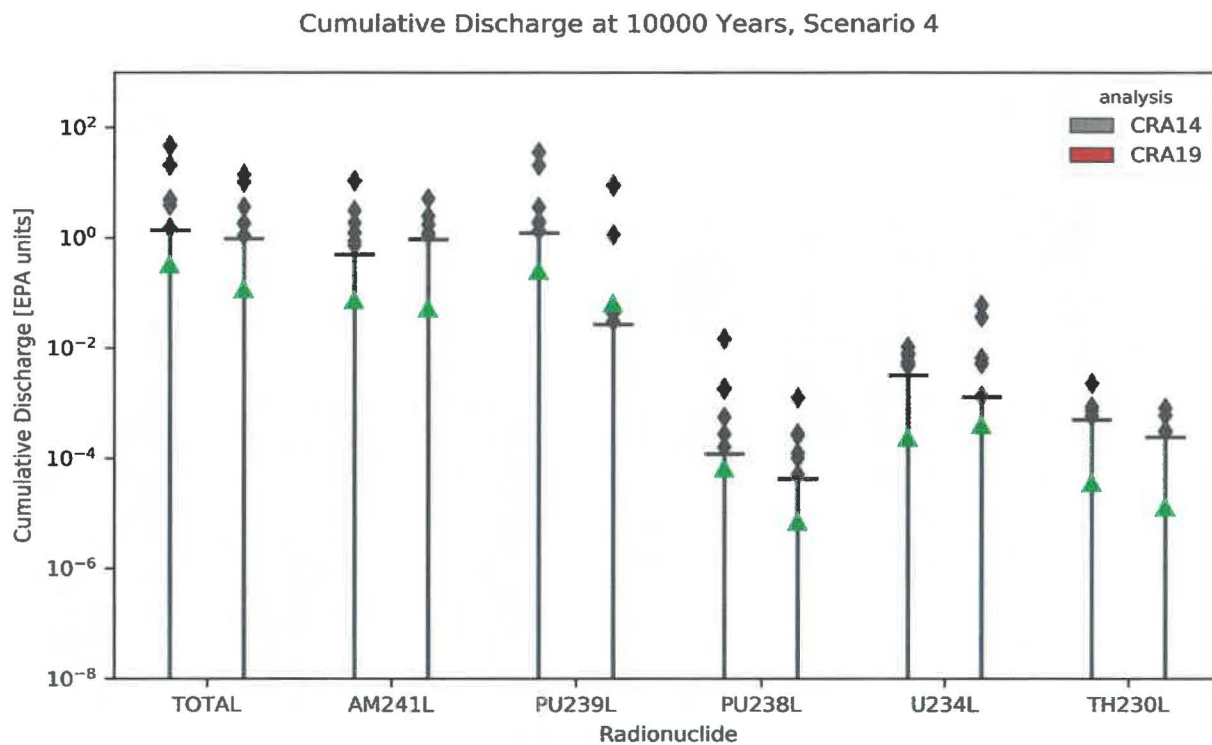


Figure 43– Cumulative Discharge at 10000 Years, Scenario 4

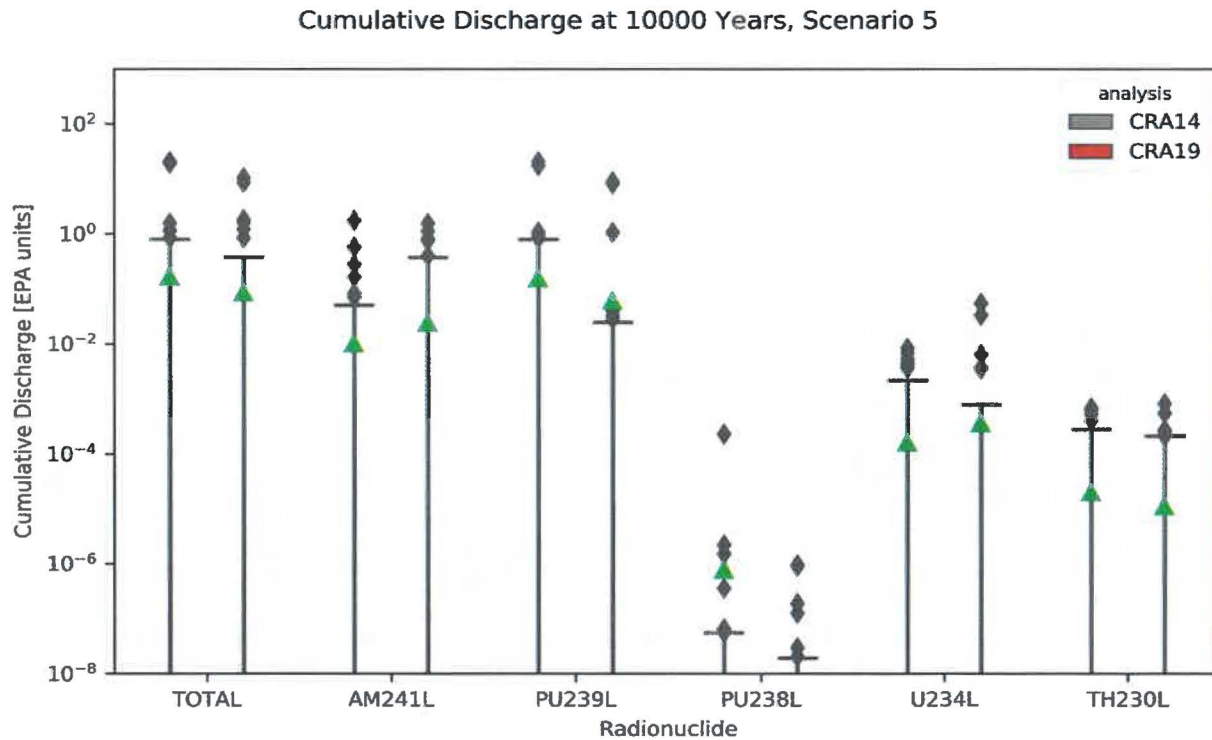


Figure 44– Cumulative Discharge at 10000 Years, Scenario 5

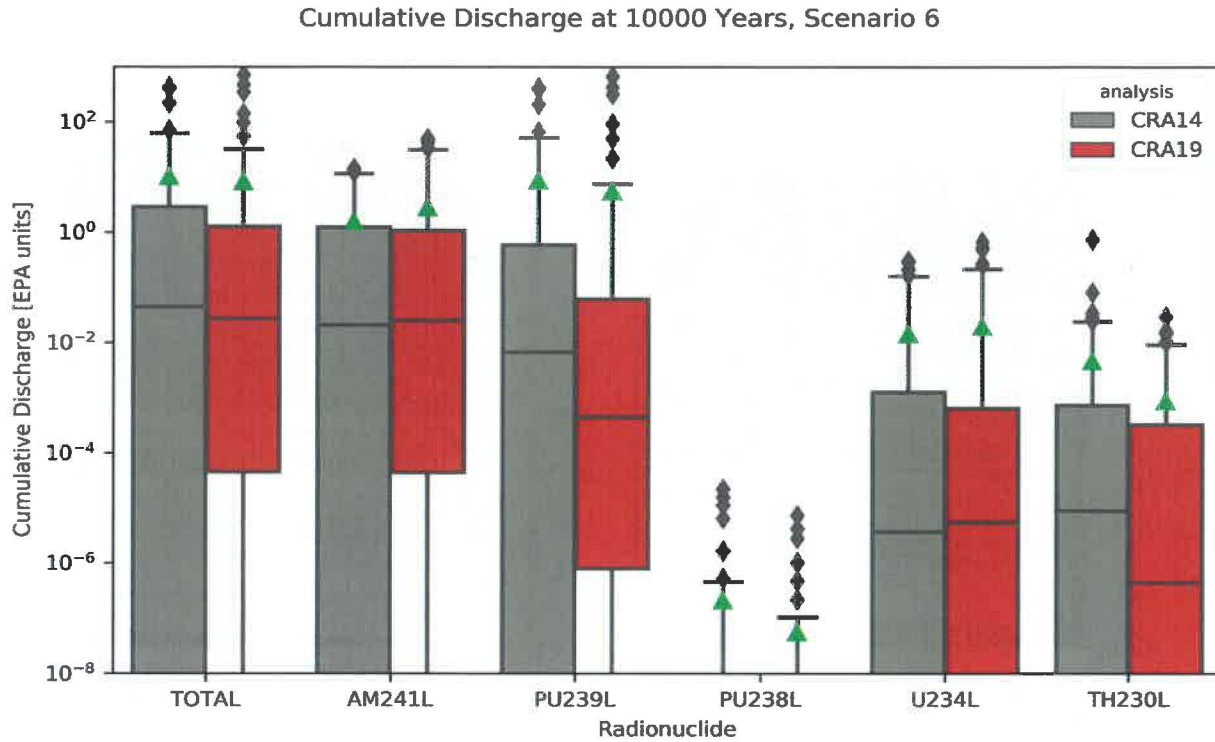


Figure 45– Cumulative Discharge at 10000 Years, Scenario 6

Figure 41 through Figure 45 show the cumulative radionuclide discharges at year 10,000 for each lumped radionuclide, for scenarios 2 through 6. It is important to note that the boxplots summarize each radionuclide distribution independently, whereas the boxplot for the “total” radionuclide discharge summarizes the distribution of sums. The means (indicated by the green triangles) are typically larger than the 75th percentile values, which indicates that they are dominated by a few simulations with large discharge values (the outliers). In general, U234L cumulative discharges (means and outliers) have increased due to the increase in its isotope-to-element mole fraction. This is significant because U(VI) is assumed to have low adsorption (i.e. low linear matrix partition coefficients, MKD0) in the Culebra, and thus is more likely to reach the LWB in the Culebra.

Because the full time-history of the *to Culebra* cumulative radionuclide discharges is used to compute *from Culebra* releases, the horsetail plots are shown for each lumped radionuclide for each of scenarios 2 through 6 in Figure 46 through Figure 65. For most simulations, especially in scenarios 2 and 3, the majority of the discharge occurs in the first few hundred years after the borehole plug degrades (which is assumed to occur 200 years after the intrusion). For scenario 6, where an E2 (non-brine-pocket penetrating) intrusion occurs at year 1000 and an E1 (brine-pocket-penetrating) intrusion occurs at year 2000, most of the discharges occur after the E1 intrusion. A few of the scenario 6 simulations show small discharges occurring prior to the year 1000 intrusion. This is an artifact of the location used to tabulate brine discharges. For scenario 6, this location is in the BRAGFLO grid layer just below Marker Bed 138 (not the layer just below the Culebra, which is the location used for scenarios 1-5) (Garner 2003). This pre-intrusion-time discharge is indicating movement of brine between the repository/DRZ and MB138.

AM241L Cumulative Discharge vs Time, Scenario 2

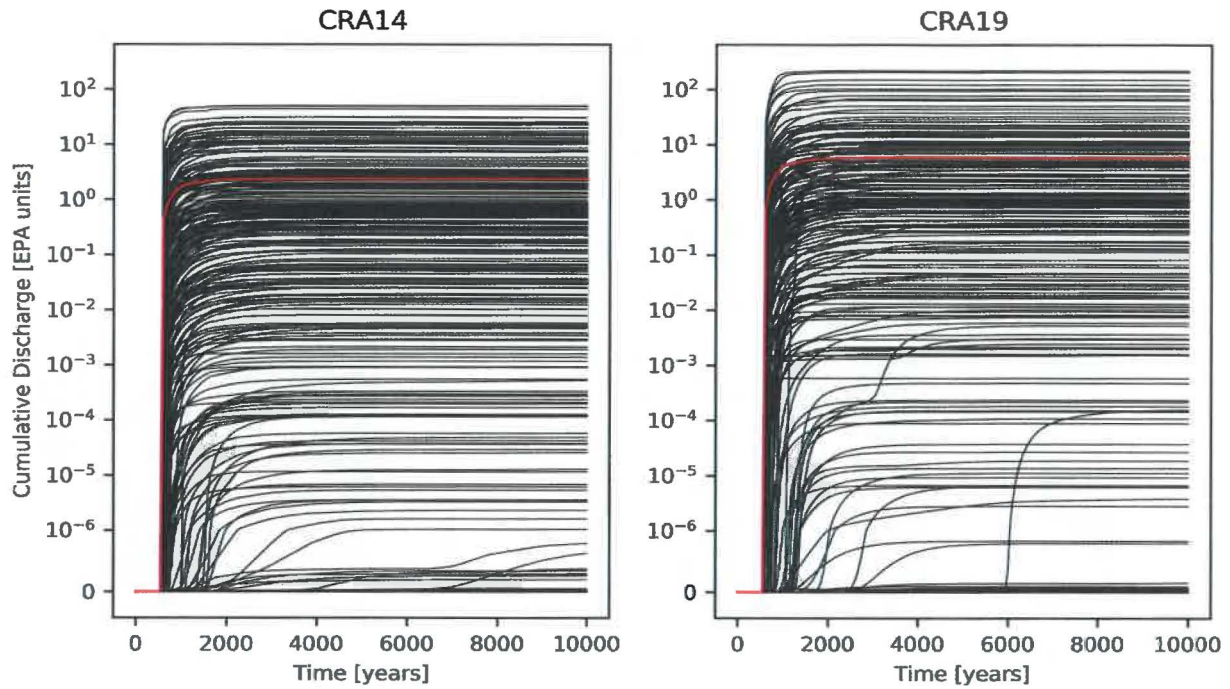


Figure 46– AM241L Cumulative Discharge vs Time, Scenario 2

PU239L Cumulative Discharge vs Time, Scenario 2

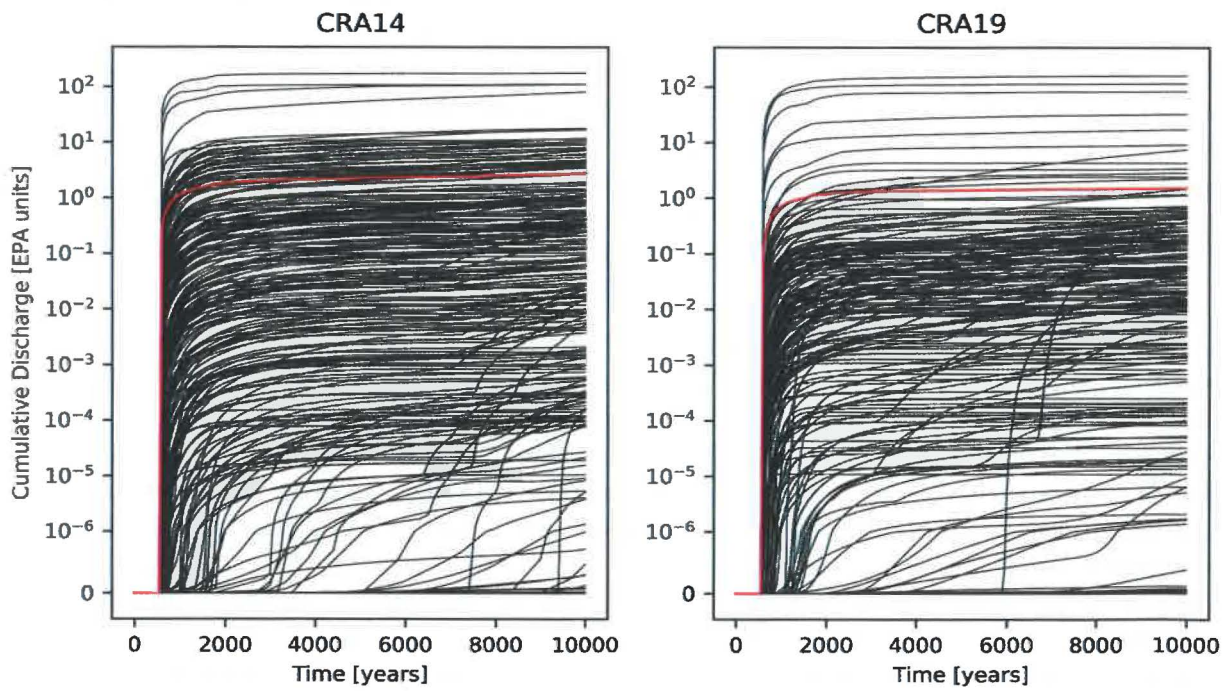


Figure 47– PU239L Cumulative Discharge vs Time, Scenario 2

U234L Cumulative Discharge vs Time, Scenario 2

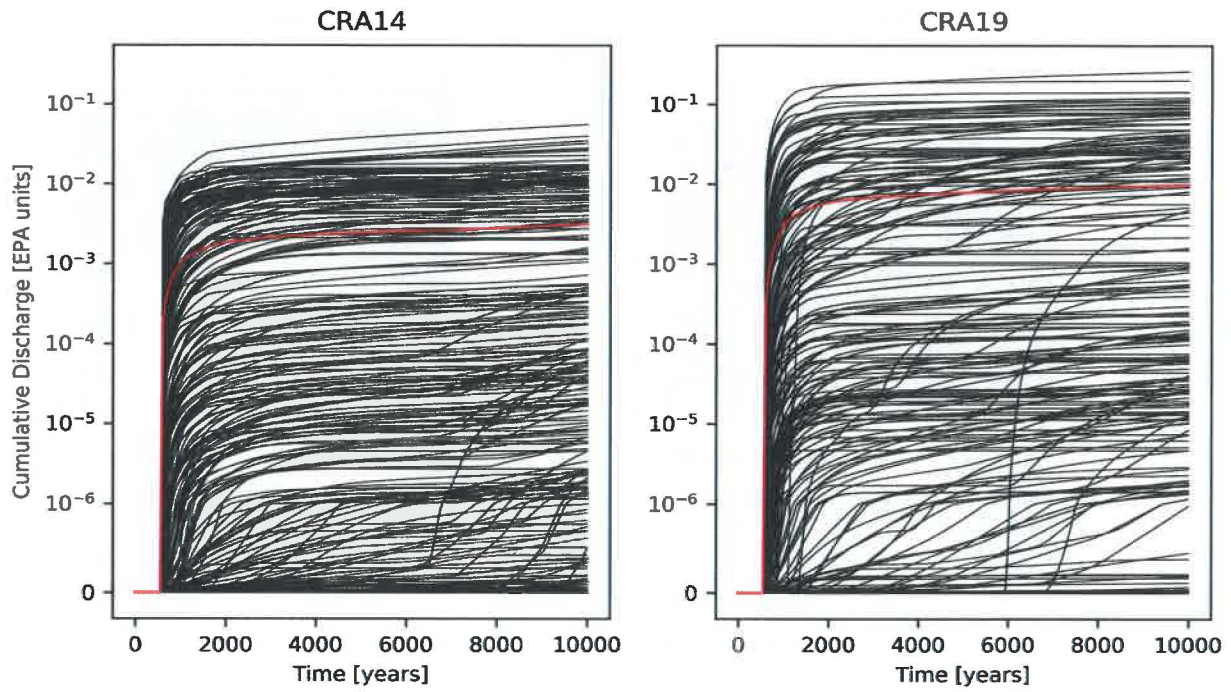


Figure 48-- U234L Cumulative Discharge vs Time, Scenario 2

TH230L Cumulative Discharge vs Time, Scenario 2

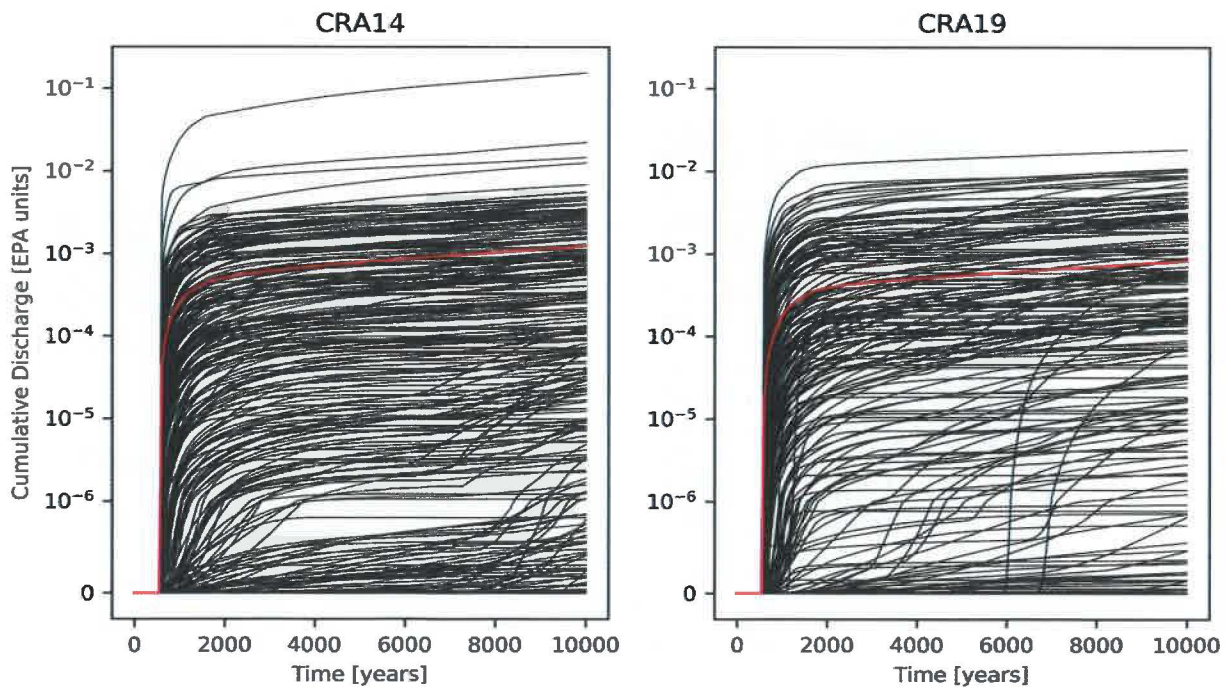


Figure 49-- TH230L Cumulative Discharge vs Time, Scenario 2

AM241L Cumulative Discharge vs Time, Scenario 3

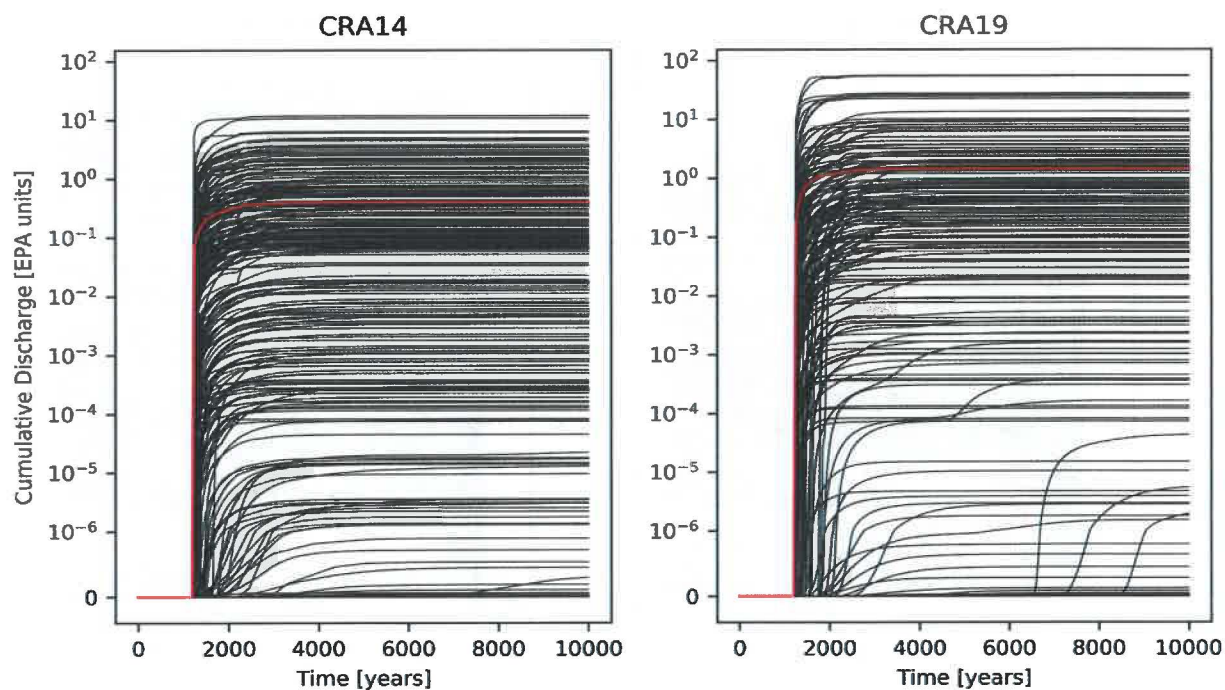


Figure 50– AM241L Cumulative Discharge vs Time, Scenario 3

PU239L Cumulative Discharge vs Time, Scenario 3

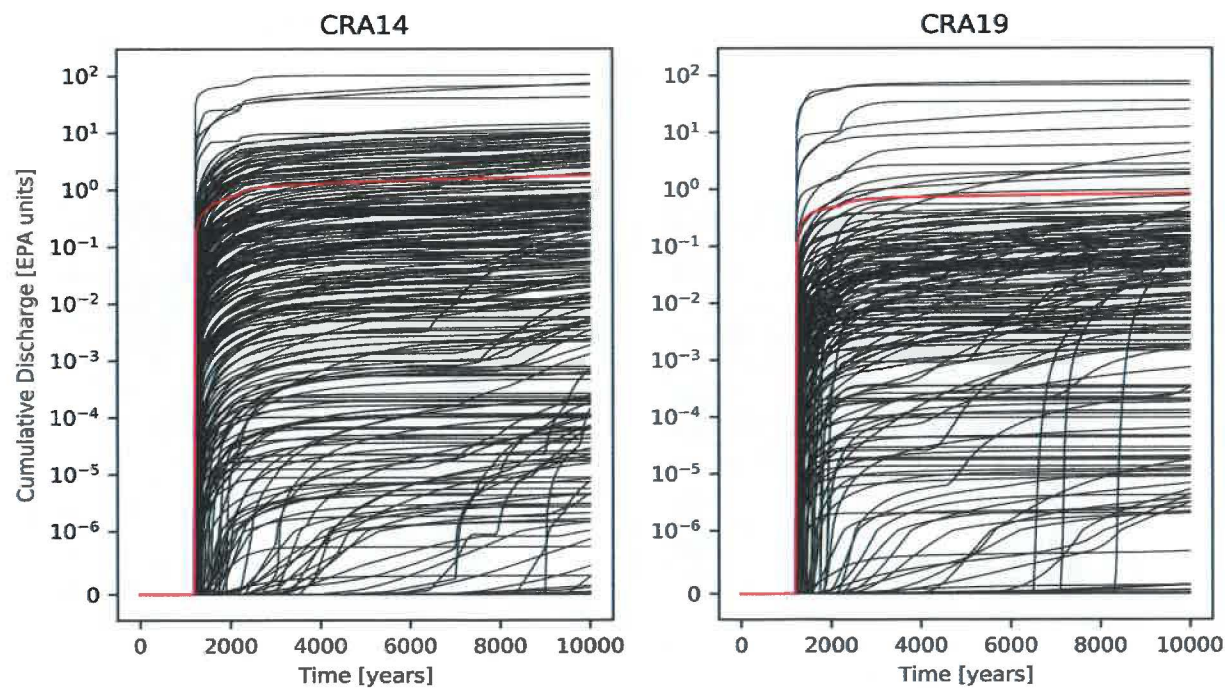


Figure 51– PU239L Cumulative Discharge vs Time, Scenario 3

U234L Cumulative Discharge vs Time, Scenario 3

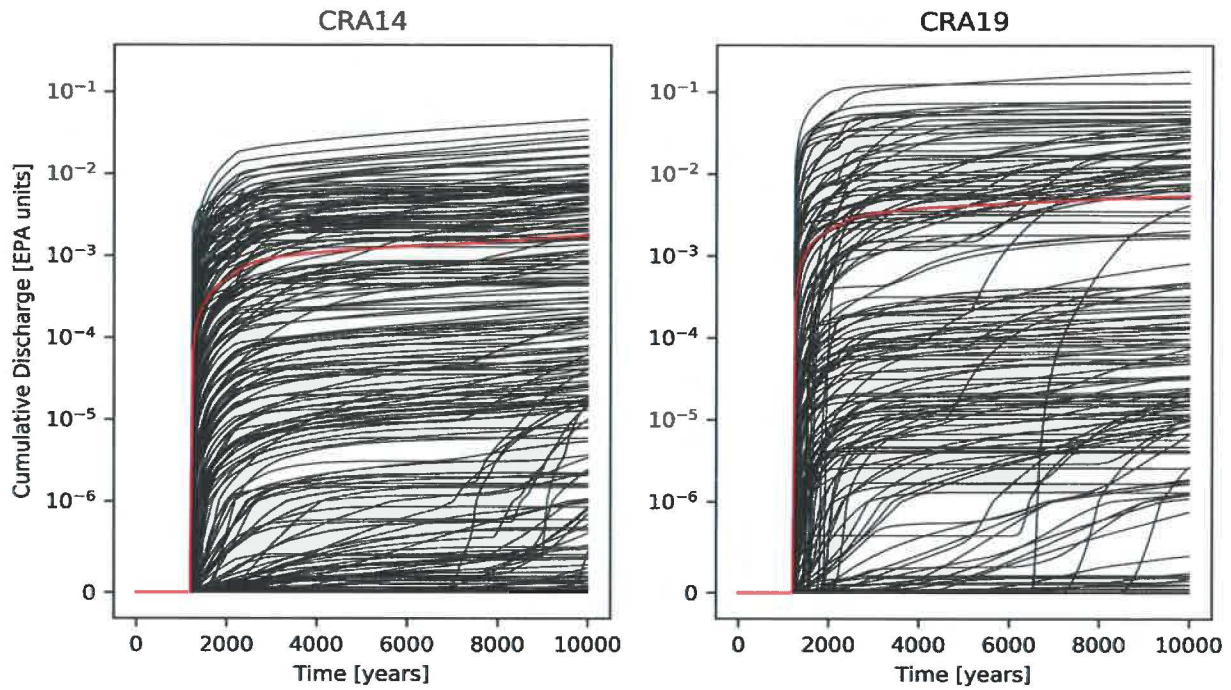


Figure 52– U234L Cumulative Discharge vs Time, Scenario 3

TH230L Cumulative Discharge vs Time, Scenario 3

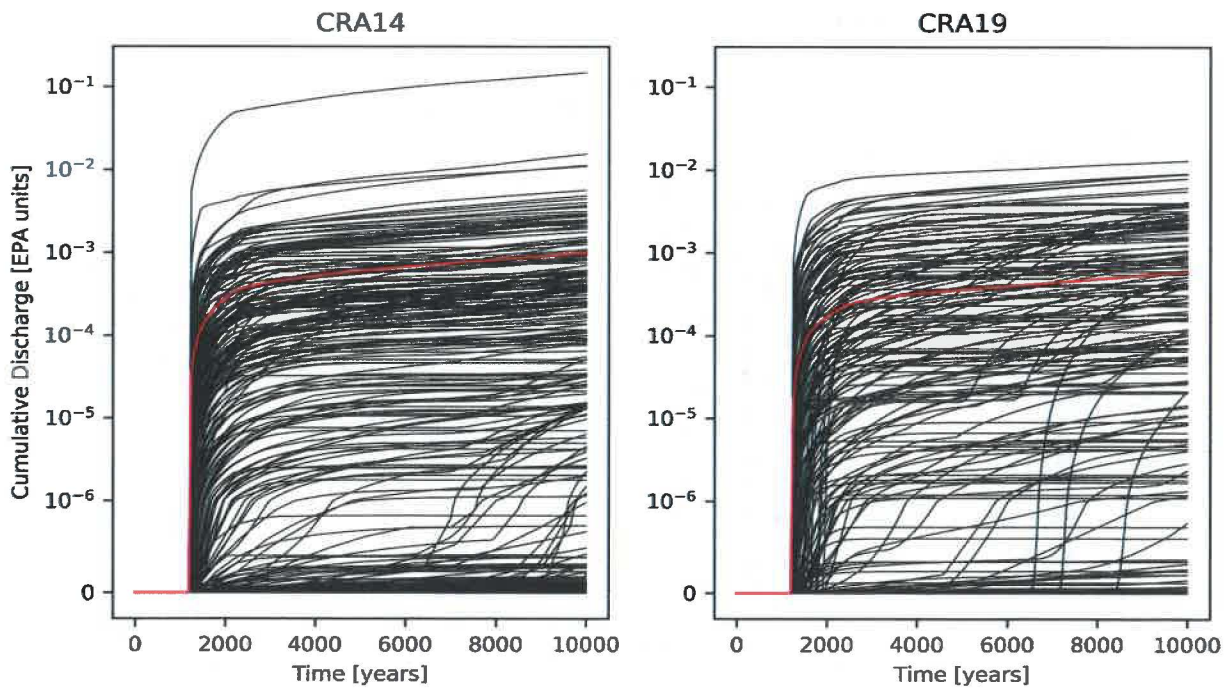


Figure 53– TH230L Cumulative Discharge vs Time, Scenario 3

AM241L Cumulative Discharge vs Time, Scenario 4

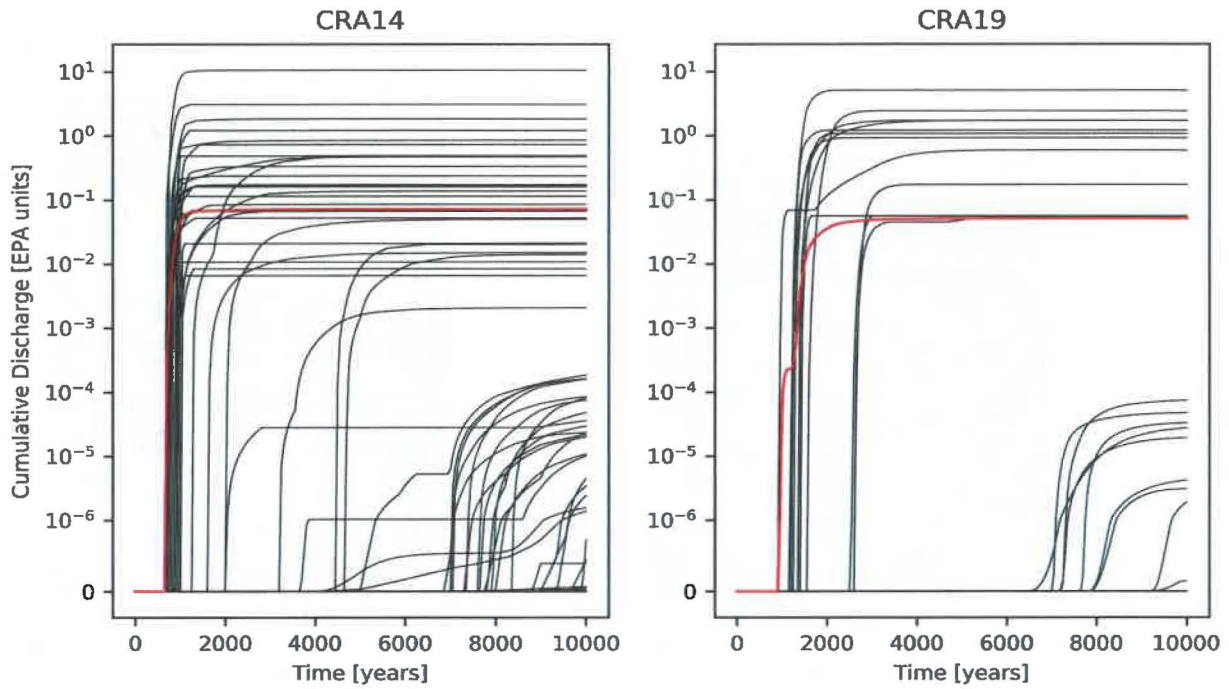


Figure 54– AM241L Cumulative Discharge vs Time, Scenario 4

PU239L Cumulative Discharge vs Time, Scenario 4

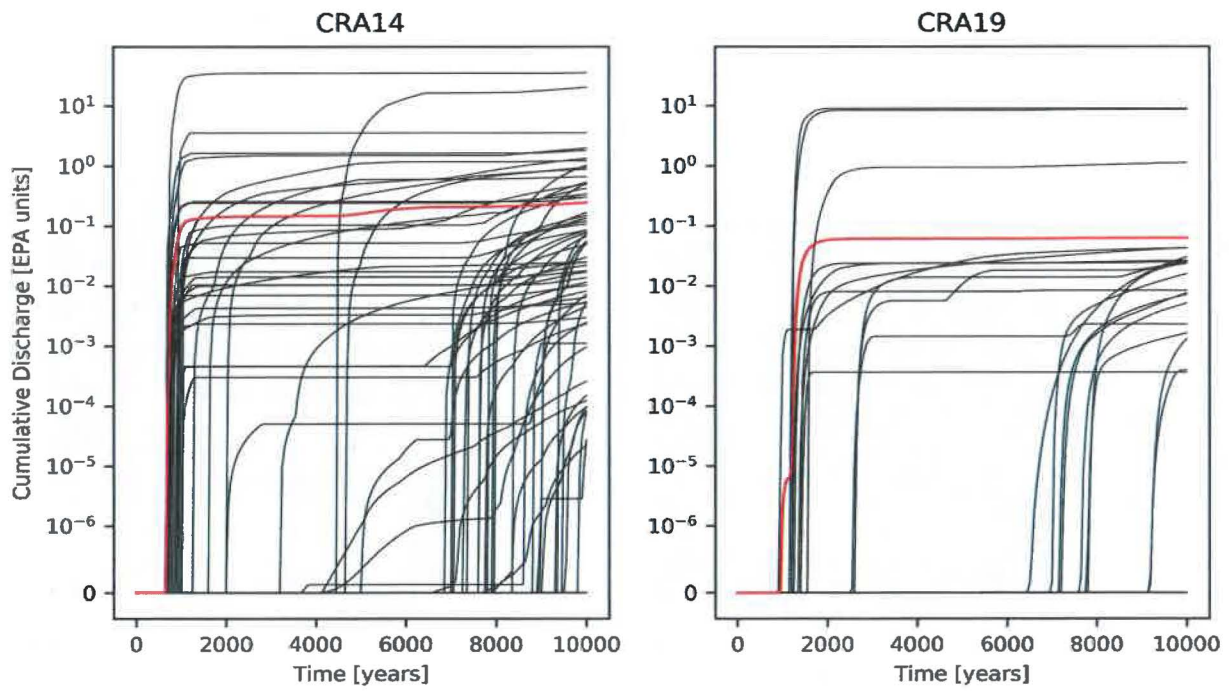


Figure 55– PU239L Cumulative Discharge vs Time, Scenario 4

U234L Cumulative Discharge vs Time, Scenario 4

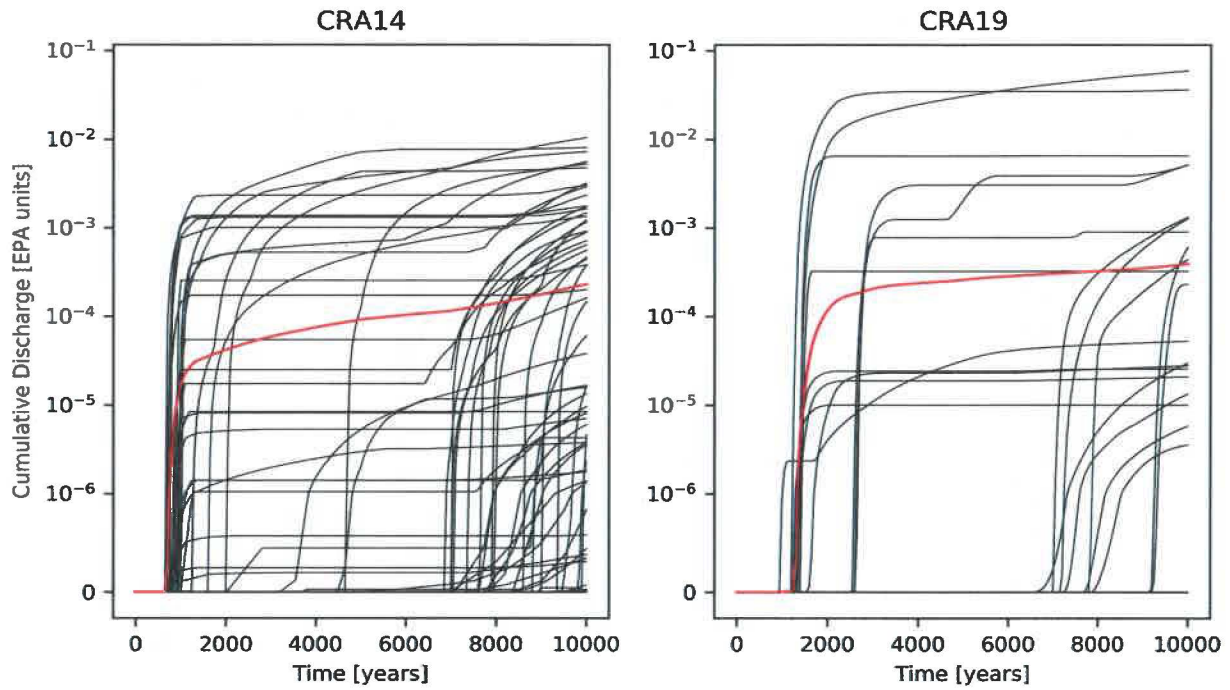


Figure 56– U234L Cumulative Discharge vs Time, Scenario 4

TH230L Cumulative Discharge vs Time, Scenario 4

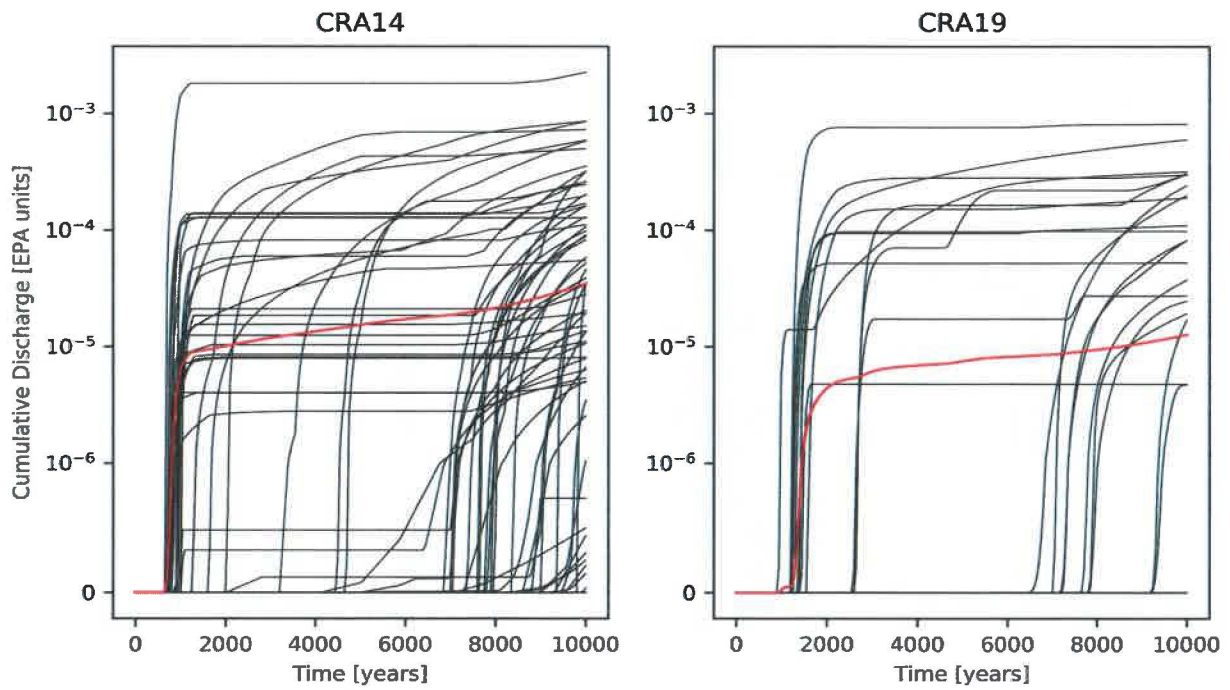


Figure 57– TH230L Cumulative Discharge vs Time, Scenario 4

AM241L Cumulative Discharge vs Time, Scenario 5

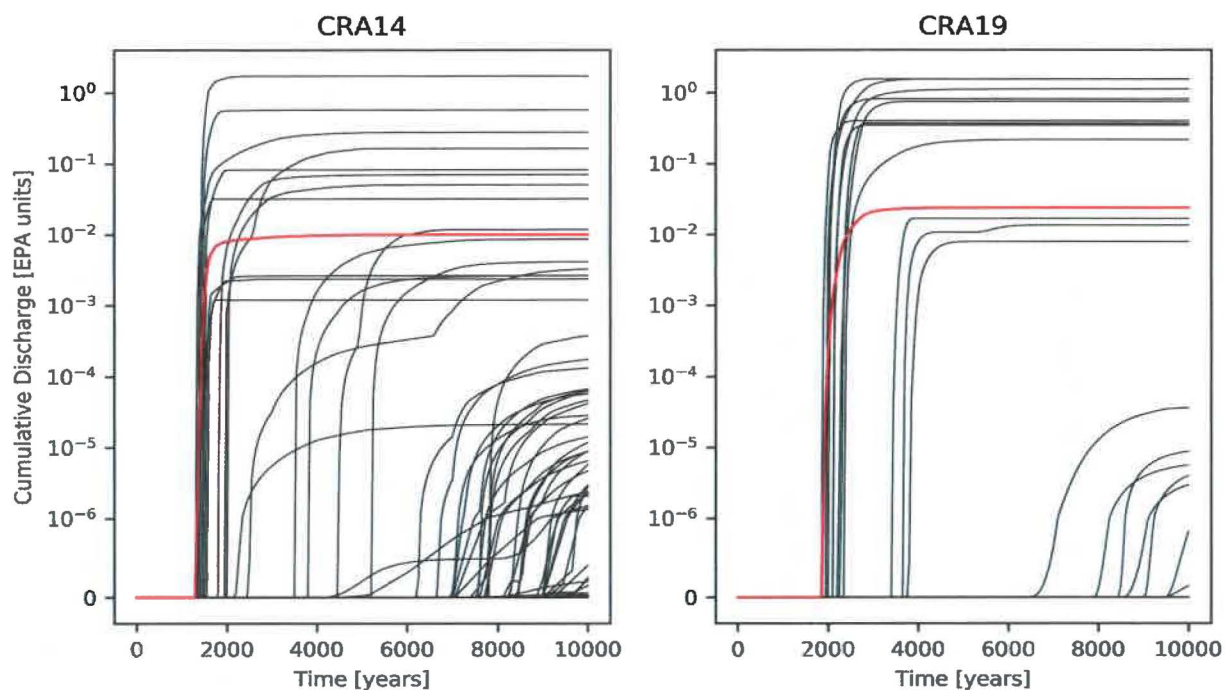


Figure 58– AM241L Cumulative Discharge vs Time, Scenario 5

PU239L Cumulative Discharge vs Time, Scenario 5

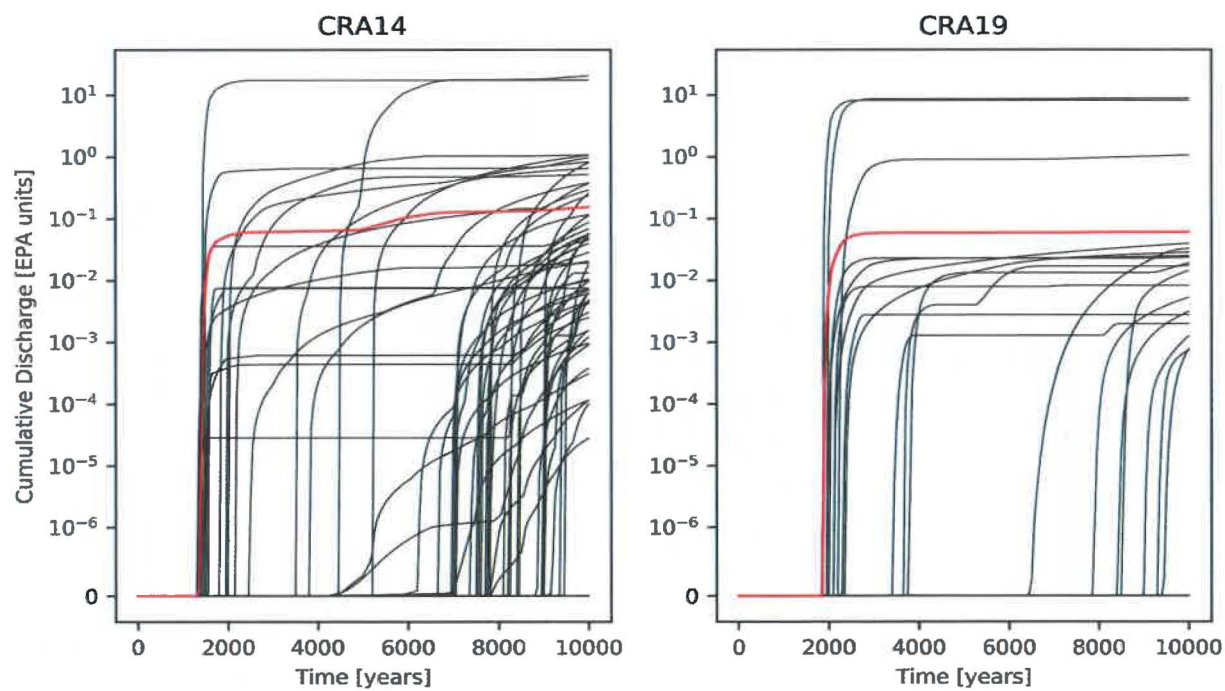


Figure 59– PU239L Cumulative Discharge vs Time, Scenario 5

U234L Cumulative Discharge vs Time, Scenario 5

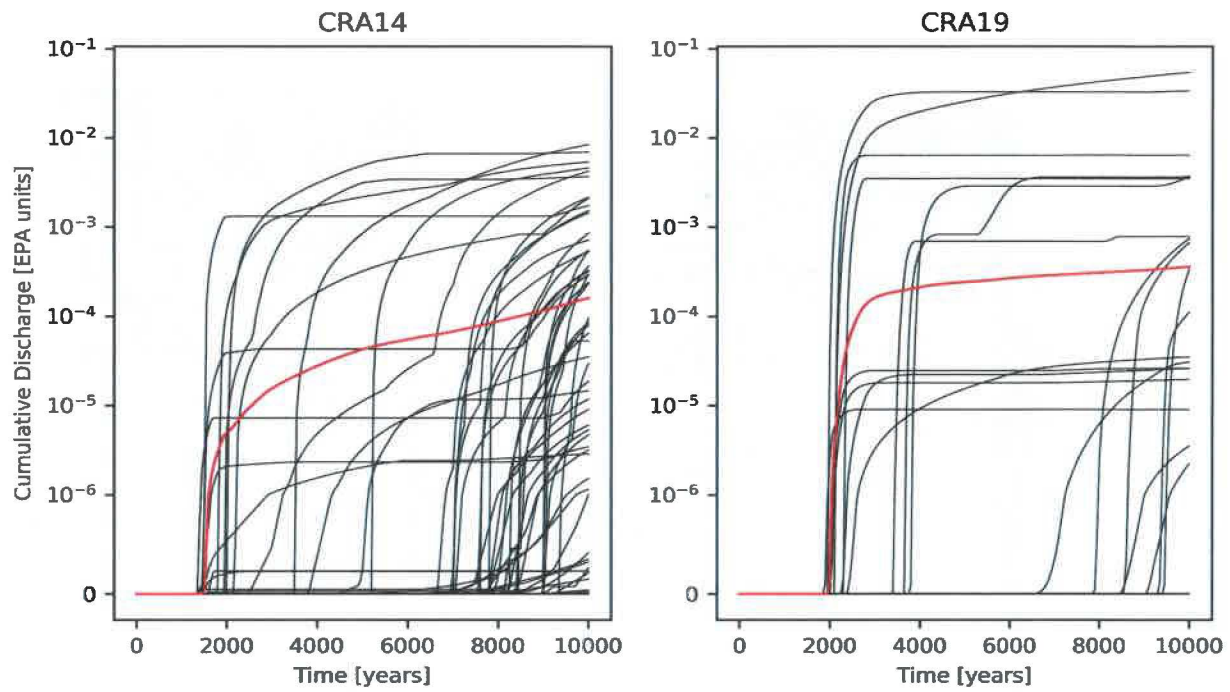


Figure 60– U234L Cumulative Discharge vs Time, Scenario 5

TH230L Cumulative Discharge vs Time, Scenario 5

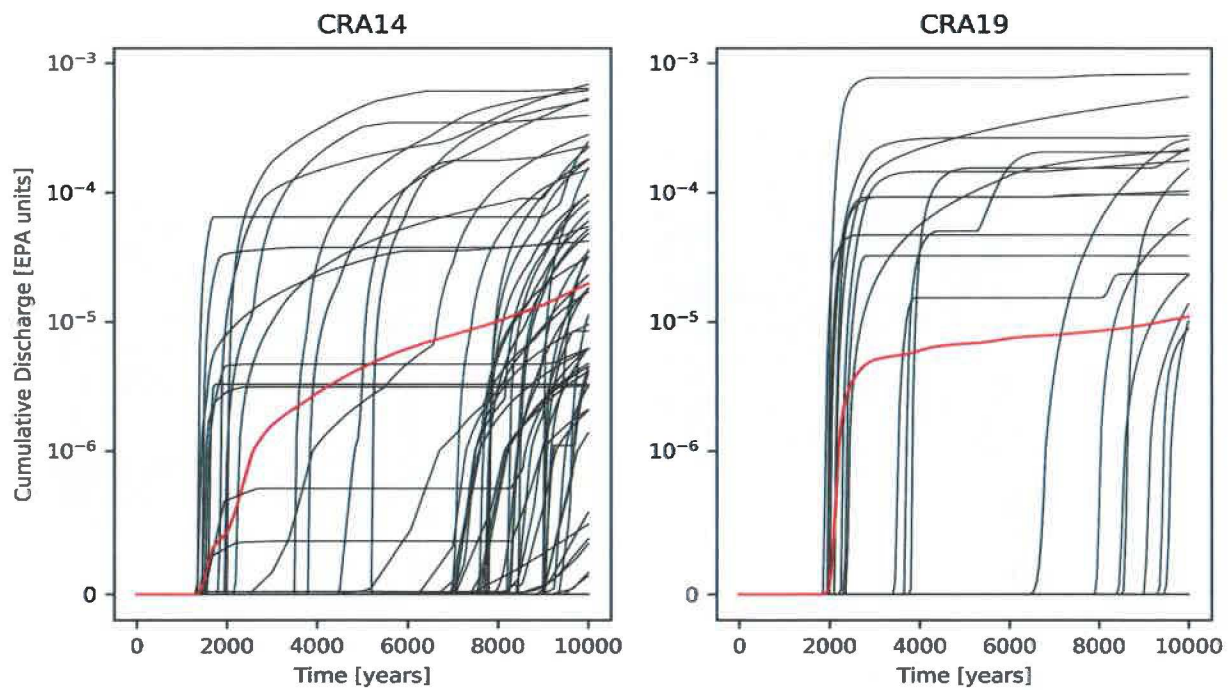


Figure 61– TH230L Cumulative Discharge vs Time, Scenario 5

AM241L Cumulative Discharge vs Time, Scenario 6

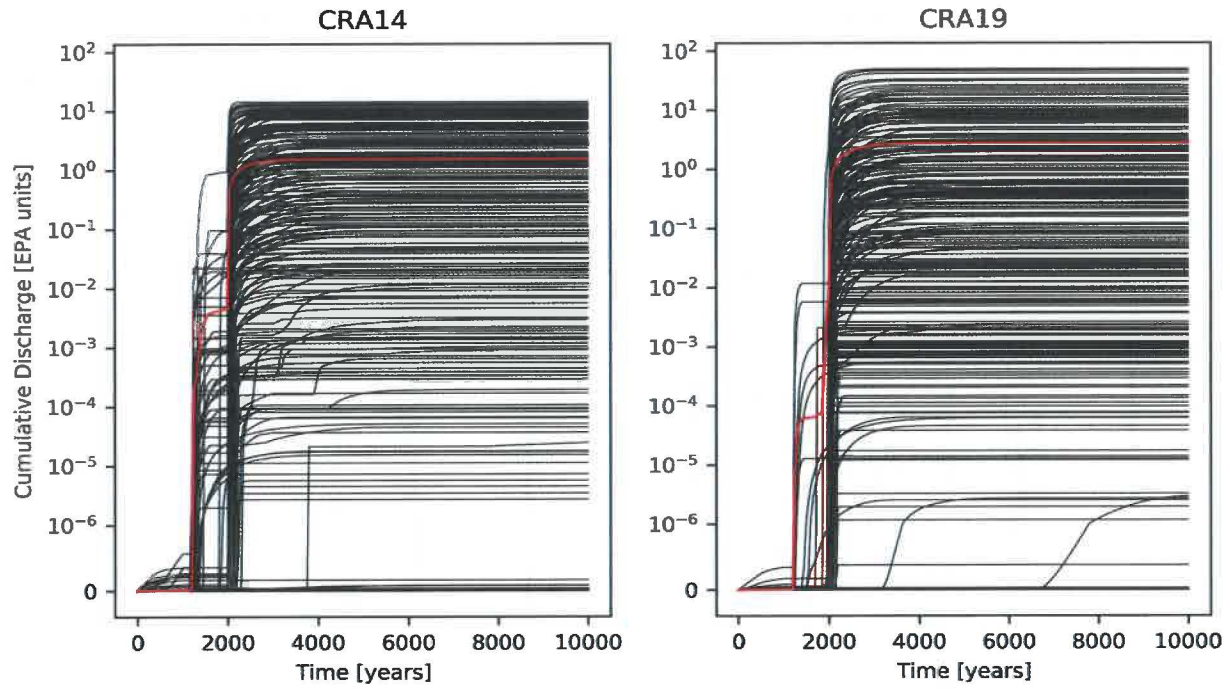


Figure 62– AM241L Cumulative Discharge vs Time, Scenario 6

PU239L Cumulative Discharge vs Time, Scenario 6

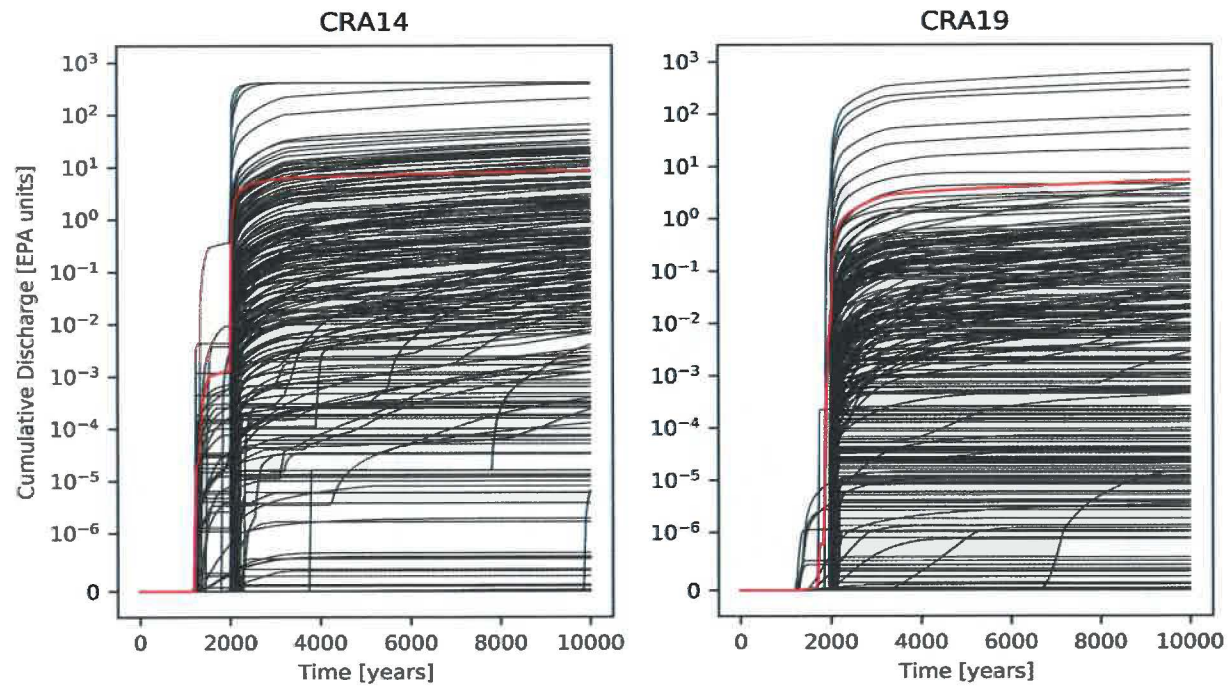


Figure 63– PU239L Cumulative Discharge vs Time, Scenario 6

U234L Cumulative Discharge vs Time, Scenario 6

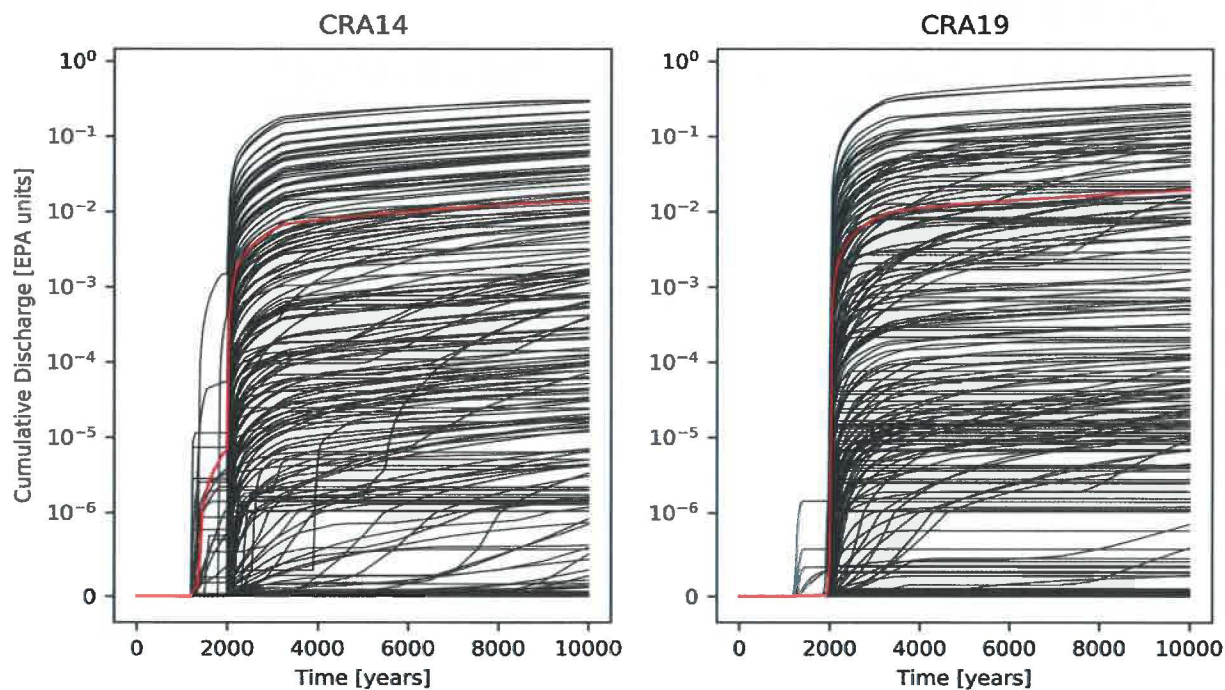


Figure 64– U234L Cumulative Discharge vs Time, Scenario 6

TH230L Cumulative Discharge vs Time, Scenario 6

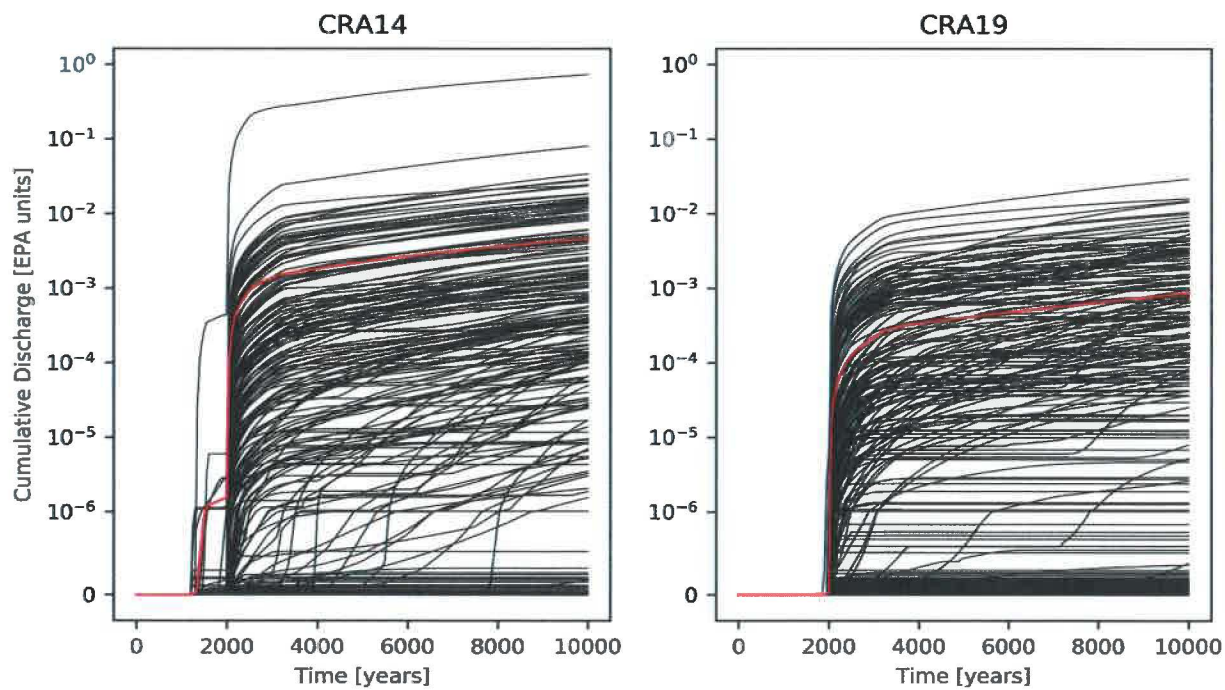


Figure 65– TH230L Cumulative Discharge vs Time, Scenario 6

5.0 SUMMARY

Numerous changes were introduced for the CRA-2019 PA that impact actinide mobilization and transport in the Salado. Most notably, the assumed An(III) baseline solubility values decreased substantially, the An(III) solubility uncertainty distribution values increased, and the An(IV) solubility uncertainty distribution values decreased. The result is that Am(III), Pu(III), and especially Pu(IV) median and mean concentrations decreased, and total mobile radioactivity concentrations decreased overall. The reduction in Pu mobile concentrations will reduce late-time releases in particular since little ^{241}Am remains in the inventory at late times. *To Culebra* cumulative radionuclide discharges remain similar overall between the CRA-2019 PA and the CRA-2014 PA calculations.

6.0 REFERENCES

- Bethune, J.B. 2019. Analysis Package for Direct Brine Releases in the 2019 Compliance Recertification Application Performance Assessment (CRA-2019 PA). Sandia National Laboratories, Carlsbad, NM. ERMS 571370.
- Brunell, S. 2019. Analysis Package for Normalized Releases in the 2019 Compliance Recertification Application Performance Assessment (CRA-2019 PA). Sandia National Laboratories, Carlsbad, NM. ERMS 571373.
- Brush, L.H. and P. Domski. 2013a. Calculation of Organic-Ligand Concentrations for the WIPP CRA-2014 PA. Sandia National Laboratories, Carlsbad, NM. ERMS 559005.
- Brush, L.H. and P. Domski. 2013c. Uncertainty Analysis of Actinide Solubilities for the WIPP CRA-2014 PA, Revision 1. Sandia National Laboratories, Carlsbad, NM. ERMS 559712.
- Brush, L.H. and P. Domski. 2013b. Prediction of Baseline Actinide Solubilities for the WIPP CRA-2014 PA. Sandia National Laboratories, Carlsbad, NM. ERMS 559138.
- Brush, L.H., P.S. Domski, and Y.-L. Xiong. 2012. Analysis Plan for WIPP Near-Field Geochemical Process Modeling. AP-153, Revision 1. Sandia National Laboratories, Carlsbad, NM. ERMS 556960.
- Clayton, D.J. 2008b. Memorandum to L. Brush (Subject: Update to the Calculation of the Minimum Brine Volume for a Direct Brine Release). 2 April 2008. Sandia National Laboratories, Carlsbad, NM. ERMS 548522.
- Clayton, D.J., R.C. Camphouse, J.W. Garner, A.E. Ismail, T.B. Kirchner, K.L. Kuhlman, M.B. Nemer. 2010. Summary Report of the CRA-2009 Performance Assessment Baseline Calculation. Sandia National Laboratories, Carlsbad, NM. ERMS 553039.
- Clayton, D.J., S. Dunagan, J.W. Garner, A.E. Ismail, T.B. Kirchner, G.R. Kirkes, M.B. Nemer. 2008. Summary Report of the 2009 Compliance Recertification Application Performance Assessment. Sandia National Laboratories, Carlsbad, NM. ERMS 548862.
- Cotsworth, E. 2005. EPA Letter on Conducting the Performance Assessment Baseline Change (PABC) Verification Test. U.S. EPA, Office of Radiation and Indoor Air, Washington, D.C. ERMS 538858.
- Cotsworth, E. 2009. EPA Letter on CRA-2009 First Set of Completeness Comments. U.S. EPA, Office of Radiation and Indoor Air, Washington, D.C. ERMS 551444.
- Day, B.A. 2019. Analysis Package for Salado Flow in the 2019 Compliance Recertification Application Performance Assessment (CRA-2019 PA). Sandia National Laboratories, Carlsbad, NM. ERMS 571368.
- Domski, P.S. 2018. Memo on the estimation of the solubility product (Log K_{sp}) for Ca₂EDTA.7H₂O, and Pitzer parameters for the Na⁺ / CaEDTA²⁻ pair. Sandia National Laboratories, Carlsbad, NM. ERMS 570202.

Domski, P.S. 2019a. An Update to the EQ3/6 Pitzer Thermodynamic Database DATA0.FM1 with the Creation of DATA0.FM4. Sandia National Laboratories, Carlsbad, NM. ERMS 571052.

Domski, P.S. 2019b. Uncertainty Analysis of Actinide Solubilities for CRA 2019. Sandia National Laboratories, Carlsbad, NM. ERMS 571179.

Domski, P.S. and C. Sisk-Scott. 2019. Prediction of Baseline Actinide Solubilities for CRA 2019 with an Updated EQ3/6 Pitzer Thermodynamic Database, DATA0.FM4. Sandia National Laboratories, Carlsbad, NM. ERMS 571178.

Fox, B. 2003. Radionuclides Expected to Dominate Potential Releases in the Compliance Recertification Application, Revision 1. Sandia National Laboratories, Carlsbad, NM. ERMS 531086.

Fox, B., Clayton, D., and Kirchner, T. 2009. Radionuclide Inventory Screening Analysis Report for the PABC-2009 Revision 0. Sandia National Laboratories, Carlsbad, NM. ERMS 551679.

Garner, J.W. 1998. Corrective Action Request W-98-003. Sandia National Laboratories, Albuquerque, NM. ERMS 249852.

Garner, J.W. 2003. Analysis Package for PANEL: Compliance Recertification Calculation. Sandia National Laboratories, Carlsbad, NM. ERMS 530165.

Garner, J.W. 2010. Analysis Package for PANEL: CRA-2009 Performance Assessment Baseline Calculations. Sandia National Laboratories, Carlsbad, NM. ERMS 553032.

Garner, J.W. and C. Leigh. 2005. Analysis Package for PANEL: CRA-2004 Performance Assessment Baseline Calculation (Revision 0). Sandia National Laboratories, Carlsbad, NM. ERMS 540572.

Ismail, A.E. and J.W. Garner. 2008. Analysis Package for Salado Transport Calculations: Compliance Recertification Application 2009. Sandia National Laboratories, Carlsbad, NM. ERMS 548845.

Jang, J.J. 2019. Analysis Plan for Derivation and Addition of Equilibrium Constants and Pitzer Interaction Parameters to the WIPP Geochemical Thermodynamic Database. AP-182, Revision 0. Sandia National Laboratories, Carlsbad, NM. ERMS 571074.

Kicker, D. and T. Zeitler. 2013. Radionuclide Inventory Screening Analysis for the 2014 Compliance Recertification Application Performance Assessment (CRA-2014 PA). Carlsbad, NM: Sandia National Laboratories. ERMS 559257.

Kicker, D.C. 2019. Radionuclide Inventory Screening Analysis for the 2019 Compliance Recertification Application Performance Assessment, Revision 1(CRA-2019 PA). Sandia National Laboratories, Carlsbad, NM. ERMS 571659.

Kim, S. 2013a. Analysis Package for Salado Transport Calculations: CRA-2014 Performance Assessment. Sandia National Laboratories, Carlsbad, NM. ERMS 560174.

Kim, S. 2013b. Analysis Package for PANEL: CRA-2014 Performance Assessment. Sandia National Laboratories, Carlsbad, NM. ERMS 560056.

Kirchner, T., A. Gilkey, and J. Long. 2014. Summary Report on the Migration of the WIPP PA Codes from VMS to Solaris, AP-162 Revision 1. Sandia National Laboratories, Carlsbad, NM. ERMS 561757.

Kirchner, T., A. Gilkey, and J. Long. 2015. Addendum to the Summary Report on the Migration of the WIPP PA Codes from VMS to Solaris, AP-162. Sandia National Laboratories, Carlsbad, NM. ERMS 564675.

Kirchner, T.A. 2014. Analysis Plan for Migration of VMS files from the HP Alpha Cluster to the Sun/Solaris Cluster and Qualification of Codes from the Alice Linux Cluster on the Sun Solaris Cluster. AP-168 Revision 0. Sandia National Laboratories, Carlsbad, NM. ERMS 561953.

Kuhlman, K.L. 2010. Analysis Report for the CRA-2009 PABC Culebra Flow and Transport Calculations, AP-144. Sandia National Laboratories, Carlsbad, NM. ERMS 552951.

Leigh, C. and Fox, B. 2005. Radionuclides Expected to Dominate Potential Releases in the Performance Assessment Baseline Calculation Revision 0. Sandia National Laboratories, Carlsbad, NM. ERMS 539634.

Leigh, C.D., J.F. Kanney, L.H. Brush, J.W. Garner, G.R. Kirkes, T. Lowry, M.B. Nemer, J.S. Stein, E.D. Vugrin, S. Wagner, and T.B. Kirchner. 2005. 2004 Compliance Recertification Application Performance Assessment Baseline Calculation, Revision 0. Sandia National Laboratories, Carlsbad, NM. ERMS 541521.

Long, J. 2013. Execution of Performance Assessment Codes for the CRA-2014 Performance Assessment. Sandia National Laboratories, Carlsbad, NM. ERMS 560016.

Long, J. 2019. Computational Code Execution and File Management for the 2019 Compliance Recertification Application Performance Assessment (CRA-2019 PA). Sandia National Laboratories, Carlsbad, NM. ERMS 571375.

Lowry, T.S. 2003. Analysis Package for Salado Transport Calculations: Compliance Recertification Application. Sandia National Laboratories, Carlsbad, NM. ERMS 530164.

Lowry, T.S. 2005. Analysis Package for Salado Transport Calculations: CRA-2014 PA Baseline Calculation. Sandia National Laboratories, Carlsbad, NM. ERMS 548363.

MacKinnon, R.J., and G. Freeze. 1997a. Summary of EPA-Mandated Performance Assessment Verification Test (Replicate 1) and Comparison With the Compliance Certification Application Calculations, Revision 1. Sandia National Laboratories, Carlsbad, NM. ERMS 422595.

MacKinnon, R.J., and G. Freeze. 1997b. Summary of Uncertainty and Sensitivity Analysis Results for the EPA-Mandated Performance Assessment Verification Test, Rev. 1. Sandia National Laboratories, Carlsbad, NM. ERMS 420669.

MacKinnon, R.J., and G. Freeze. 1997c. Supplemental Summary of EPA-Mandated Performance Assessment Verification Test (All Replicates) and Comparison With the Compliance Certification Application Calculations, Revision 1. Sandia National Laboratories, Carlsbad, NM. ERMS 414880.

Mariner, P.E. 2019. A summary of humic colloid parameter values to be implemented in the CRA-2019 Deferred Performance Assessment. Sandia National Laboratories, Carlsbad, NM. ERMS 571250.

Reed, D., J. Swanson, and F. Stanley. 2019. LANL/ACRSP Parameter Recommendations for the CRA-2019 Deferred Performance Assessment Revision 1. Los Alamos National Laboratory, Carlsbad, NM. LCO-ACP-24.

- Sarathi, R.S. 2019a. Memo: Explanation of CAPMIC definition and usage in PA calculations. ERMS 570685. Sandia National Laboratories. Carlsbad, NM.
- Sarathi, R.S. 2019b. Design Document and User's Manual for PANEL Version 5.00. Sandia National Laboratories, Carlsbad, NM. ERMS 570821.
- Sarathi, R.S. 2019c. Requirements Document, Validation Plan, and Validation Document for PANEL Version 5.00. Sandia National Laboratories, Carlsbad, NM. ERMS 570820.
- Sarathi, R.S. 2019d. Intrusion-time shifting software problem for NUTS. SPR19-002. Sandia National Laboratories, Carlsbad, NM. ERMS 570979.
- Sarathi, R.S. 2019e. Change Control Form for PANEL Version 5.00. Sandia National Laboratories, Carlsbad, NM.
- Shinta, A.A. 1997. User's Manual for NUTS, Version 2.05. Sandia National Laboratories, Albuquerque, NM. ERMS 246002.
- Sisk-Scott, C. 2019a. Analysis Plan to Update the WIPP Geochemical Thermodynamic Database (DATA0.FM1) to DATA0.FM4 for CRA-2019. AP-183, Revision 1. Sandia National Laboratories, Carlsbad, NM. ERMS 571001.
- Sisk-Scott, C. 2019b. Calculation of Organic-Ligand Concentrations for the WIPP CRA-2019 Deferred PA. Sandia National Laboratories, Carlsbad, NM. ERMS 571011.
- U.S. Congress. 1992. WIPP Land Withdrawal Act, Public Law 102-579, 106 Stat. 4777, 1992; as amended by Public Law 104-201, 110 Stat. 2422, 1996.
- U.S. Department of Energy (DOE) 1996. Title 40 CFR Part 191 Compliance Certification Application for the Waste Isolation Pilot. U.S. Department of Energy Waste Isolation Pilot Plant, Carlsbad Area Office, Carlsbad, NM. DOE/CAO-1996-2184.
- U.S. Department of Energy (DOE) 2004. Title 40 CFR Part 191 Compliance Recertification Application for the Waste Isolation Pilot Plant, 10 vols., U.S. Department of Energy Waste Isolation Pilot Plant, Carlsbad Area Office, Carlsbad, NM. DOE/WIPP 2004-3231.
- U.S. Department of Energy (DOE). 1996. Title 40 CFR Part 191 Compliance Certification Application for the Waste Isolation Pilot Plant (October). Appendix WCA. DOE/CAO-1996-2184. Carlsbad, NM: Carlsbad Field Office.
- U.S. Department of Energy (DOE). 1996. Title 40 CFR Part 191 Compliance Certification Application for the Waste Isolation Pilot Plant (October). Appendix SCR. DOE/CAO-1996-2184. Carlsbad, NM: Carlsbad Field Office.
- U.S. Department of Energy (DOE). 1996. Title 40 CFR Part 191 Compliance Certification Application for the Waste Isolation Pilot Plant (October). Appendix MASS. DOE/CAO-1996-2184. Carlsbad, NM: Carlsbad Field Office.
- U.S. Department of Energy (DOE). 1996. Title 40 CFR Part 191 Compliance Certification Application for the Waste Isolation Pilot Plant (October). Appendix SOTERM. DOE/CAO-1996-2184. Carlsbad, NM: Carlsbad Field Office.
- U.S. Department of Energy (DOE). 2014. Title 40 CFR Part 191 Subparts B and C Compliance Recertification Application 2014, Appendix PA-2014. DOE/WIPP 14-3503. Carlsbad, NM: Carlsbad Field Office.

U.S. Department of Energy (DOE). 2014. Title 40 CFR Part 191 Subparts B and C Compliance Recertification Application 2014, Appendix MASS-2014. DOE/WIPP 14-3503. Carlsbad, NM: Carlsbad Field Office.

U.S. Department of Energy (DOE). 2014. Title 40 CFR Part 191 Subparts B and C Compliance Recertification Application 2014, Appendix SCR-2014. DOE/WIPP 14-3503. Carlsbad, NM: Carlsbad Field Office.

U.S. Department of Energy (DOE). 2014. Title 40 CFR Part 191 Subparts B and C Compliance Recertification Application 2014, Appendix SOTERM-2014. DOE/WIPP 14-3503. Carlsbad, NM: Carlsbad Field Office.

U.S. Environmental Protection Agency (EPA). 2017. Criteria for the Certification and Recertification of the Waste Isolation Pilot Plant's Compliance with the Disposal Regulations; Recertification Decision. July 19, 2017. Office of Radiation and Indoor Air, Docket EPA-HQ-OAR-2014-0609-0079.

U.S. Environmental Protection Agency (EPA). 1993. "40 CFR 191: Environmental Radiation Protection Standards for the Management and Disposal of Spent Nuclear Fuel, High-Level and Transuranic Radioactive Wastes; Final Rule." *Federal Register*, vol. 58 (December 20, 1993): 66398–416.

U.S. Environmental Protection Agency (EPA). 1996a. "40 CFR Part 194: Criteria for the Certification and Recertification of the Waste Isolation Pilot Plant's Compliance with the 40 CFR Part 191 Disposal Regulations; Final Rule." *Federal Register*, vol. 61 (February 9, 1996): 5223–45.

U.S. Environmental Protection Agency (EPA). 1998. 40 CFR 194, Criteria for the Certification and Recertification of the Waste Isolation Pilot Plant's Compliance with the Disposal Regulations: Certification Decision: Final Rule, *Federal Register*. Vol. 63, 27354-27406.

U.S. Environmental Protection Agency (EPA). 2006. 40 CFR 194, Criteria for the Certification and Recertification of the Waste Isolation Pilot Plant's Compliance with the Disposal Regulations: Certification Decision: Final Rule, *Federal Register*. Vol. 71, 18010-18021.

U.S. Environmental Protection Agency (EPA). 2010. 40 CFR Part 194 Criteria for the Certification and Recertification of the Waste Isolation Pilot Plant's Compliance With the Disposal Regulations: Recertification Decision, *Federal Register* No. 222, Vol. 75, pp. 70584-70595, November 18, 2010.

Van Soest, G.D. 2018. Performance Assessment Inventory Report – 2018. INV-PA-18, Revision 0. Los Alamos National Laboratory, Carlsbad, NM.

WIPP PA Parameter Database. <http://bto.sandia.gov>.

Xiong, Y.-L. 2013. Analysis Plan for Derivation of Thermodynamic Properties Including Pitzer Parameters for Solubility Studies of Iron, Lead and EDTA. AP-154, Revision 2. Sandia National Laboratories, Carlsbad, NM.

Zeitler, T.R. 2019b. Analysis Package for Parameter Sampling in the 2019 Compliance Recertification Application Performance Assessment (CRA-2019 PA). Sandia National Laboratories, Carlsbad, NM. ERMS 571367.

Zeitler, T.R. 2019. Analysis Plan for the 2019 WIPP Compliance Recertification Application Performance Assessment. Sandia National Laboratories, Carlsbad, NM. ERMS 571150.